The Hong Kong Polytechnic University
Department of Building Services Engineering

Control and Design for a Multi-Evaporator Air-Conditioning (MEAC) System

Pan Yan

A thesis submitted in partial fulfillment of the requirements

for the Degree of Doctor of Philosophy

May 2012

Certificate of Originality

I hereby declare that this thesis is my own work and that, to the best of my knowledge and belief, it reproduces no material previously published or written, nor material that has been accepted for the award of any other degree or diploma, except where due acknowledgement has been made in the text.

PAN YAN

Department of Building Services Engineering

The Hong Kong Polytechnic University

Hong Kong SAR, China

May, 2012

Abstract

Multi-evaporator air-conditioning (MEAC) systems are widely used in small- and medium-sized buildings, offering many advantages over conventional chilled water based air-conditioning systems in terms of installation convenience, high design flexibility, being easy to maintain and commission, better indoor thermal comfort control and higher energy efficiency. Although a number of capacity control algorithms have been developed based on system simulation, no experimental-based capacity controller developments for MEAC systems may be identified, except where the capacity controller developed for an MEAC system was based on a model obtained through system identification, which cannot be generically applied to other MEAC systems. On the other hand, the pipelines in an MEAC system are usually complicated, causing a large refrigerant pressure drop, which could in turn further lower evaporating temperature, increase condensing temperature, reduce system's operating efficiency and result in refrigerant mal-distribution among evaporators. Furthermore, different designs for an MEAC system would affect its operating performance and total power input, but no previous studies on applying the Constructal Theory to the refrigerant pipework layout design of an MEAC system for minimizing the total power requirement have been reported. Therefore, a comprehensive research program consisting of developing a novel capacity control algorithm, and investigating the effects of large pressure drop along a refrigerant distribution pipework on the operating performance in a dual-evaporator air

conditioning (DEAC) system, discovering the best possible pipework layout design of MEAC systems for minimizing the total power input requirement using the Constructal Theory has been carried out and is reported in this thesis.

This thesis starts with reporting the development of a novel capacity control algorithm (NCCA) for a DEAC system, a typical MEAC system. The controller imitated On-Off control of a single-evaporator A/C system (SEAC) in each indoor unit of the DEAC system by using variable-speed compressor and electronic expansion valves (EEVs). Experimental tests validated its control accuracy and robustness. However, indoor air temperature controlled using the NCCA may still be subjected to significant fluctuations under certain operating conditions due to the use of temperature dead-band and time delay for compressor start-up, and the interaction among indoor units. An improved novel capacity control algorithm (INCCA) was therefore further developed, and further controllability tests carried out. The test results showed that the INCCA was simple but could effectively restrain the magnitude of temperature variations and avoid the frequent altering in compressor speed.

Secondly, the thesis presents a modeling study on the effects of refrigerant pipeline length on the operational performance of a DEAC system. To facilitate the intended modeling study, a physical-based steady-state mathematical model has been developed. The model contained a sub-module which was specifically devoted to

accounting for the influence of refrigerant pipeline length on system operational performance. The model has been validated by comparing its prediction results with the experimental results previously reported by others. Using the model developed, the effects of refrigerant pipeline length on the operating performance of the DEAC system have been studied and are reported, and the layout optimization of a DEAC system was studied for the highest possible operational efficiency. Simulation results indicated that the DEAC system's COP decreased with an increase in the refrigerant pipeline length. The simulation results also suggested that for a DEAC system, its highest COP would be resulted in when the outdoor unit was located equally between the two indoor units and its lowest COP when the outdoor unit was located close to either of the indoor unit.

Thirdly, this thesis documents an analytical study of applying the Constructal Theory to discovering the best possible refrigerant pipework layout design in MEAC systems for minimizing the total power requirement. Two approaches that might be used in the study were considered. The first approach was based on the first law of thermodynamics and consisted of changing the configuration of an MEAC system in such a way that the work required per unit of heat removed from an indoor space was reduced. The second approach was based on the second law of thermodynamics, aiming at reducing the irreversibility of the system. It was shown that the use of the two approaches would yield equivalent results. However, the first approach was simpler and more familiar with for people, because it did not require the calculation

and discussion of entropy generation. Therefore the first approach was adopted in the study. The study started from a single-room case (SEAC systems), and was extended to a dual-room case (DEAC systems) and finally to a multi-room case (MEAC systems). Two ways to arrange the refrigerant pipework were considered. One was to position the refrigerant pipework inside room(s) and the other outside the room(s). The analytical study results show that for an SEAC system, its heat exchanger (i.e., indoor unit) area was fixed by the cooling load it had to deal with, while for a DEAC system and an MEAC system, their total heat exchanger areas were decided by the total cooling load they had to handle. The heat exchanger area in each room however was influenced by the location of the outdoor unit of the MEAC system when the distance among all rooms was fixed. This suggested that if the cooling load in one room was specified, the operating performance of an MEAC system would be influenced by the design of its pipework. The study results for all the three study cases also indicated that the optimum diameters of refrigerant pipelines were independent of their lengths. This can guide the designer of an MEAC system to calculate an optimum pipeline diameter and find out the total heat exchanger area first, and then to determine the pipelines length and heat exchanger area in each room as a function of the total system cost and outdoor unit position.

Publications Arising from the Thesis

Journal Papers

1. **Pan Yan**, Xu Xiangguo, Xia Liang, Deng Shiming. A modeling study on the effects of refrigerant pipeline length on the operational performance of a dual-evaporator air conditioning system. *Applied Thermal Engineering*, 39 (2012) 15-25 (Based on Chapter 5).

2. **Pan Yan**, et al. Experimental study of a novel capacity control algorithm for a multi-evaporator air conditioning system. *Applied Thermal Engineering*, In Press (Based on Chapter 4).

3. **Pan Yan**, et al. Thermodynamics of cooling with evaporator and distribution lines (Based on Chapter 6 and under preparation).

Acknowledgements

I must express my gratitude to my Chief Supervisor, Professor Deng Shiming, and my Co-Supervisor, Dr. Chan Mingyin, Assistant Professor, both from the Department of Building Services Engineering (BSE), The Hong Kong Polytechnic University, for their excellent guidance, caring patience, and providing me with an excellent environment for doing research. Without their encouragements and guidance, this study would not have been materialized.

My special thanks go to the Research Grant Council (RGC) of Hong Kong and The Hong Kong Polytechnic University for financially supporting this project. I would like to thank Dr. Xu Xiangguo for helping me develop my simulation model and carry out the experimental work. I would also like to thank Dr. Pan Dongmei, who's a good friend of mine, for her helps. Furthermore, I would like to thank Dr. Xia Liang, Miss Qu Minglu and Miss Li Ning for their helps during my study. In addition, I wish to express my gratitude to the technicians in the Heating, Ventilation and Air Conditioning Laboratory of the BSE Department for their supports during my experimental work.

I also wish to thank Professor Adrian Bejan of Duke University, USA, who accepted me as a visiting student to his research laboratory between January and May, 2012.

Last but not least I wish to express my gratitude and love to my beloved parents for their supports, patience and understandings.

Table of Contents

List of Figures

List of Tables

Nomenclature

Variable	Description	Unit
A	area	m^2
A_f	fin surface area	m^2
A_{tu}	outside tube surface area	m^2
B_1. B_3	parameters defined by Eqs. (6.30), (6.76) and (6.92)	DL
B_m	integrated refrigerant thermophysical property	DL
B_o	refrigerant boiling characteristics number	DL
c_L	total cost per unit C_E	m^2
c_T	pipeline cost per unit C_E	$/$m^2$
C_1-C_5	constants used in Eq.(5.20)	DL
C_6,C_7	coefficients used in Eqs. (6.14) and (6.15)	DL
C_E	cost per area of evaporator	$/$m^2$
C_L	cost per area of refrigerant pipeline	$/$m^2$
C_T	total cost	$
C_o	refrigerant convection characteristics number	DL
C_p	specific heat at constant pressure	kJ/(kg·K)
COP	coefficient of performance	DL
d	diameter	m
d_c	tube collar diameter	m
d_h	hydraulic tube diameter	m
D	cylinder bore (in Chapter 5) or diameter (in Chapter 6)	m
e	relative difference	DL
E	On-Off control signal for EEV	DL
EC_{ev}	actual pulse output of the EEV	DL
f	friction factor	DL
F	refrigerant volumetric flow rate	L/min

f_c	turbulent skin-friction coefficient of condenser	DL
f_e	turbulent skin-friction coefficient of evaporator	DL
F_{cm}	input frequency of VFD	Hz
Ff_r	dimensionless factor of refrigerant property	DL
Fr	*Froude* number	DL
g_r	refrigerant mass flux	kg/(s·m^2)
h	specific enthalpy	kJ/kg
i_1-i_5	the index of iteration number	DL
j	*Colburn* factor	DL
j_1-j_7	parameters used in Eqs. (5.42) and (5.61)	DL
$K1$, $K2$	parameters used in Eq. (5.93)	DL
K_E	parameter used in Eq. (6.26)	DL
K_{ev}	valve opening per unit of pulse output	m^2
K_L	parameter used in Eq. (6.27)	DL
K_T	parameter used in Eq. (6.28)	DL
l	length (used in Chapter 5)	m
L	length (used in Chapter 6)	m
L_{cm}	stroke of cylinder	m
$LMTD$	log mean temperature difference	K
$\dot{m}$	mass flow rate	kg/s
m	the number of rooms	DL
n	length ratio	DL
N	polytropic index	DL
Nu	Nusselt number	DL
NR	number of longitudinal tube rows	DL
P	pressure	bar
ΔP	pressure difference	bar
ΔP_m	compressor discharge pressure	bar

PL_{cm}	number of electrode couple of the motor	DL
PI_f	fin pitch	m
PI_L	louver pitch	m
Pr	Prandtl number	DL
q	heat transfer flux	W/m^2
Q	heat transfer rate	W
R	combined total thermal resistance	(m·K)/W
r_c	refrigerant latent heat of vaporization	kJ/kg
Re	Reynolds number	DL
S	entropy	J/K
s_{cm}	slip factor of the motor	DL
S_{cm}	rotational speed of compressor	r/s
SD	standard deviation	$^{\circ}C$
S_1	transverse tube pitch	m
S_2	longitudinal tube pitch	m
t	time	s
T	temperature	K
ΔT	Temperature difference	$^{\circ}C$
U	overall heat transfer coefficient	$W/(m^2 \cdot K)$
V	volume	m^3
w_{cm}	compressor specific work	kJ/kg
W	total power required by installation	W
W_{cm}	electrical work input to compressor (used in Chapter 5)	W
W_P	pumping power	W
W_R	power required for compression	W
X	additional control signal for EEV	DL
Y	improved On-Off control signal for EEV	DL

Greek symbols

α	convective heat transfer coefficient	W/(m^2·K)
β	order used in Eq. (6.15)	DL
δ_f	fin thickness	m
ε	absolute roughness of pipe wall	m
ζ_a	dehumidifying augmentation factor	DL
η	efficiency	DL
η_a	fin surface efficiency	DL
η_f	fin efficiency	DL
η_{mec}	mechanic coefficient	DL
η_{motor}	motor coefficient	DL
η_R	compression ration	DL
θ_l	louver angle	degree (°)
λ_{cm}	overall displacement coefficient	DL
$\lambda_{f,e}$	thermal conductivity tube fin metal	W/(K·m)
λ_l	leakage coefficient	DL
λ_p	pressure loss coefficient	DL
λ_r	refrigerant thermal conductivity	W/(K·m)
λ_t	the temperature coefficient	DL
λ_v	compressor volumetric coefficient	DL
λ_w	indicated coefficient	DL

μ_a	air dynamic viscosity	kg/(m·s)
μ_r	refrigerant dynamic viscosity	kg/(m·s)
ξ_{ev}	expansion valve flow coefficient	DL
ρ	density	kg/m^3
ς	local loss coefficient	DL
υ	velocity	m/s
χ	dryness fraction	DL
$\overline{\chi}$	mean dryness fraction	DL
ω	moisture content	g/(kg dry air)

Subscripts

1, 2…	room/indoor unit number
a	air or ambient
avg	average
B	building or room
c	condenser
cm	compressor
dr	dry
ds	de-superheating
e	evaporator
ev	expansion valve
E	evaporator
gen	generation
h	enthalpy
i	inside
I, II	branch number

L	pipeline
li	liquid
m	mass flow rate
max	maximum
o	outside
opt	optimum
P	pressure
Q	cooling capacity
r	refrigerant
R	refrigerator plant
sc	sub-cooling
set	setting point
sh	superheated
T	temperature
tp	two-phase
va	vapor
wt	wet
wl	wall

Note: DL = Dimensionless

List of Abbreviations

A/C	air-conditioning
ANN	artificial neural networks
COP	coefficient of performance
CSR	compressor speed ratio
DEAC	dual-evaporator air-conditioning
DX	direct-expansion
EEV	electronic expansion valve
FPFA	fan-coil plus fresh air
FSR	fan speed ratio
INCCA	improved novel capacity control algorithm
LGU	load generating unit
MEAC	multi-evaporator air-conditioning
MIMO	multi-input-multi-output
NCCA	novel capacity control algorithm
PDE	partial-differential equations
RTD	resistance temperature device
SEAC	single-evaporator air conditioning
TEAC	three-evaporator air-conditioning
TEV	thermal expansion valve
VCC	vapor compression cycle
VFD	variable frequency drive
VRV	variable refrigerant volume

Chapter 1

Introduction

For pursuing a high quality living and working environment with less energy consumption, multi-evaporator air-conditioning (MEAC) systems are widely used in small- to medium-scale buildings due to their advantages of installation convenience, high design flexibility, being easy to maintain and commission, better indoor thermal comfort control and higher energy efficiency. Although both a single-evaporator air-conditioning (SEAC) system and an MEAC system are operated based on vapor compression cycle, there exists a number of noticeable differences between them. Usually in an MEAC system, there are two or more evaporators (or indoor units) installed in parallel without any pressure regulators, which results in strongly coupled operational parameters in each indoor unit. This feature requires that different control algorithms be used for MEAC systems. However, only a limited number of reported studies on the modeling and control of MEAC systems could be identified in the open literature. Although a number of capacity control algorithms have been developed based on system simulation, no experimental-based capacity controller developments for MEAC systems could be identified, except where the capacity controller developed for an MEAC system was based on a model obtained through system identification, which cannot be generically applied to other MEAC systems.

On the other hand, the refrigerant pipelines in an MEAC system are usually complicated, resulting in a potentially large refrigerant pressure drop which in turn could lower evaporating temperature, increase condensing temperature, reduce system operational efficiency and further lead to refrigerant mal-distribution among evaporators. Neglecting the influences of pipelines length and fittings on the operational performance can be problematic for an MEAC system. Nonetheless, only a few studies have been so far carried out to look into this issue. Furthermore, since the pipework in MEAC systems are complicated and different layout designs would have significant impacts on the operational efficiency and input power requirement. Therefore, finding out the best possible layout design for MEAC systems are very important in order to achieve the highest possible operational efficiency.

This thesis begins with an extensive literature review on a number of issues related to the design and control for MEAC systems. Firstly, the detailed configurations of both outdoor unit and indoor units in MEAC systems and the connection between them to form a complete system, and the MEAC systems equipped with certain special features are reviewed. A review on the previous studies on the operational performances of MEAC systems and the effects of refrigerant pipework on the operational parameters in an MEAC system, including refrigerant flow distribution, evaporating pressure or temperature, and energy efficiency under different cooling load fractions in different conditioned rooms, is then presented. Thirdly, a review on the previous studies on modeling of MEAC systems and their components such as evaporator, condenser, expansion valve and compressor is reported. This is followed by reviewing various issues related to the capacity control and advanced control

strategies developed for or adopted in MEAC systems. Furthermore, Constructal Theory, which can be potentially applied to discovering the best possible layout design for MEAC systems, is introduced. Finally, a number of important issues where further in-depth research work has been identified, including developing capacity control strategies for MEAC systems, evaluating the influence of the refrigerant pressure drop along pipelines on MEAC systems' operational performances and discovering the best possible design for MEAC systems by using the Constructal Theory for the highest possible system operational efficiency. There are the expected targets of investigation in the research project reported in this thesis.

The research proposal covering the aims and objectives, the project title and the methodologies adopted in this project is presented in Chapter 3.

Chapter 4 reports on developing a novel capacity control algorithm (NCCA) for a dual-evaporator air-conditioning (DEAC) system, which imitated On-Off control for an SEAC system in each indoor unit of an MEAC system by using variable-speed compressor and electronic expansion valves (EEVs). The control algorithm is presented and the experimental validation about control accuracy and robustness reported. The experimental results showed, however, that indoor air temperature controlled using NCCA may still be subjected to significant fluctuations at certain operating conditions due to the use of temperature dead-band and time delay for compressor start-up, and the interaction among indoor units. An improved novel capacity algorithm (INCCA) was further developed and related controllability tests were also carried out.

A modeling study on the effects of refrigerant pipeline length on the operational performance of a dual-evaporator air-conditioning (DEAC) system is presented in Chapter 5. A physical-based steady-state mathematical model has been developed and is reported. The model has a sub-module specifically devoted to accounting for the influence of refrigerant pipeline length on system operational performance. The model has been validated by comparing its prediction results with the experimental results previously reported by others. The results of the modeling study on the effects of refrigerant pipeline length on the operational performance of the DEAC system for the highest possible operational efficiency are presented.

An analytical study of applying the Constructal Theory to discovering the best possible refrigerant pipework layout design of MEAC systems for minimizing the total system power requirement is reported in Chapter 6. Two approaches that might be used in the study were considered. The first approach was based on the first law of thermodynamics and consisted of changing the configuration of an MEAC system in a way that the work required per unit of heat removed from an indoor space was reduced. The second approach was based on the second law of thermodynamics, aiming at reducing the irreversibility of the system. It was shown that the use of the two approaches would yield equivalent results. However, the first approach was simpler and more familiar with for people, because it did not require the calculation and discussion of entropy generation. Therefore the first approach was adopted in the study. The study started from a single-room case (SEAC systems), and was extended to a dual-room case (DEAC systems) and finally to a multi-room case (MEAC systems). Two ways to arrange the refrigerant pipework were considered. One was to

position the refrigerant pipework inside room(s) and the other outside the room(s). The analytical study results are reported.

The Conclusions of the thesis and the proposed future work are presented in the final Chapter.

Chapter 2

Literature Review

2.1 Introduction

For pursuing a high quality living and working environment with less energy consumption, the use of air-conditioning (A/C) becomes increasingly important. The latest developments of A/C technology, which is featured by high efficiency, operation and control convenience, are continuously being seen all over the world. Modern A/C system emerged in early 1900s following the invention of the first A/C systems designed by Willis Carrier to improve the printing quality in a printing plant [Margaret 1972]. At first, A/C systems were mostly applied to increasing productivity and product quality in various industrial processes. However, with gradual improvements in living standard, A/C systems gradually started to find applications in non-industry processes, such as buildings and transportations, so as to provide people with a thermally comfortable environment to live or work in. For example, residential sales of air conditioners expanded dramatically in 1950s [Margaret 1972]. Currently, A/C systems can be found in almost all types of buildings: commercial, residential, industrial and institutional, etc.

Different types of A/C systems have been designed for different purposes and functions in different buildings. A variable refrigerant volume (VRV) A/C system is a typical example. It consists of indoor units (from one up to 60 units) connected to a common outdoor unit by refrigerant pipework. In a VRV system, refrigerant mass

flow rate is varied using either an inverter controlled variable-speed compressor or multiple compressors of varying capacity to satisfy the cooling and/or heating requirements within air conditioned spaces served by the VRV A/C system. The first VRV A/C system appeared in 1982 in Japan. Since then, VRV A/C systems have gained a greater and greater popularity due to their inherent advantages over conventional A/C systems, such as high energy efficiency, flexibility in design and installation and compactness in configuration, etc. Currently, VRV A/C systems are widely seen in various small- to medium-scale buildings.

As mentioned, there can be one or more indoor units (evaporators) in a VRV A/C system. Consequently, two broad types of VRV A/C systems are identified: a single-evaporator air-conditioning (SEAC) system and a multi-evaporator air-conditioning (MEAC) system. In an MEAC system, one common outdoor unit is connected to a number of indoor units. Although both an SEAC and an MEAC system are operated based on vapor compression cycle (VCC), there exist a number of noticeable differences between the two systems. In an MEAC system, the operational parameters in each indoor unit are strongly coupled and its pipework complicated due to more than one of varying capacity indoor units connected in parallel. Consequently, different approaches have been adopted to study SEAC and MEAC systems, respectively. Unlike an SEAC system, an MEAC system could be operated with some of its indoor units providing cooling and others providing heating, simultaneously and independently. This implies more flexibility with respect to operational modes for users, and might thus offer a greater energy saving potential when simultaneous heating and cooling are required in different parts of a building.

Because of their obvious advantages, in Japan, MEAC systems are used in approximately 50% of small- to medium-scale commercial buildings (up to 6500 m^2) and one-third of large-scale commercial buildings (more than 6500 m^2) [Goetzler 2007]. In Mainland China, MEAC systems took 30% of the A/C market share in 2009 [M&EI 2009]. In the U.S., MEAC systems are gaining more attentions as more people become familiar with the MEAC technology [Masuda et al. 1991, Amarnath and Blatt 2008].

This Chapter presents a critical literature review on various issues related to studying MEAC systems. At first, a review of the configurations of MEAC systems is reported, which is followed by presenting a review on the studies of operational performances for MEAC systems. Thirdly, a review of mathematical modeling methods for complete MEAC systems and their main components is presented. Fourthly, various issues related to developing capacity control strategies for MEAC systems are reviewed. Finally, the Constructal Theory, which can be used to discover the best possible system design for the minimized system power consumption, is briefly introduced. A number of important issues, where further in-depth research studies for MEAC systems are required, have been identified and are summarized in conclusion.

2.2 Configurations of MEAC systems

The detailed configurations of both outdoor and indoor units of an MEAC system and the connection between the outdoor unit and indoor units to form a complete system will be introduced at first. Then MEAC systems equipped with certain

special features will also be covered in this Section.

2.2.1 Outdoor unit and its main components

An outdoor unit in an MEAC system mainly consists of a compressor, a condenser and a high pressure refrigerant receiver.

Usually, a variable-speed compressor is used in an MEAC system. Its speed variation is achieved through normally using a frequency inverter [Amarnath and Blatt 2008]. By varying the supply frequency of a frequency inverter to the compressor, its speed as well as the discharge refrigerant mass flow rate are varied, so that the required cooling loads in conditioned spaces can be satisfied. Therefore, an MEAC system equipped with variable-speed compressor can actively respond to the fluctuations in space load conditions [Masuda et al. 1991, Xia et al. 2002, Afify 2008, Aynur 2008]. Very often, inverter-driven scroll compressors are also used in MEAC systems because they provide variable refrigerant mass flow rate without potential risk of harmonic current emission [Cho and Kim 2000, Chen et al. 2002a, b]. Their advantages may include continuous control, low noise level, reduced vibration, low-start current and quick control response [Hu and Yang 2005, Cuevas and Lebrun 2009]. A scroll compressor uses two interleaving scrolls to pump, compress or pressurize refrigerant. Often, one of the scrolls is fixed, and the other orbits eccentrically without rotating, thereby trapping and pumping or compressing pockets of refrigerant fluid between the scrolls. A further method for producing the compression motion is to co-rotate the scrolls, in synchronous motion, but with offset centers of rotation [Park et al. 2002, Chen et al. 2002a, b].

Air-cooled condensers were used in all MEAC systems up to 2008. Recently, the introduction of water-cooled MEAC systems has extended the potential application of MEAC technology [Aynur 2010]. Generally, an air-cooled condenser is of fin-and-tube type and a water-cooled condenser plate type. In a water-cooled MEAC system, a cooling tower is required [Aynur 2010]. A water-cooled condenser provides a connection between refrigerant circuits and cooling water circuits. The pressure in water circuit pipelines is lower than that in refrigerant circuits, which in turn reduces the risk of leakage [Website_1 2006, Li et al. 2009]. The shortcoming of a water-cooled MEAC system is however the intermediate heat exchange between water and refrigerant, which would increase irreversible heat loss and reduce system performance [Li et al. 2009].

2.2.2 Indoor unit and its main components

An indoor unit in an MEAC system generally consists of a heat exchanger, temperature sensors, a fan, an accumulator and an EEV. The progression of the number of indoor units was from two indoor units operating with a single outdoor unit, to four to eight units in the late 1980s, then to 16 units in the early 1990s, to 32 units by 1999 and to 40 units by 2003. Currently, the advancement in MEAC technology allows as many as 60 or more indoor units to be operated with one outdoor unit, with the cooling/heating capacity of each indoor unit ranging from 1.4 to 17.5 kW [Amarnath and Blatt 2008, Website_4 2011].

Indoor units might be wall-mounted or floor-mounted and can be of ceiling-cassette type, concealed ducted type, etc. Temperature sensors are usually located at

evaporator outlet for control purpose. According to the difference between indoor air temperature and its setting, the refrigerant mass flow rate through indoor units is regulated by using EEV [Aynur 2010]. An indoor air fan is usually also of variable-speed type and users can control the fan speed by themselves via a remote controller.

The function of an EEV in a refrigeration system is similar to that of a thermostatic expansion valve (TEV), except that the refrigerant temperature at the exit of an indoor unit is sensed electronically. Although EEVs are more expensive than other types of expansion valves, they are more and more widely used due to their advantages, such as a faster response to load variation, a wider range of flow rate regulation and a higher control precision [He et al. 1997, Aprea and Mastrullo 2002, Li et al. 2004, Chen and Deng 2006, 2010]. A further benefit of using EEVs in an MEAC system is that EEVs could be opened or shut down during operation so that it is possible to have individual control of providing air conditioning in different spaces. Some of the indoor units may be turned off by fully closing their matching EEVs, while the others are in operation [Aynur 2010, Goetzler 2007]. Therefore, EEVs are widely applied to MEAC systems as a throttle regulator [Website_4 2011].

2.2.3 Pipework connecting an outdoor unit and its matching indoor units

An outdoor unit and indoor units in an MEAC system are connected via a refrigerant pipework. Currently, the maximum pipe length in an MEAC system can be over 1000 m [Website_1 2006]. Theoretically, the maximum length of a refrigerant pipeline is determined by compressor power input and the refrigerant flow resistance. Therefore, there would be a maximum allowable height difference and a maximum

allowable total refrigeration pipeline length [Website_1 2006, Website_2 2009]. Generally, two-pipe or three-pipe configurations are common for MEAC systems. A two-pipe (a high pressure refrigerant gas pipe and a low pressure liquid pipe) MEAC system is commonly used for cooling or heating only depending on season. A three-pipe (a high pressure refrigerant gas pipe, a low pressure gas pipe and a low pressure liquid pipe) MEAC system can however provide cooling and heating simultaneously in different parts of a building, which may occur in winter in medium- to large-scale buildings with an inner zone and an outer zone in each floor [Amarnath and Blatt 2008].

2.2.4 MEAC systems with special features

Special features may be incorporated into an MEAC system to meet different requirements at different operating conditions.

To recover the rejected heat from an A/C system decreases not only the consumption of primary energy for heating purposes such as domestic hot water heating, but also the calefaction to the surrounding by heat rejection from A/C systems [Gu et al. 2004, Shen et al. 2008]. Usually, the rejected heat may be used to generate low-temperature hot water. Shi et al. [2003] showed that the energy efficiency ratio (EER) of an air conditioner when operated in a heat recovery mode was twice as much as that in a non-heat recovery mode. For an MEAC system, heat recovery could be incorporated when heating and cooling take place simultaneously to transfer heat between the pipes supplying refrigerant to cooling and heating indoor units, which is a unique feature for MEAC systems. The study by Hai et al. [2006a] showed that an

experimental MEAC system with heat recovery can meet the demand of concurrent heating and cooling through the switch of solenoid valves. The experimental results demonstrated that the system can deal with the load in each room, and its EER was increased remarkably.

In addition, an MEAC system itself does not have ventilation provisions. It is therefore necessary to consider ventilation provisions when employing an MEAC system for achieving high indoor air quality [Aynur et al. 2008a, b, c, Aynur 2010]. Ventilation provisions may be incorporated into an MEAC system in a number of ways. One is to place an indoor unit of the MEAC system inside a ventilation duct. A dedicated outdoor air handling unit may also be used, and an MEAC system would have to only deal with space load. In addition, heat recovery ventilators can be introduced to reduce the cooling loads imposed on MEAC systems [Amarnath and Blatt 2008].

2.3 Operational performance of MEAC systems

Normally, indoor units or evaporators in an MEAC system are directly connected in parallel through refrigerant pipework without using pressure regulators. Hence, evaporating pressures or temperatures in all these evaporators are pretty close to each other [Chen et al. 2005, Winkler et al. 2008]. These evaporators are working simultaneously with a common compressor and a condenser, resulting in highly coupled system operational parameters. Consequently, a change in the thermal condition in one room may cause changes in evaporating pressures and temperatures in all other evaporators [Chen et al. 2005]. Therefore, the relationships among

operational parameters in an MEAC system, including refrigerant flow distribution, evaporating pressure or temperature and energy efficiency under different cooling load fractions in different conditioned rooms, are highly coupled. This has thus attracted a great deal of research attentions.

On the other hand, in an actual MEAC system, its refrigerant pipework can be much more complicated with a long total pipe length and a large number of fittings such as elbows and valves. A longer pipeline with more fittings would cause a greater refrigerant pressure drop [Wijaya and Spatz 1995], which in turn could further lower evaporating temperature, increase condensing temperature, reduce system's operational efficiency and result in refrigerant mal-distribution among evaporators [Lee and Yoo 2000]. Therefore, the influence of pipeline length with fittings on the operational performance of an MEAC system deserves more research attention.

2.3.1 Measured operational performance of MEAC systems

The earlier published studies on the operational performance of MEAC systems appeared in 1990s [Fujita et al. 1992, Okuzawa 1992]. At that time, instead of using variable-speed compressors, twin rotary constant-speed compressors were used. Fujita et al. [1992] examined the output cooling capacity and refrigerant flow distribution in an MEAC system with two indoor units. The indoor thermal comfort, the reliability and working efficiency of the system were improved by the use of a control technology based on the EEVs and twin rotary compressors. It was further suggested that the reduction of the number of On-Off operation could provide comfort and help save energy. Okuzawa [1992] optimized the control over the degree

of refrigerant superheat in an MEAC system with four to six indoor units by using a PI control algorithm which improved the system's response to load variation.

With the technology advancement in variable-speed compressors and EEVs, more advanced control strategies that can lead to a reliable system operation, a high efficiency and a better indoor thermal environment have been implemented in MEAC systems. The operational performances of MEAC systems equipped with a variable-speed compressor and EEVs gained an increasingly more research attention, and a number of studies have been carried out to investigate the influences of varying both compressor speed and EEV openings on the operational performance of MEAC systems. Park et al. [2001] studied the impacts of varying compressor speed and EEV openings on the output cooling capacity of an MEAC system. The study showed that, at a fixed compressor speed, the MEAC system could provide variable cooling capacity by changing EEV openings to satisfy the cooling load in each indoor unit. A parabolic relationship between COP variation and the opening area of an EEV was demonstrated. Therefore, there existed an optimum EEV opening with respect to COP variation. However, at a fixed compressor speed, the cooling capacity within only a certain range may be supplied through varying the opening of EEVs. Park et al. [2007] further noticed that for an MEAC system, the lowest operating compressor speed satisfying the imposed cooling load on the system should be selected in order to achieve the highest possible COP. A set of equations obtained using linear regression were given by Hu and Yang [2005], who tested and obtained the relationship between the opening of EEVs and the percentage output capacity of a variable-capacity scroll type compressor in an MEAC system having five indoor

units.

A distinguished feature of an MEAC system is the complicated relationship among its coupled operational system parameters. Choi and Kim [2003] established a dual-evaporator air-conditioning (DEAC) experimental system and studied the coupled relationship among its operational parameters. Firstly, the influence of return air temperature on the system operational parameters was studied. It was found out that a change in return air temperature to one indoor unit, when the return air temperature to the other indoor unit remained unchanged, would influence the total cooling capacity, power consumption and the coefficient of performance (COP) when both compressor speed and EEV openings were fixed. These results agreed well with that reported by Domanski and Didion [1983]. Secondly, the impact of changing the opening of one EEV, with the opening of the other EEV fixed, on system performance was also investigated. It was shown that at a constant compressor speed, the cooling capacity of one indoor unit was increased when the opening of its matching EEV was increased. However, the cooling capacity of the other indoor unit was lowered even the opening of its matching EEV remained unchanged. Therefore, it was suggested that two EEVs should be simultaneously controlled to obtain an appropriate capacity balance between the two indoor units in a DEAC system, even though the operating conditions in only one of indoor units were changed. Furthermore, the study results also showed that evaporating pressures in both indoor units as well as condensing pressure increased with an increase in the opening of one EEV only.

The cooling load in a space is determined by many factors, such as the size,

orientation, internal setting and occupancy of the space, etc. Therefore, the cooling load in different rooms served by an MEAC system will be different. Consequently, the influence of varying cooling load ratio, which is defined as the fraction of the cooling load in one room to the sum of all cooling loads from all rooms, on system performance has been studied. Park et al. [2007] investigated the effects of the variation of load ratio on system performance for a DEAC system. The total cooling load of the system was fixed in the study. The study results showed that the compressor power input and system COP varied with the change in load ratio. The former was increased and the latter decreased with an increase in load ratio. It was suggested that the reason for power input increase was due to an increase in compressor operating frequency, which increased with load ratio even when the total space cooling load remained unchanged.

Hu and Yang [2005] demonstrated that an MEAC system having five indoor units and a variable-capacity scroll compressor could achieve zoning control because the system could provide exact cooling capacity for each of the indoor units under part load condition. In this study, EEVs were used as a control device to adjust the refrigerant mass flow rate when space cooling load was varied. Xia et al. [2002] tested the performance of an MEAC system with five indoor units, using six calorimeters. The outdoor unit and five indoor units were each placed in one of the calorimeters. The test results suggested that the system COP did not change significantly at different part load ratios. This was partly because the two compressors used in the system were arranged in “tandem”, which helped yield a better part load performance. Joo et al. [2011] carried out a series of experiments to

understand the relationship between the operational performance and part load ratio. The COP values and the average cooling and heating capacities at their full load conditions were compared to those at part load conditions at each operating mode, i.e., cooling-only, heating-only, cooling-main, heating-main and heat recovery. In addition, the effects of EEVs' openings and fan speed on system performance were discussed in order to optimize the cooling and heating capacities under part load conditions in both cooling-main and heating-main modes. It was indicated that for all operating modes, the compressor speed ratios (CSRs) were strongly dependent on the number of operating indoor units in the main path. For both cooling-only and heating-only modes, the averaged heating capacity and cooling capacity per unit could be properly controlled by varying the CSRs. However, for both cooling-main and heating-main modes under part load conditions, there was a large imbalance between cooling capacity and heating capacity even when the CSRs were optimized. Therefore, in order to obtain a designed capacity in both cooling-main and heating-main modes, the refrigerant mass flow rate through an indoor unit in the sub-path was controlled by adjusting its matching EEVs' opening, at an optimized CSR. Furthermore, the average heating capacity per unit was increased with a decrease in the outdoor fan speed ratio (FSR), while the average cooling capacity per unit decreased, providing a better capacity balance. However, the COP was decreased by 12.7% with a decrease in FSR from 100% to 22.5%. In heat recovery mode, the average cooling capacity and heating capacity per unit were increased with an increase in the CSR, while the COP was decreased.

To be able to provide heating and cooling simultaneously is one of distinguished

advantages for MEAC systems, which may be called as heat recovery MEAC systems. Kang et al. [2009] conducted an experimental study on an MEAC system with four indoor units operated under five modes: cooling-only, heating-only, cooling-main, heating-main, and heat recovery. The last three modes: cooling-main, heating-main and heat recovery, were inspired by the concept of heat recovery to achieve a better energy performance. In cooling-main mode, the rate of the bypass refrigerant mass flow to a heating-operated indoor unit was optimized by controlling its matching EEV's opening. The study showed that the power consumption in the cooling-main mode was decreased by 11.1% from that in the cooling-only mode due to a decrease in refrigerant mass flow rate. In heating-main mode, the refrigerant mass flow rate to a cooling-operated indoor unit was optimized by adjusting its matching EEV's opening. The EERs in the heating-only and heating-main modes were 3.29 and 3.63, respectively. In heat recovery mode, it was found out that the system COP decreased with an increase in compressor speed because the rate of increase in the output cooling capacity was higher than that of the compressor power input when compressor speed was increased. Furthermore, the system COP in heat recovery mode was higher than that in all other modes since the heat rejected from the condenser and some of evaporators were utilized.

Zhou et al. [2007, 2008] developed a new module that may be incorporated into EnergyPlus, a well-known building energy simulation program, to evaluate the level of energy-use for VRV systems, covering both SEAC and MEAC systems. The energy consumptions for three popular A/C systems, namely, a variable air volume (VAV) system, a VRV system, and a fan-coil plus fresh air (FPFA) system, were

numerically studied using the module developed at the EnergyPlus platform. A generic office building was modeled where the three A/C systems were installed. The energy consumption of the three A/C systems in the office building was the focus of the study and the study results helped designers' evaluation and decision-making on selecting different A/C systems in the early stages of building design. Simulation results showed that as compared to the use of the VAV system and FPFA system, energy savings at 22.2% and 11.7%, respectively, were expected when using the VRV system.

2.3.2 Effects of refrigerant pipework on the operational performances of an MEAC system

Although most published studies related to MEAC systems focused on operational system performances, there have been a limited number of studies where the complicated refrigerant pipework in a VAV system was the study focus.

Hirao et al. [1992] described a technology for predicting the operational performance of an air-to-air heat pump system with long refrigerant pipelines and large differences in installation level. Shah et al. [2004a] evaluated the pressure drops along the suction pipeline from each evaporator exit to the compressor suction in an MEAC system by using the well-known Darcy-Weisbach Equation. However, the primary objective was to evaluate the refrigerant mass flow rate at each evaporator outlet, instead of evaluating the total pressure drop for the MEAC system. Shao et al. [2008] and Shi et al. [2008] established a generic model for complex refrigeration systems based on a two-phase fluid network. This model consisted of sub-models for

refrigerant pipelines and system components, and could be used to evaluate the system performance and to optimize system design at all operating conditions. However, the focus was on building a generic simulation model which can be used to study different complex refrigeration systems, but not on the influence of the refrigerant pipework on system performance.

2.4 Modeling of MEAC systems

More and more research attention has been paid to studying A/C systems using modeling approach because of its cost effectiveness compared to using experimental approach. Mathematical modeling has been hence extensively used to investigate the operational performance of an A/C system, to demonstrate the controllability of a control strategy, to verify the optimization design of a configuration and to detect and diagnose system faults, etc. [Qi 2009].

A large number of published studies in open literature are available on modeling both steady-state and dynamic behaviors of A/C systems. The models available can be classified into two types: physical and empirical. A physical model, which can reflect the physical insight of a real system, is built based on physical principles and expressed using mathematic equations. However, an empirical model can be established using different methods such as regression analysis, polynomial curve fit, artificial neural networks (ANN) and system identification, with possibly high adaptability. There exist however some unsolvable problems in an empirical modeling method because of the imperfection of the method itself and the limitation of a model developer's understandings [Diaz et al. 1999, Pacheco-Vega et al. 2001,

Singh et al. 2006, Ding 2007].

Graph Theory, which has been used in many subject areas, such as electric circuit network and fluid network, is a modeling approach different from either the physical or empirical modeling approach. It converts a specific problem into a graph of nodes and verges. A refrigeration cycle can be usually depictured on a *p*-*h* diagram. When applying Graph Theory modeling approach to A/C or refrigerant systems, the refrigerant flow direction must be added in order to truly reflect the refrigeration cycle, and a complete refrigeration cycle will become a directed graph composed of multiple nodes [Liu et al. 2004, Ding 2007]. Comparing with other modeling approach, Graph Theory modeling is flexible in describing complicated refrigerant circuit arrangement [Liu et al. 2004].

To develop a high quality model for an engineering system, the requirements for modeling at least include: (1) accuracy, (2) rapidness and (3) stability. These three requirements may conflict with one another, and then a compromise has to be made [Ding 2007]. Generally, to achieve a high modeling accuracy for key system components, such as a heat exchanger, distributed-parameter modeling approach may be used, which can reflect well the distributive characteristic of the operational parameters in such a component [Chen 2005, Qi 2009]. However, because of distributed nature, using such a modeling approach is time-consuming with potential poor calculation stability. On the other hand, for the purpose of testing control strategies and studying dynamic response of a complete engineering system, a full understanding of the details of certain system components may not be necessary. Therefore, lumped-parameter modeling approach may be used. Although it is relative

simple and difficult to reflect the detailed distribution of parameters along the dimension of a system component, it is more useful in studying the overall performance of a system, and consequently usually more effective in carrying out research work related to system control [Ding 2007]. A partial-lumped parameter modeling approach is a compromise between the distributed- and lumped-parameter modeling approaches [Deng 2000, Domanski 1991]. With this approach, a system component, e.g., evaporator or condenser, is divided into several zones but lumped-parameter modeling is adopted in each zone. For a condenser, usually three zones, i.e., a superheated zone, a two-phase zone and a sub-cooling zone, are assumed. For an evaporator, two zones, i.e., a two-phase zone and a superheated zone, are usually designated. Both the accuracy and the computational speed for a partial-lumped parameter modeling approach are between those of the distributed- and lumped-parameter modeling approaches. There is little difference between the prediction accuracy using a partial-lumped parameter modeling approach and a distributed-parameter modeling approach, but the computational speed when using a partial-lumped parameter modeling approach is obviously faster than that when using a distributed-parameter modeling approach, so a partial-lumped parameter modeling approach is suitable for system modeling when the accuracy requirement is not too high [Qi 2009].

Both an SEAC system and an MEAC system are operated based on vapor compression refrigerant cycle, and consist of four basic components, i.e., a compressor, one or more evaporators, the same number of expansion valves as that of evaporators and a condenser. Essentially, the same component models might be

used for either an SEAC system or an MEAC system. After many years of developments, different component models for A/C systems are extensively available for different applications. It is commonly acknowledged that a complete MEAC system is more complicated than that of an SEAC system due to the fact that two or more evaporators are connected in parallel so that system operational parameters are highly coupled. Furthermore, modeling the refrigeration pipelines in an MEAC system is also increasingly important as a complicated refrigerant pipework in an MEAC system could also significantly affect its operational performance, as mentioned in Section 2.3.2.

2.4.1 Heat exchanger modeling

Heat exchanger modeling has always been in the spotlight of simulation-based research work for HVAC and Refrigeration systems. Many investigations on heat exchangers modeling have been carried out using lumped-parameter modeling approach [Chi and Didion 1982, Nyers and Stoyan 1994, Vargas and Parise 1995], and distributed-parameter modeling approach [MacArthur 1984, Bensafi et al. 1997]. Partial-lumped parameter modeling approaches were used by Deng [2000] and Domanski [1991], where a condenser was divided into three zones, i.e., two-phase, superheated and sub-cooling zone and an evaporator two zones, i.e., two-phase, and superheated zone. Zhang and Zhang [2006] developed a distributed-parameter model for a direct-expansion (DX) evaporator in a vapor compression refrigeration system, using moving boundary approach to describe the transient behavior of the DX evaporator. This model allowed the superheated region in the evaporator to be included or excluded. A time-variant, rather than a constant, mean void fraction was

employed to improve the robustness of a traditional moving boundary model under larger disturbances.

Since the correlations of air-side heat transfer coefficients would significantly affect the modeling accuracy for a heat exchanger, a set of relatively simple correlations for an average heat transfer coefficient for different heat exchangers, such as plate-finned tube, flat fins or wavy and louvered fins, have been developed [Gray and Webb 1986, Turaga et al 1988, Webb 1990, Corberan and Melon 1998]. Currently, the most commonly enhanced heat transfer surface used in DX A/C systems is of louvered fin type that can provide a higher average heat transfer coefficient. Wang et al. [1999 and 2000] proposed general heat transfer correlations for louvered fin geometry having round tube configuration under dry and wet conditions, respectively. A total of 49 samples of louvered fin-and-tube heat exchangers with different geometric parameters, including louver pitch, louver height, longitudinal tube pitch, transverse tube pitch, tube diameter, and fin pitch were included in the correlations developed.

ANN has also been useful in modeling a heat exchanger. Diaz et al. [1999] developed an ANN-based model for a heat exchanger. Pacheco-Vega et al. [2001] studied the heat transfer phenomena in a fin-tube refrigerating heat exchanger with limited amount of experimental data using ANN modeling approach. Islamoglu [2003] carried out the heat transfer analysis on a wire-on-tube type heat exchanger using limited experimental data and ANN modeling approach.

Graph Theory modeling approach can also be used to describe detailed structures of

an evaporator. A practical way was to number each tube and refrigerant flow direction within a single tube first, so that a directed graph was created, then an adjacent matrix was built [Liu et al. 2004]. With the help of the concepts of directed graph and graph-based search algorithms in Graph Theory, Liu et al. [2004] developed a general steady-state distributed-parameter model for a fin-and-tube heat exchanger. This model made it possible to analyze the operational performance of an evaporator with complex refrigerant circuits.

2.4.2 Compressor modeling

A compressor turns the low pressure vapor refrigerant into high pressure vapor refrigerant such that it can be condensed in a condenser to reject heat to a second fluid (e.g., air, water) to complete a refrigeration cycle. Compared to an evaporator or a condenser, the dynamics of a compressor may be negligible, so that quasi-steady modeling is usually adopted. This is achieved by assuming that a compressor reaches its specified operating speed instantly. Generally, a polytropic compression process is assumed and a mathematical model for a compressor can be established by using the traditional thermodynamic approach [Domanski and Mclinden 1992, Browne and Banasal 1998].

On the other hand, a compressor may also be represented by an empirical correlation using the actual performance data with the aid of curve fitting or regression analysis. This approach can achieve a better approximation but required a set of detailed tested compressor performance data from manufacturers or in-situ test.

2.4.3 Expansion valve modeling

An expansion device in a refrigeration system controls the refrigerant mass flow and balances the system pressure. Commonly, an expansion valve can be represented by a steady-state model due to its very small thermal inertia. Refrigerant expansion is generally treated as an isenthalpic process when modeling an expansion valve. MacArthur [1984] represented an expansion valve by an orifice equation. Park et al. [2007] developed an empirical correlation for predicting the mass flow rate passing through an EEV by modifying a single-phase orifice equation with consideration of EEV's geometries and operating conditions. Geometric parameters that were included in the empirical correlation were orifice diameter, orifice length and the EEV opening. One representative model for expansion valves was developed by Damasceno et al. [1990], based on the specifications given by manufacturers and the empirical fittings for one set of distributor nozzle and tube size.

2.4.4 Developing and solving MEAC system models

Component-based approach is usually adopted when modeling a complete MEAC system, and there are two main methods for solving a component-based MEAC system model: (1) simultaneous solving method and (2) sequential solving method [Winkler et al. 2008].

For the first method, all the model equations, often of non-linear nature, and initial and boundary conditions are solved simultaneously using the Euler Method or Newton-Raphson Method or Runge-Kutta Method, etc. Commercial software

packages have been developed to help solve these non-linear equations [Klein and Alvarado 2002, Masy 2006, Masy 2008]. Very often it can be difficult to find out the cause if divergence occurs during solving model equations, and thus calculation stability is not easily ensured. On the other hand, when applying this method to a developed system model whose structure is normally fixed, additional component sub-model cannot be easily inserted into the system model, and thus the flexibility of system simulation might be compromised [Ding 2007 ,Winkler et al. 2008]. Therefore, as far as MEAC system simulation is concerned, this solving method is not popular. Gordon et al. [1999] and You et al. [2010] respectively solved their dynamic MEAC system models using the simultaneous solving method. A set of coupled one dimensional partial-differential equations (PDEs) were formulated for major system components by applying mass, momentum and energy conservation, and all the equations were solved simultaneously.

The second method, i.e., sequential solving method, can be more conveniently used since the component models were established first and treated as “black-box” objects. Only the knowledge of how the component sub-models were connected was required when using this method to solve a complete model. A set of initial values for model inputs were assumed. If the convergence criterion was not satisfied, the assumed initial values would be updated and then the iteration had to be repeated. Winkler et al. [2008] studied the influence of setting initial values for the inputs to an A/C system model on computational speed. Component sub-models were run several times prior to solving the system model and it was shown that better initial values can help reduce the required computational time. The sequential solving method had

clear physical meaning in solving a system model and was easy to debug to ensure the calculation stability [Ding 2007].

A number of MEAC system models were solved using sequential solving method [Zhang and Zhang 2011]. For example, Park et al. [2001] and Chen et al. [2005] solved a steady-state MEAC system model and a dynamic MEAC system model using the sequential solving method, respectively. Component sub-models were first developed. The mass flow rates passing through a compressor and through EEVs were used as convergence criterions when solving MEAC system models using the sequential solving method.

Shao et al. [2008] and Shi et al. [2008] developed a model to predict the performance of complex refrigeration systems using a two-phase fluid network. The two-phase network consisted of nodes and branches. A node was the joint of two or more branches. Different types of branches can be used depending on the components contained in these branches. A compressor was always in Branch 0. For a branch containing condenser or evaporator, the branch was a factual one; otherwise, it was a fictitious one. Factual and fictitious branches were represented by different index so that only factual branches would be solved. A node–branch incidence matrix was usually employed to describe the connection between nodes and branches in the fluid network. The calculations of heat transfer, pressure loss and refrigerant charge were accomplished using distributed-parameter sub-models for components, and the complete system model concerned the balance of conservation equations between nodes and branches. Basically, the solution algorithm consisted of only one iteration loop.

System identification method was used by Lin and Yeh [2007a, b] to obtain a linear, low-order model for a three-evaporator A/C (TEAC) system. The compressor speed and the three EEVs openings were intuitively selected as the inputs and the wall temperature of the two-phase region in each evaporator and the associated degree of superheat as the outputs. This was because the former determined the heat absorbing capacity, and the latter dictated the operational efficiency and ensured the safe operation of the compressor. Based on this linear low-order model identified from experiments, a control strategy was developed.

2.4.5 Pipework modeling

When a large-scale pipework was present in an A/C system, the refrigerant pressure drop along pipelines would be significant and thus would impact on system performance. This was particularly true for an MEAC system whereof pipework was much more complicated than that in an SEAC system. The pressure drop would affect evaporating or condensing pressure in an A/C system. Furthermore, compressor suction pressure and degree of refrigerant superheat would also be affected, and hence the refrigerant state at compressor suction, which was very important in evaluating refrigerant mass flow rate passing through a compressor, might not be correct [Qi 2009].

In those lumped-parameter models for heat exchangers, the refrigerant pressure drop across a heat exchanger was often neglected or assumed at a fixed value. According to the correlations provided by Pierre [1964], the refrigerant pressure drop across a heat exchanger was proportional to the square of refrigerant mass flow rate.

Although there were many reported studies on the pressure drop for various refrigerants including R134a inside a heat exchanger [Cavallini et al. 2001], a general average pressure drop correlation was in fact hard to be established because an average pressure drop would be closely related to the configuration of internal tube surface of a heat exchanger and its geometry such as circuitry arrangements, etc.

Unfortunately, not much research work on modeling the refrigerant pipework in MEAC systems to study the effects of the pressure drop along refrigerant pipeline on system performance may be identified.

2.5 Capacity control strategies developed for MEAC systems

The control objective for an MEAC system is basically to maintain the desired indoor air temperature in each conditioned space at its set-point at the lowest possible energy consumption under various operating conditions. In order to fulfill the objective, the mass flow rate of refrigerant entering each evaporator must vary in accordance with the cooling load it deals with. On the other hand, the output cooling capacity should match the total cooling load from all conditioned spaces by regulating the compressor speed. This could not only reduce the fluctuation of air temperatures inside the conditioned spaces but also improve the energy efficiency, particularly during part load operation of an MEAC system.

The early studies published on the control of MEAC systems were carried out by Masuda et al. [1991] and Okuzawa [1992]. Constant-speed compressors were On-Off controlled, which was not difficult to implement. However, its disadvantages

were that it was difficult to maintain indoor air temperatures within a suitable range, and refrigerant mass flow rate cannot be distributed precisely.

The application of variable-speed compressor to MEAC systems enabled a great step forward in their capacity control. It was reported that a variable-speed compressor can vary its output cooling capacity between 20% and 100% of the full capacity. Therefore, the use of a variable-speed compressor can offer a greater energy saving, particularly in part load condition. Yang and Lee [1991] presented an analysis for an inverter-driven variable-speed A/C system used in a hot and humid region. The results indicated that the use of variable-speed compressors could provide an annual energy saving of 20%. Cohen et al. [1974] studied the energy saving potential for a variable-speed A/C system on a seasonal basis and it was found out that the system would be operated more efficiently at part load condition by using a variable-speed compressor, due to the reduced frictional losses and the reduced pressure ratio imposed on the compressor. In the past, variable-speed compressors were generally regarded as being suitable only for use in small-scale A/C systems, but not in medium- or large-scale A/C systems due to the lack of sufficient development and component integration. Fortunately, in recent years medium- to large-scale variable-speed compressors have been greatly improved in various aspects and widely used in large-scale A/C systems [Park et al. 2002]. Qureshi and Tassou [1996] made theoretical and practical comparisons of various capacity control methods at full and part load conditions, and the study results showed that a variable-speed operation was the most energy efficient technique for an A/C system.

An EEV also plays an important role in capacity control of an A/C system. Inside an

EEV, there is a stepping motor that can accurately drive the valve needle up and down according to the number and phase order of electronic pulses to adjust the opening of throttling area. A precise refrigerant mass flow rate distribution can therefore be made. In a variable-speed compressor SEAC system, its EEV usually controls the refrigerant mass flow rate entering its evaporator based on the degree of superheat at the exit of the evaporator, and the compressor speed is modulated according to room temperature [Cerri and Battisti 1994, Scalabrin and Bianco 1994, Qureshi and Tassou 1996]. However, it is much difficult to apply this control strategy to an MEAC system directly, since the operational parameters in an MEAC system were strongly coupled and the change in the operating condition in one indoor unit would significantly affect that in other indoor units.

Usually, an A/C system is nonlinear. He et al. [1997, 1998] demonstrated that there were strong cross-coupling effects among various operational parameters in a vapor compression refrigeration cycle, such as evaporating temperature, condensing temperature and degree of superheat, etc. Therefore, a proper coordination between the openings of EEVs and compressor speed would improve the control behavior of degree of superheat, and the ability to withstand external disturbances while effectively modulating the system cooling capacity. Despite the fact that variable-speed compressors are standard provision and EEVs are usually used as throttling devices in MEAC systems, appropriate control strategies are necessary to ensure the accurate indoor thermal environment control and efficient system operation. Over the years various attempts have been tried to develop different control strategies for MEAC systems. Shah [2004a] reported a study on dynamic modeling and control of

MEAC systems. Although a brief discussion on closed loop control strategies was presented, no actual controllability tests of these strategies were carried out and reported.

With the rapid developments of powerful and flexible direct digital technologies, advanced control strategies, such as fuzzy logic control, system identification, etc., have also been increasingly applied to MEAC systems.

Fuzzy logic control has been viewed as an alternative to the standard PID control in various applications due to its robustness, fast time response and easy implementation. The core part of fuzzy logic control is the control rules that are derived from the experiences of experts and the previous knowledge about a controlled object. Chen et al. [2005] carried out a simulation study, where a self-tuning fuzzy control strategy was applied to an MEAC system with three evaporators and a variable-speed compressor. The suction pressure was taken as a controlled variable to regulate compressor speed while indoor air temperature to regulate the opening of individual EEVs. This control strategy consisted of three main parts: fuzzifying, fuzzy reasoning and defuzzifying. To improve the performance using the fuzzy control system, a self-tuning modifying factor, α, was incorporated. It was shown that the adoption of the self-tuning modify factor achieved the following control results: when the deviation of a controlled variable from its setting, such as suction pressure or room air temperature, was relatively large, more weighting was given to the control action of the current fuzzifying value, to increase the response speed; otherwise, more weighting was given to the control of difference of the current fuzzifying value, to decrease the overshoot. Simulation results showed that

the proposed control strategy could achieve the desired control accuracy for the controlled parameters, i.e., the room air temperatures, without considerable oscillation. However, no experimental validation of the control algorithms was conducted.

Lin and Yeh [2007a, b] designed a feedback controller for a TEAC system through system identification which produced a low-order linear model. The three evaporating temperatures were controlled by the openings of the matching EEVs in order to maintain the indoor temperatures at their set-points without steady-state errors. Compressor speed was used to control the degree of superheat at the exit of three evaporators. The experimental results indicated that the controller developed based on the model could successfully regulate the indoor temperatures and maintain the steady-state degree of superheat. Furthermore, based on the low-order linear model obtained from system identification, a control strategy with flow distribution capability proposed for MEAC systems to accommodate different thermal demands in different rooms was reported by Lin and Yeh [2009a, b]. By performing steady-state analysis on the controlled system and utilizing the identified system parameters, the mechanism of flow distribution can be analytically explained. Experimental results indicated that the proposed strategy could successfully regulate the indoor temperatures, despite that the reference settings in respective rooms were different and the settings were altered in the middle of the control process. Furthermore, a framework for mode switching control for a DEAC system was proposed. The framework was basically an integration of a controller and a dynamic compensator. The controller, which possessed the flow-distribution capability, was intended to

provide a nominal performance. While mode switching was achieved by varying the reference settings in the controller, the dynamic compensator was used to improve the transient responses immediately after the switching. Experimental results indicated that the proposed framework could achieve satisfactory indoor temperature regulation and provide bumpless switching between different modes of operation. However, in these studies, the mathematical model obtained through system identification and the controllers developed based on the model may not be applicable to other MEAC units having different configurations and/or being operated under other operating conditions, thus not generic.

2.6 A brief introduction to the Constructal Theory

The Constructal Theory was developed by Adrian Bejan in the late 90's. *Constructal* is a word created by Bejan, coming from the Latin verb *construere*, which is to construct, in order to designate the natural tendency of all flow systems to construct flow configurations, such as rivers, trees and branches, lungs and also the engineered forms coming from the constructal design-generation [website_5 2010].

The Constructal Theory teaches how to construct the flow architecture and provides a new way of thinking with epistemological and philosophical implications [Rosa et al. 2004, Bejan 2005]. The Constructal Theory focuses on the construction of optimal flow architecture. The flow architecture (shape or structure) is deduced, not assumed in advance [Reis 2006].

2.6.1 The Constructal Theory

The Constructal Theory holds that every flow system exists with purpose (or objective, function). The constructal designs allow the system to flow more easily, to measurably move more current farther and faster for less unit of useful energy consumed [Bejan and Lorente 2010, Bejan 2006]. This theory, also known as the Constructal Law, was stated by Bejan [2006] in 1996, as follows: “For a finite-size system to persist in time (to live), it must evolve in such a way that it provides easier access to the imposed currents that flow through it.” The Constructal Law represents three steps toward making “design in nature” a concept and law-based domain in science [Bejan and Lorente 2010]:

- Life is flow: all flow systems are live systems, the animate and the inanimate.

- Design generation and evolution is a phenomenon of physics.

- Designs have the universal tendency to evolve in a certain direction in time.

The Constructal Law is a first principle of physics that accounts for all designs and evolutions in nature. It holds that shape and structure arise to facilitate flow. The designs that arise spontaneously in nature reflect this tendency: they allow entities to flow more easily to measurably move more current farther and faster for less unit of useful energy consumed.

2.6.2 The application of the Constructal Theory

The Constructal Law is a summary of all design generation and evolution phenomena in nature. Flow architectures are ubiquitous in both natural and engineered systems. They evolve toward better performance, and persist in time (they survive) while the older disappear [Bejan 1996, Bejan and Almogbel 2000, Bejan and Lorente 2004]. Thus, the Constructal Theory could be used to explain the structures of natural flow and optimize flow architectures as well. For example, a heat engine is supposed to extract maximum useful work from heat currents that flow between systems at different temperatures. Performance is a measure of the degree to which each system realizes its purpose. The design of engineered systems evolves in time toward configurations that offer better performance, i.e., better achievement of their purpose. The system purpose is global and it should be under existing global constraints, including the space allocated to the system, available material and components, allowable temperature, pressure or stress ranges, etc.

The Constructal Theory has been applied to various natural and engineered systems. The distinctive feature of the Constructal Theory is that flow structure is not assumed in advance for an optimization process, but is its consequence. Optimization of tree networks for volume-to-point and point-to-volume movement is a special flied where the Constructal Theory is applied to engineering [Wechsatol et al. 2001, Lorente et al. 2002, 2003]. The purpose of the optimization depends on the characteristics of a problem, for example, minimization of pumping power, maximization of heat exchange under the constrains of total volume or total surface area, available materials (pipes), the physical limitation, etc. Optimization of flow

geometry proceeds hierarchically from elemental cells (the smallest scale) to larger constructs (higher order scale).

For example, the Constructal Theory could be used to guide designing hot water distribution to a growing number of users spreading over an area. The optimization of such a flow tree might be pursued under several objectives: (1) maximization of the temperature of the hot water received by the most disadvantaged user; (2) minimization of the heat loss over the entire piping network or (3) maximization of the hot water temperature averaged over all the users [Wechsatol et al. 2001]. The constraints may range from the size and shape of the area to be served by piping systems to the amount of insulation and the total volume occupied by the pipes. Strategies that have been proposed include the constructal sequence and the "one-by-one growth", where, at each step in time, one new user is added to an existing network. Lorente et al. [2002, 2003] found out that several strategies could lead to similar tree flows, and thus comparable levels of global performance. One strategy was based on the observation that the lowest flow resistance was achieved for a pipe when it had the shortest path possible on the area allocated to it. This method was important because it allowed the optimization to be performed locally.

The augmentation of a heat transfer system is also an important application of the Constructal Theory [Alebrahim and Bejan 1999, Almogbel and Bejan 1999, Bejan and Almogbel 2000, Biserni et al. 2004]. Matos et al. [2004a, b] carried out a three-dimensional numerical and experimental geometric optimization study on the maximization of the total heat transfer rate between a bundle of finned tubes in a given volume and external flow. Kraus [2003] used the Constructal Theory for

finding out the optimum longitudinal fin of rectangular profile with tip heat loss. Bonjour et al. [2004] optimized the design of dendritic fins for a coaxial two-stream heat exchanger. These studies showed that depending on system size, the best configuration can be either a radial pattern or a tree of fins.

The Constructal Theory could be used to explain and model the flow structure in the nature. Rosa et al. [2004] in a recent review article gave a broad list of allometric scaling laws involving the geometric parameters of river channels and river basins. The Constructal Theory views the naturally occurring flow structures (their geometric form) as the end result of a process of area to point flow access optimization with the objective of providing minimal resistance to flow [Errera and Bejan 1998]. In addition, the Constructal Theory has been applied to a model of the long-term behavior (climate) of the atmospheric and oceanic circulation that is the largest flow system on Earth [Bejan and Reis 2005, Reis and Bejan 2006].

An MEAC system usually has a complicated refrigerant pipework and different pipework layouts, as reviewed in Section 2.3.2, which impacts on system's operational performance. Therefore, an MEAC system is an ideal candidate to apply the Constructal Theory, with respect to its pipework layout design. However, no previous studies on applying the Constructal Theory to discovering the best possible pipework layout design of an MEAC system might be identified.

2.7 Conclusions

With the pursuing of high quality living and comfortable working environment, more

and more attentions have been paid to improving indoor thermal environmental control using A/C systems. MEAC systems have been widely used in small- to medium-scale buildings in recent years due to their advantageous characteristics over conventional A/C systems, such as high energy efficiency, flexibility in design and installation and compactness in configuration. In addition, comparing with SEAC systems, each indoor unit in an MEAC system could operate in heating and/or cooling mode independently, implying more flexible operating modes for users, and offering potential energy savings when heating and cooling are required simultaneously in different zones of an air conditioned building.

An extensive literature review on various issues related MEAC technology has been carried out and is reported in this Chapter. Most existing research and development efforts focused on introducing basic unit configurations, reporting measured operational performances of MEAC systems, and developing various capacity control strategies, etc. Three main issues, where further research efforts are urgently required, are identified as follows:

- Although a number of capacity control algorithms were developed based on the system simulation, no experimental-based capacity controller developments and their controllability tests for MEAC systems may be identified, except where the capacity controller developed for an MEAC system was based on a model obtained through system identification, which cannot be generically applied to other MEAC systems, as pointed out in Section 2.5. Hence, while acknowledging that different capacity control algorithms may co-exist, openly developing an effective and robust capacity control strategy for MEAC systems

to ensure adequate control accuracy for controlled indoor air parameters such as temperature and with adequate experimental controllability tests is urgently desired.

- In an actual MEAC system, its pipelines are much more complicated than those in an SEAC system, with a much longer total pipeline length, a larger installation height difference, and more pipe fittings such as elbows and valves, as mentioned in Section 2.2.3. A long pipeline with a large height difference and many fittings would cause a great refrigerant pressure drop [Wijaya and Spatz 1995], which could in turn further lower evaporating temperature, increase condensing temperature, reduce system's operational efficiency [Lee and Yoo 2000] and result in refrigerant mal-distribution among evaporators as compared to what would happen in an SEAC system. Neglecting the influence of the length of pipelines with fittings on the operational performance may be reasonable for an SEAC system, but can be problematic for an MEAC system. Furthermore, for new MEAC system designing, guidelines are needed so as to optimize refrigerant pipework layout for the best possible system operational efficiency. Nonetheless, as reported in Section 2.3.2, no previous studies on the influence of complicated refrigerant pipework in an MEAC system on its operational performance may be identified. Although the relationships among the coupled operational parameters in an MEAC system have been extensively studied and the method of evaluating the pressure drop along refrigerant pipelines is available, the influence of the large pressure drop along a refrigerant distribution pipework on the operational performance in an MEAC system has

not yet been studied.

- The Constructal Theory is a powerful tool in constructing flow architectures. It has been widely applied to other engineering systems, as mentioned in Section 2.6. However, no previous studies on applying the Constructal Theory to MEAC system's design may be identified. Given that an MEAC system has a complicated pipework of several hundred meters long with height differences; it will be an ideal candidate for the application of the Constructal Theory, to discover the best possible pipework layout design, for the highest possible operational efficiency, at the fixed initial installation costs.

The extensive literature review presented in this Chapter has identified a number of important subject topics, as summarized above, where further in-depth research studies on developing capacity control strategies of MEAC systems, evaluating the influence of the refrigerant pressure drop along pipelines on MEAC systems' operational performances by using the Constructal Theory to discover the best possible pipework design configuration for an MEAC system for minimizing the system energy consumption, are urgently required. There are the expected targets of investigation to be reported in this Thesis.

Chapter 3

Proposition

3.1 Background

From the literature review presented in Chapter 2, it is evident that MEAC systems are widely used in small- to medium-scale buildings due to their advantages of high energy efficiency, flexibility in design and installation and compactness in configuration. Compared with an SEAC system, the operational parameters in an MEAC system are usually highly coupled. The refrigerant pipework in an MEAC system is much more complicated because there is more than one evaporator connected in parallel without pressure regulators. Therefore, the outcomes of many existing studies related to an SEAC system may not be directly applicable to the corresponding issues in an MEAC system. Consequently, when carrying out research work related to MEAC systems, the following issues including developing an appropriate capacity control strategy, studying the influence of the complicated refrigerant pipework on system performance and discovering the best possible pipework layout design for the highest possible operational efficiency need to be addressed.

An appropriate capacity control strategy for an MEAC system can maintain the desired indoor thermal environment in each conditioned space served by the MEAC system. However, there have been only limited studies on developing capacity control strategies for MEAC systems, with most of them being simulation based.

Consequently, there is a strong need to develop an effective and robust experimentally validated capacity control algorithm for MEAC systems.

In addition, with a large-scale pipework, the refrigerant pressure drop along pipelines in an MEAC system would be significant and would thus affect system performance. The literature review presented in Chapter 2 reveals that no previous studies on the influence of complicated refrigerant pipework in an MEAC system on its operational performance have been carried out. Therefore, the influence of the large pressure drop along a refrigerant pipework on the operational performance in an MEAC system needs to be studied.

Furthermore, in an MEAC system, its refrigerant pipework layout design can significantly impact the system performance. It is therefore necessary to discover the best possible refrigerant pipework design for the highest possible system operational efficiency. On the other hand, the Constructal Theory teaches how to construct the flow architecture, and constructal designs allow the system to flow more easy and to measurably move more current father and faster for less unit of useful energy consumed. Given that an MEAC system has a complicated pipework of several hundred meters long, it is an ideal candidate for the application of the Constructal Theory. However, no previous studies on applying the Constructal Theory to the design of MEAC systems may be identified. Therefore, the application of the Constructal Theory to discovering the best possible pipework layout design of an MEAC system for the highest possible operational efficiency is necessary.

3.2 Project title

This thesis focuses on three major pieces of work related to the control and design for MEAC systems: (1) experimentally developing and validating an effective and robust capacity control strategy for an MEAC system; (2) studying the influence of the pressure drop along a refrigerant distribution pipework on the operational performance in an MEAC system; (3) applying the Constructal Theory to discovering the best possible refrigerant pipework layout design of an MEAC system for the highest possible operational efficiency. The proposed research project is therefore entitled "Control and design for a multi-evaporator air conditioning (MEAC) system".

3.3 Aims and objectives

The objectives of the research work reported in this thesis are as follows:

- To experimentally develop and validate an effective and robust capacity control strategy for a DEAC system, a typical MEAC system;

- To investigate the influence of the pressure drop along a refrigerant distribution pipework on the operational performance of a DEAC system, through a modeling study;

- To apply the Constructal Theory to discovering the best possible pipework layout design of an MEAC system for the highest possible system operational efficiency.

3.4 Research methodologies

Experimental, numerical and analytical methods will be employed throughout the project. Firstly, when developing an effective and robust capacity controller for the DEAC system, a control algorithm, which imitated the On-Off control for an SEAC system in each indoor unit of the DEAC system by using variable-speed compressor and EEVs, will be proposed. Controllability tests under various settings for experimentally validating the novel capacity control algorithm will be carried out. Furthermore, the control algorithm might be further improved based on the experimental results and controllability tests for the improved control algorithm will be carried out as well. All the experimental work will be carried out in a DEAC experimental rig specifically developed for this project in the HVAC Laboratory in the Department of Building Services Engineering, The Hong Kong Polytechnic University.

Secondly, when studying the influence of refrigerant pipework on system operational performance, a physical-based steady-state mathematical model with a sub-module specifically established for investigating the influence of refrigerant pipe length on system operational performance for a DEAC system, will be developed. This model will be validated using the results from previously reported experimental studies by other researchers. The simulation results will be analyzed and the effects of refrigerant pipe length on the operational performance of the DEAC system modeling investigated.

Thirdly, the Constructal Theory will be applied to discovering the best possible pipework layout design of an MEAC system, for the highest possible operational efficiency at the fixed initial installation costs. Two approaches may be used. The first approach is based on the first law of thermodynamics and consisted of changing the configuration of an MEAC system in such a way that the work required per unit of heat removed from an indoor space is reduced. The second approach is however based on the second law of thermodynamics, aiming at reducing the irreversibility of the system. The study will be started from single-room cases (SEAC systems), and is to be extended to dual-room cases (DEAC systems) and to multi-room cases (MEAC systems). Two ways to arrange the refrigerant pipework will be considered. One is to position the refrigerant pipework inside room(s) and the other outside the room(s).

Chapter 4

Development of a novel capacity control algorithm for an MEAC system

4.1 Introduction

As reported in Chapter 2, the use of MEAC systems is advantageous in terms of installation convenience, high design flexibility, being easy to maintain and commission, better indoor thermal comfort control and higher energy efficiency [Goetzler 2007]. Variable-speed compressors, instead of constant-speed compressors, are standard provisions for MEAC systems. EEVs are usually used as throttling devices because of their control stability and capacity control accuracy [Choi and Kin 2003]. Nonetheless, it still remains a challenge to ensure that each indoor unit gets the exact amount of refrigerant flow required for space cooling.

A limited number of reported studies on MEAC systems may be identified with most existing efforts focusing on introducing basic unit configuration, operation and function [K. Simizu 1990, Lijima1992]. Others were related to fundamental system modeling or experimental work [Park et al. 2001, Xia et al. 2002, Choi and Kim 2003, Shi et al. 2003, Xia et al. 2003, Hu and Yang 2005, Hai et al. 2006]. From the studies by Part et al [2001] and Choi and Kim [2003], it was clearly demonstrated that the changes in operational parameters of one indoor unit in a DEAC system would definitely affect those of the other.

Shah et al. [2004] developed a generic model for commercial application and presented a brief discussion on closed loop control strategies. However, no actual controllability tests of these strategies were carried out and reported. Lin and Yeh [2007] reported a study on designing a feedback controller for a three-evaporator air-conditioning (TEAC) system through experimental identification which produced a low-order linear model suitable for controller design. The feedback controller designed was multi-input-multi-output (MIMO) based and possessed a cascade structure for dealing with fast and slow system dynamics. However, the mathematical model obtained through system identification and the controller developed based on the model may not be applicable to other MEAC systems with different configurations and/or being operated under other operating conditions, thus not generic.

Chen et al. [2005] carried out a simulation study on developing a dynamic model and control algorithms for a TEAC unit equipped with a variable-speed compressor and EEVs. A novel control algorithm was proposed and its controllability numerically tested with the TEAC model developed. A self-tuning fuzzy algorithm with a modifying factor was incorporated into the controller. The results of controllability tests showed that the proposed control algorithms could achieve the desired control accuracy for the controlled variables. However, no experimental validation of both the mathematical model and control algorithms was conducted.

Although several control algorithms were developed based on the system simulation [Shah et al. 2004, Chen et al. 2005, Lin and Yeh 2007], no experimental-based capacity controller developments and their controllability tests for MEAC systems

may be identified in open literature, except the controller developed through system identification. Hence, while acknowledging that different capacity control algorithms may co-exist, developing an effective and robust capacity control strategy openly for MEAC systems to ensure adequate control accuracy for controlled indoor air parameters such as temperature and with adequate experimental controllability tests is urgently desired.

In the study reported in this Chapter, an NCCA, which imitated the On-Off control of an SEAC system for each indoor unit, was developed for an MEAC system jointly using a variable-speed compressor and EEVs. Controllability tests under various test conditions for experimentally validating the NCCA were carried out using a DEAC experimental rig and satisfactory test results obtained. Based on the test results, the NCCA was further modified and improved test results with better control accuracy obtained.

4.2 The development of the NCCA for an MEAC system

For an MEAC system, as illustrated in Fig. 4.1, the EEV placed in each conditioned room may be given two functions, one to control the degree of superheat when its matching indoor unit was turned on and the other to act as a stop valve to turn off the supply of refrigerant to the unit when the indoor air temperature setting was reached. Therefore, two signals should be fed back to each EEV, the degree of superheat at the evaporator outlet and the room air dry-bulb temperature. Furthermore, the supply air fan in an indoor unit may be locally controlled at different speeds. A dead-band of ±0.5 ºC in indoor air temperature setting should be normally allowed for an On-

Off controlled SEAC system to avoid frequent switching-on and -off of a compressor. Therefore, such a ±0.5 ºC dead-band was also incorporated into NCCA for each EEV connected to its matching indoor unit of the MEAC system.

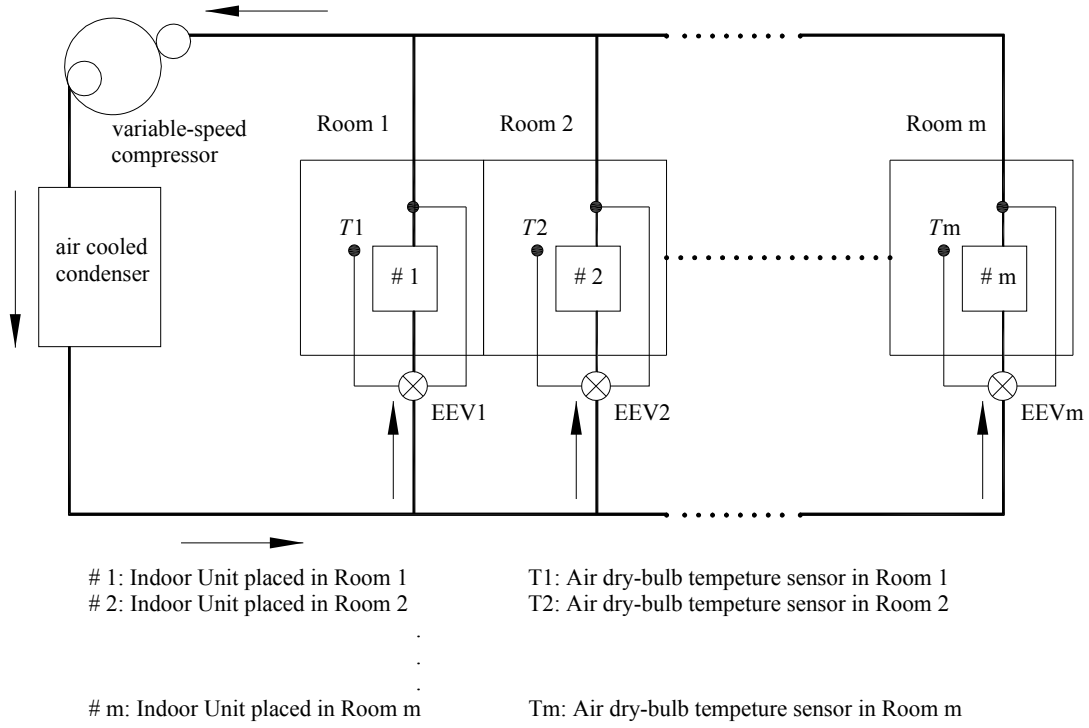

Fig. 4.1 Schematics of an MEAC system

In an MEAC system having m numbers of indoor units, for the i^{th} ($1 \le i \le m$) indoor unit serving i^{th} room with its indoor air temperature setting $T_{set,i}$, an On-Off control signal for the EEV connected to the i^{th} indoor unit, EEV_i, at a time point t, $E(t)_i$, was defined as:

$$\text{If } T(t)_i \ge T_{set,i} + \Delta T \qquad E(t)_i = 1 \tag{4.1}$$

$$\text{If } T_{set,i} - \Delta T < T(t)_i < T_{set,i} + \Delta T \qquad E(t)_i = E(t-1)_i \tag{4.2}$$

$$\text{If } T(t)_i \le T_{set,i} - \Delta T \qquad E(t)_i = 0 \tag{4.3}$$

where $T(t)_i$ is the actual room air temperature at t time point, and t-1 is the last time point. When $E(t)_i = 1$, EEV_i functioned to control the degree of refrigerant superheat, and when $E(t)_i = 0$, EEV_i was closed. However, when the indoor air temperature was within the dead-band, the operational status of EEV_i at t time point would be the same as it was at t-1 time point. Furthermore, the On-Off Status of an EEV determined the On-Off status of its matching indoor unit. This was to say when EEV_i was closed; the i^{th} indoor unit was turned off. Consequently, the total number of possible operational combinations for indoor units at any time point may be evaluated by:

$$\sum_{i=0}^{m} C_m^i = C_m^0 + C_m^1 + C_m^2 + ... + C_m^{m-1} + C_m^m \tag{4.4}$$

where m is the total number of indoor units in an MEAC system. Taking a DEAC system as an example, where m=2, the number of possible operational combinations at any time point may be evaluated by $\sum_{i=0}^{2} C_2^i = 4$, as detailed in Table 4.1. The number of opened EEVs or the number of indoor unit being operated at a specific time point, then may be communicated to a capacity controller developed based on the NCCA to determine required compressor speed, as shown in Table 4.1.

Table 4.1 Control logics for determining compressor speed at different operational combinations of indoor units for a DEAC system

Combination serial number	On-status for individual EEV	Corresponding design space cooling load	Compressor speed to be assigned by the controller
1	none	0	$S_{cm} = 0$
2	EEV_1	Q_1	$S_{cm} = f(Q_1)$
3	EEV_2	Q_2	$S_{cm} = f(Q_2)$
4	$EEV_1 + EEV_2$	$Q_1 + Q_2$	$S_{cm} = f(Q_1 + Q_2)$

On the other hand, the design space cooling load in individual rooms, Q_i (i=1~m), can be evaluated using standard cooling load calculation method [ASHRAE 2004, ASHRAE 2007], and then input to the controller. Moreover, the relationship between compressor speed in an MEAC system and its output cooling capacity, or the required space cooling load, can be made available either from compressor manufacturer or experimentally, as follows:

$$S_{cm} = f(Q) \tag{4.5}$$

where S_{cm} is compressor speed and Q the total space design cooling load, which is the summary of the design cooling loads from all rooms where indoor units are operated at that time point. For example, in Table 4.1, if only EEV_2 is opened, indoor unit 2 is then operated, and the compressor speed is to be determined by $S_{cm} = f(Q_2)$

(serial number 3 in Table 4.1). If both EEV_1 and EEV_2 are opened, or indoor unit 1 and 2 are operated, then the compressor speed is determined by $S_{cm} = f(Q_1 + Q_2)$.

Based on the NCCA detailed above, a capacity controller has been developed and tested using an experimental DEAC rig.

4.3 The experimental DEAC rig and conditions

4.3.1 The experimental rig

An experimental DEAC rig consisting of a DEAC system and three simulated spaces (two indoor rooms and one outdoor space) were specifically built up to carry out the controllability tests for the NCCA developed. Using a DEAC system to represent an MEAC system could help reduce the cost for experimentation and simplify the developmental work without however losing the essential representing characteristics of an MEAC system.

The schematics of the DEAC experimental rig are shown in Fig. 4.2. Inside each of the two simulated indoor rooms, there was a load generating unit (LGU) so that indoor sensible and latent cooling loads may be simulated. The air dry-bulb temperatures in the two indoor rooms were jointly influenced by the LGU and the indoor unit of the DEAC system. On the other hand, the temperature and humidity in the outdoor room were jointly controlled by an existing separate DX A/C system and a LGU inside the outdoor room. The detailed specifications of the major components used in the DEAC experimental rig are listed in Table 4.2. R22 was used as the working fluid in the experimental rig.

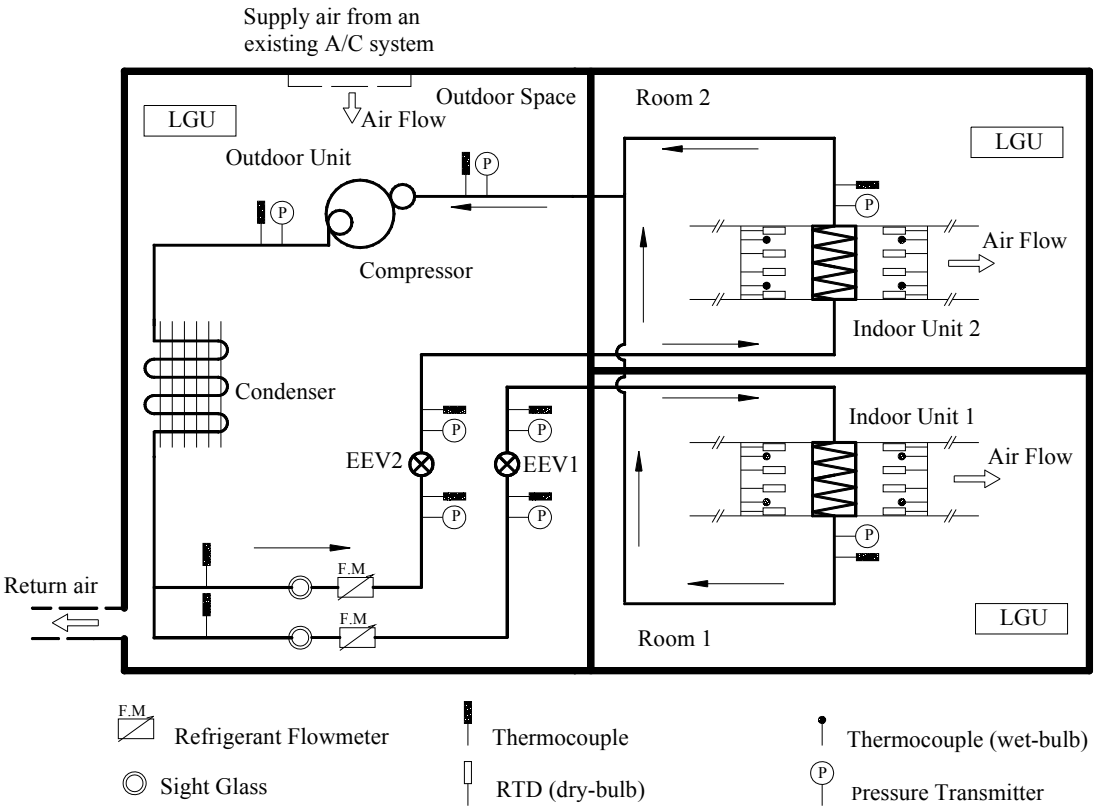

Fig. 4.2 Schematics of the experimental DEAC rig

The experimental rig was fully instrumented for measuring all of its operational parameters, which may be classified into three types, i.e., temperature, pressure and flow rate. All measurements were computerized, and all sensors and measuring devices were able to output direct current signal of 4-20 mA or 1-5 V, which were transferred to a data acquisition system for logging and recording.

Table 4.2 Specifications of the major components used in the experimental DEAC rig

Name	Specifications	
EEV	Number:	2
	Pulse Range:	0~480 Pulse
	Rated Capacity:	5.3 kW
	Port Diameter:	1.4 mm
Compressor	Number:	1
	Allowable Frequency Range:	15~110 Hz
	Rated Capacity:	8.23 kW at 75 Hz
	Displacement:	30.4 ml/rev
Condenser	Number:	1
	Fin Type	Plate Fin
	Fin Pitch:	2.1 mm
	Transverse Tube Pitch:	26 mm
	Longitude Tube Pitch:	21.66 mm
Evaporator (indoor unit)	Number:	2
	Fin Type	Plate Fin
	Fin Pitch:	2.0 mm
	Transverse Tube Pitch:	25 mm
	Longitude Tube Pitch:	21.65 mm

For each indoor unit (evaporator), eight dry-bulb temperature sensors and four wet-bulb temperature sensors were placed at both up- and down-stream of an indoor unit. The dry-bulb temperature sensors were of platinum Resistance Temperature Device (RTD) type, using three-wire Wheatstone bridge connection and with a pre-calibrated accuracy of ±0.1 °C. Thermocouples (Type K) were used for measuring air wet-bulb temperatures.

Refrigerant pressures in various locations of the refrigerant circuit in the experimental rig were measured using pressure transmitters with an accuracy of ±0.13% of full scale reading. Refrigerant temperatures were measured by thermocouples (Type K). The refrigerant mass flow rate passing through each of the two indoor units was measured by a refrigerant flow meter with a reported accuracy of ±1.6% of full scale reading.

To obtain the air mass flow rate passing through an indoor unit, a short air duct connected to the return grill of the indoor unit was added. Air velocities inside the air duct at three evenly distributed measuring points were measured using an air velocity transducer with an accuracy of 1.0%. The average return air velocity was obtained by averaging the measured air velocities at the three measuring points and the air flow rate was evaluated from multiplying the averaged air velocity by the cross-section area of the air duct.

Photos showing the experimental DEAC rig are given in Appendix A.

4.3.2 Experimental conditions

Two sets of controllability tests were carried out. In the first set having four tests, indoor air dry-bulb temperatures in both rooms remained unchanged at their setting of 24.5 °C during the tests, but the space cooling load in either room was altered at a time, as detailed in Table 4.3. In the second set acting three tests, however, while cooling loads generated by LGU in both rooms remained unchanged at 0.75 kW during the tests, indoor air temperature in either room was altered from 24.5 °C to a new value at a time, also as detailed in Table 4.3.

For each of the tests listed in Table 4.3, the test duration was 4800 s. In the first half of the duration, i.e., 2400 s, all experimental conditions and settings remained unchanged, and the experimental DEAC rig was operated at a steady-state condition. The changes as specified in Table 4.3 were then introduced at 2400 s and each test went on for the other 2400 s duration (second half).

During all tests, when indoor air temperature reached its setting, the corresponding indoor unit was shut off by closing the matching EEV, but the supply fan in indoor unit remained operating at the same speed before the EEV was closed. However, in Test 2 and Test 3 when cooling load in a room was set to zero, the corresponding indoor unit was completely shut off by closing the matching EEV and switching off the supply fan. The settings of degree of superheat for the two indoor units were the same at 3 °C. Furthermore, in the simulated outdoor space, the air dry bulb and wet bulb temperatures were maintained at 32±0.15 °C and 18.1±0.1 °C respectively, using the existing separate DX A/C system and the LGU placed there.

Table 4.3 Experimental conditions (Tests 1-7)

Set One				
Test	Room	fixed indoor air setting point (°C)	changes in cooling load (kW)	
			Before	After
1	1	24.5	0.75	0.75
	2	24.5	0.75	0.375
2	1	24.5	0.75	0.75
	2	24.5	0.75	0
3	1	24.5	0.75	0
	2	24.5	0.75	0.75
4	1	22.5	0.75	0.75
	2	24.5	0.75	0.375
Set Two				
Test	Room	fixed cooling load (kW)	changes in indoor air setting point (°C)	
			Before	After
5	1	0.75	24.5	24.5
	2	0.75	24.5	22.5
6	1	0.75	24.5	26.5
	2	0.75	24.5	24.5
7	1	0.75	24.5	26.5
	2	0.75	24.5	21.5

On the other hand, according to the detailed technical specification of the compressor used in the experimental rig, the relationship between output cooling capacity and input electrical supply frequency to the compressor was linear. Therefore, based on the simulated load, the supply frequency with two indoor units operating was twice as much as that with one indoor unit operating. In the current study, the electric supply frequency to the compressor was set at 52 Hz when two indoor units were operated.

4.4 Experimental results and discussions

Using the experimental DEAC rig and following the experimental conditions specified in the Section 4.3 and Table 4.3, seven tests to examine the controllability of the NCCA were carried out and the test results are presented in Fig. 4.3 to Fig. 4.9.

In this section, a detailed discussion on the results obtained in Test 1 and shown in Fig. 4.3 is given, since they are representative to the control characteristics for a DEAC system. The discussions for results from other Tests, however, are therefore relatively brief.

Figure. 4.3 shows the variations of indoor air dry-bulb temperatures in both rooms and refrigerant flow rates in Test 1. As shown in Fig. 4.3, the variation frequencies and magnitudes in room air temperature T_1 and T_2 were similar in the first half of the test duration (before 2400 s). However, the variation patterns for refrigerant flow rates passing through indoor units, F_1 and F_2, were different. Since the initial

conditions in two rooms were different, T_2 reached the low boundary of the ±0.5 °C dead-band earlier than T_1. When T_2 reached its low boundary of dead-band, i.e. $T_2 \le T_{set,2} - \Delta T$, EEV_2 was shut off and the supply frequency to compressor was reduced to 26 Hz. When T_1 reached its low boundary of dead-band later, both EEV_1 and compressor were shut off. Therefore, the On-Off control for indoor unit 2 was implemented by opening/closing EEV_2 while that of indoor unit 1 was implemented by switching On-Off compressor. This caused the difference in variation patterns for refrigerant flow to F_1 and F_2.

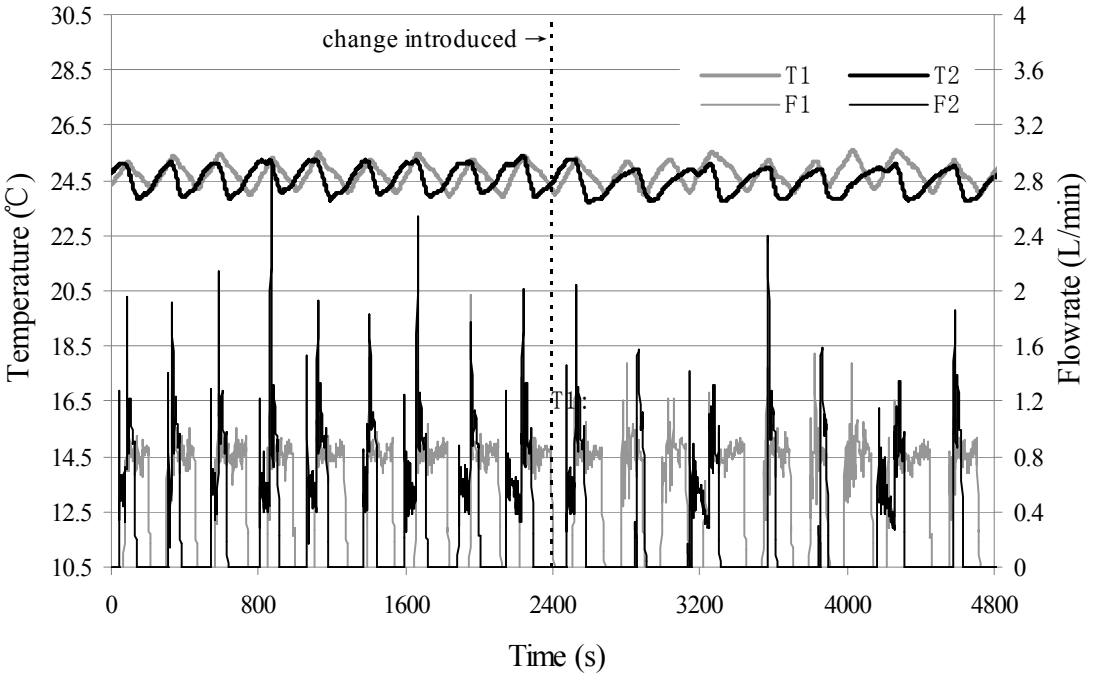

T1: Air temperature in Room 1 F1: Refrigerant flow passing through indoor unit 1

T2: Air temperature in Room 2 F2: Refrigerant flow passing through indoor unit 2

Fig. 4.3 Variations of indoor air dry-bulb temperatures and refrigerant flow rates in Test 1

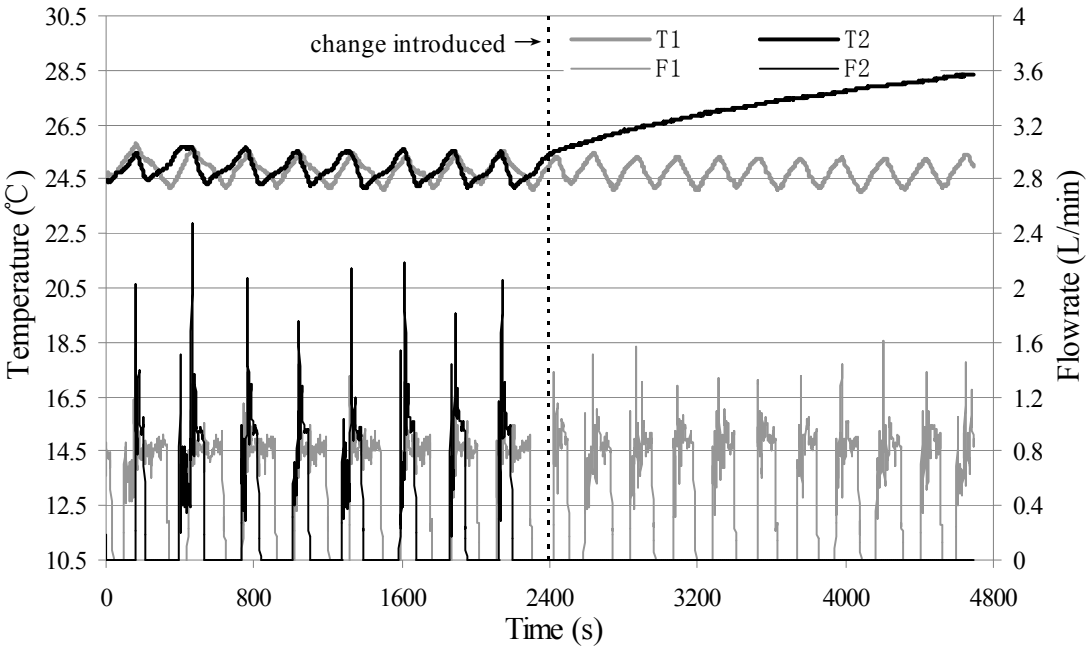

Fig. 4.4 Variations of indoor air dry-bulb temperatures and refrigerant flow rates in Test 2

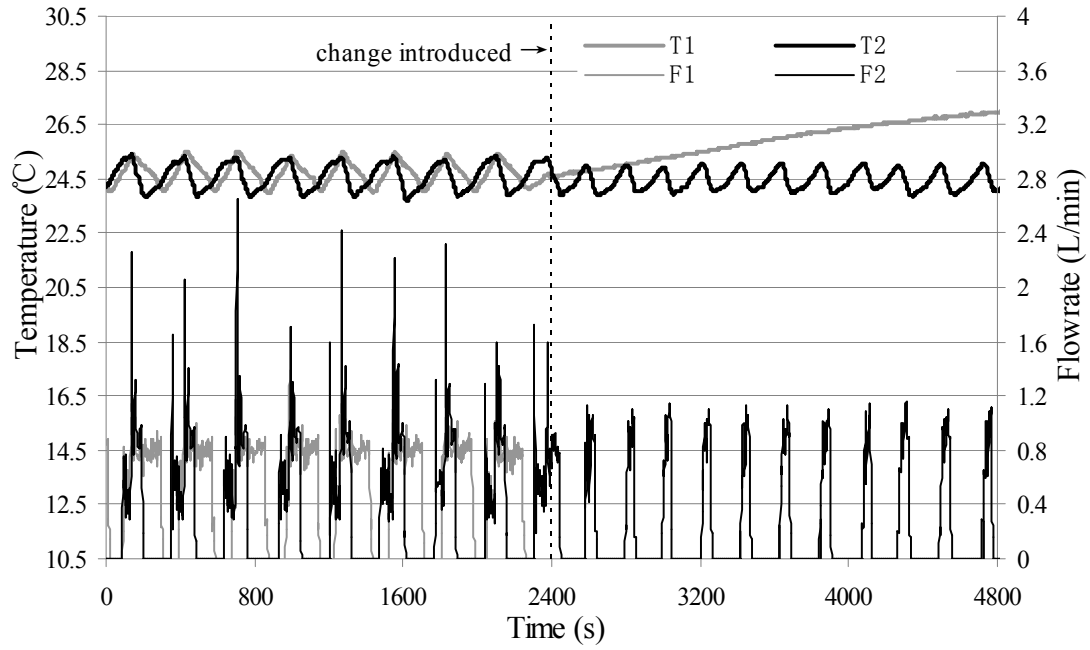

Fig. 4.5 Variations of indoor air dry-bulb temperatures and refrigerant flow rates in Test 3

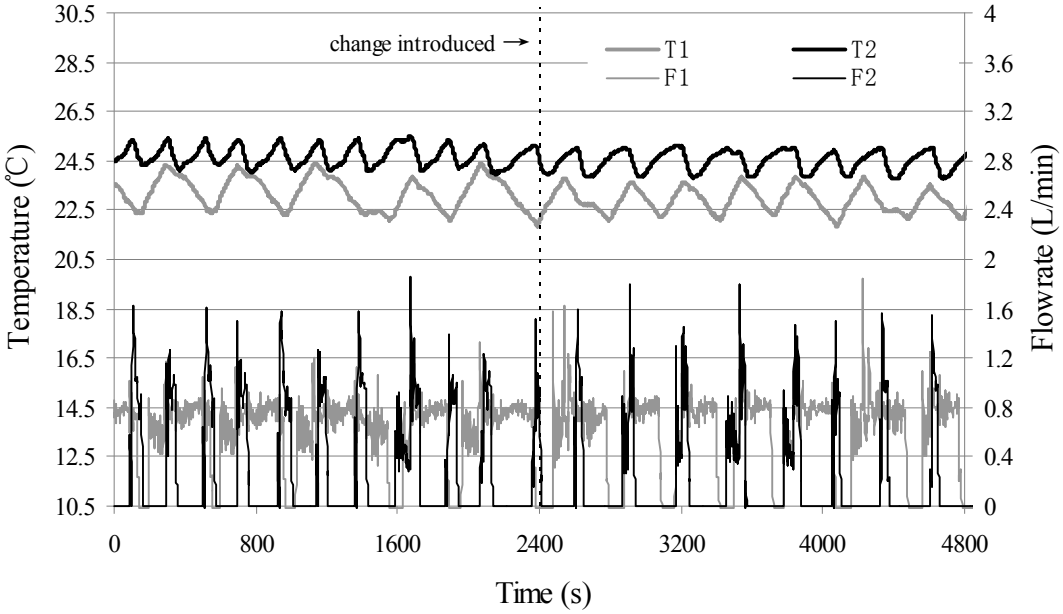

Fig. 4.6 Variations of indoor air dry-bulb temperatures and refrigerant flow rates in Test 4

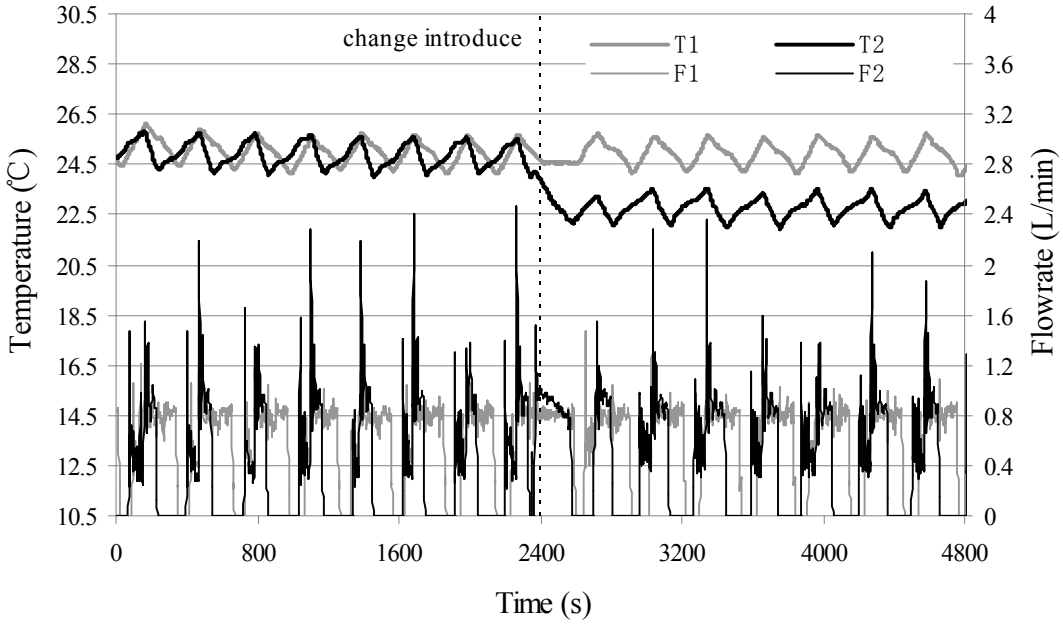

Fig. 4.7 Variations of indoor air dry-bulb temperatures and refrigerant flow rates in Test 5

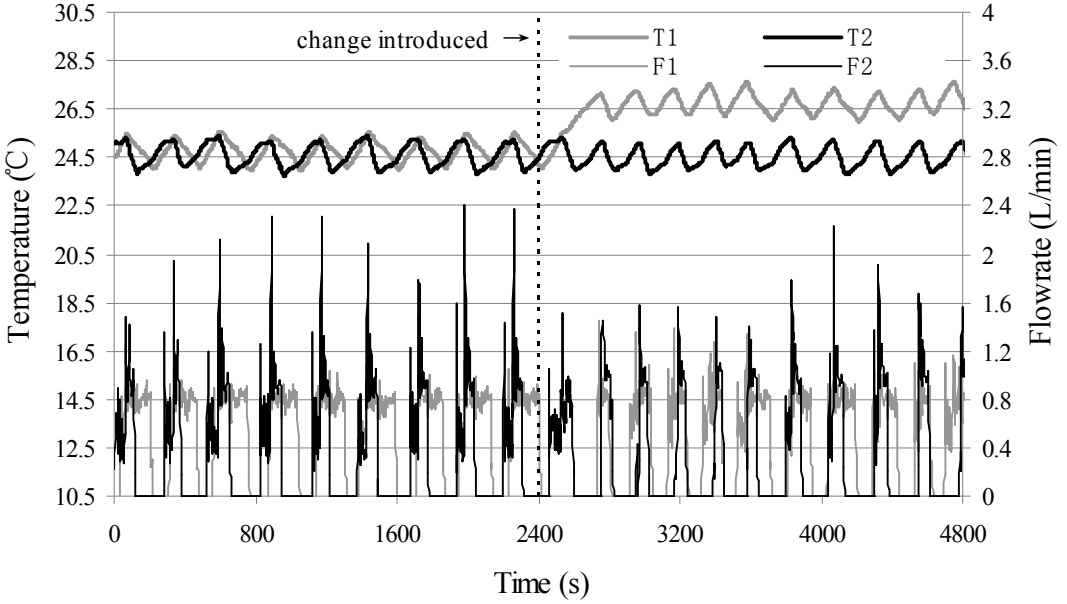

Fig. 4.8 Variations of indoor air dry-bulb temperatures and refrigerant flow rates in Test 6

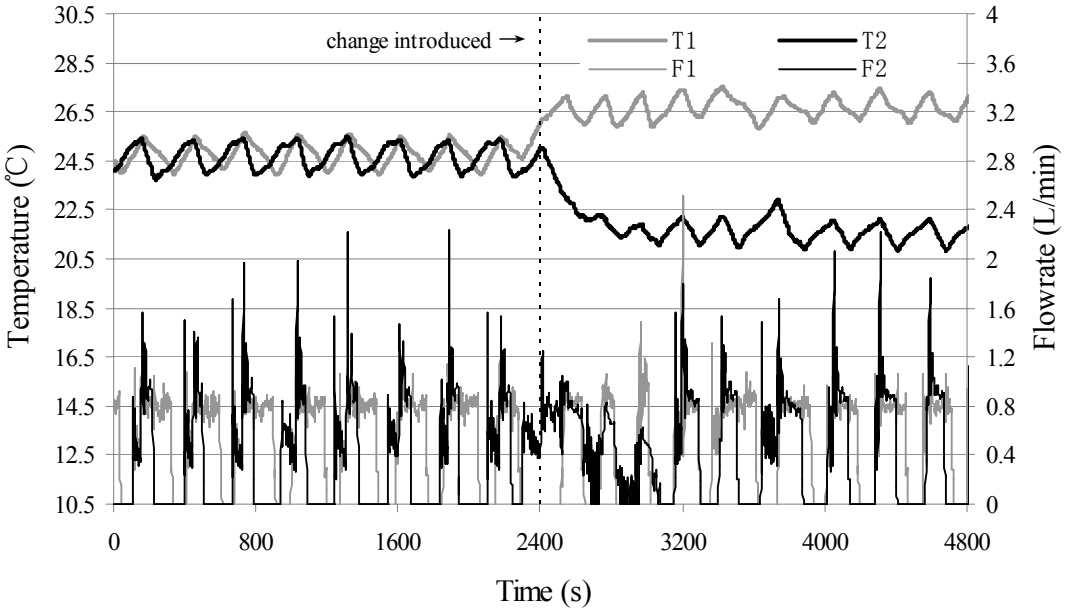

Fig. 4.9 Variations of indoor air dry-bulb temperatures and refrigerant flow rates in Test 7

It should be further noted that there was a delay of two minutes for compressor start-up due to safety protection. This could prolong the off-time duration of an indoor unit, of which the On-Off control was implemented by opening/closing EEV. Taking the time period of 2000 s - 2300 s as an example, T_2 reached its low boundary of the dead-band and EEV_2 was shut off at 2005 s. Afterwards T_1 reached its low boundary of the dead-band at 2100 s, and both EEV_1 and compressor were shut off. When T_2 reached its high boundary of the dead-band at 2143 s, i.e., $T_2 \geq T_{set,2} + \Delta T$, a starting signal was sent to both EEV_2 and compressor. EEV_2 was immediately opened and the refrigerant rushed into indoor unit 2 due to the pressure difference. However, at the time instant, the compressor was still off due to the time delay so that indoor unit 2 could not provide the required cooling capacity. The compressor was not turned on until 2220 s (2100+120). Therefore, the actual off-period duration of indoor unit 2, which was determined by the operation of an EEV, was longer than that of indoor unit 1, which was determined by the operation of a compressor.

Theoretically, the variation magnitude in T_2 should be greater than that in T_1 due to longer off-period duration when the cooling loads in two rooms were identical. T_2 may reach its low boundary of the dead-band later than T_1 in the next variation cycle due to a larger overshoot in T_2. This may consequently lead to the swap of operation control for the two indoor units, i.e., the operation of indoor unit 1 may be determined by the operation of EEV and that of indoor unit 2 by the operation of compressor. However, as shown in Fig. 4.3, T_2 increased slower than T_1 during an off-time duration and decreased faster during an on-time duration, suggesting that although both the inputs to two LGUs and the sizes of two rooms were the same, the

disturbance was existed, leading to different actual cooling loads for the two rooms. The heat transfers between the outdoor air and indoor air in the two rooms was a main factor.

After the cooling load in Room 2 was reduced from 0.75 kW to 0.375 kW at 2400 s, the off-period for indoor unit 2 was further prolonged and its on-period further shortened. However, the change in cooling load in Room 2 did not cause T_1 and T_2 to be out of control.

In this study, Standard Deviation (*SD*) was used to describe the deviation of the actual indoor air dry-bulb temperatures from their corresponding average values:

$$SD = \sqrt{\frac{\sum_{i=1}^{t} \left(T_i - T_{\text{avg},i}\right)^2}{t}} \tag{4.6}$$

The statistical analyses for the measured indoor dry-bulb temperature in Tests 1-7, are listed in Table 4.4. It can be seen that in Test 1, after cooling load in Room 2 was reduced, the averaged value and *SD* for T_2 were decreased, while those for T_1 did not however have visible changes. It should be noted that there was no specific method in the novel control algorithm to distribute refrigerant flow into the two indoor units. The refrigerant flow was automatically distributed by the opening of the two EEVs while they were used to control the degree of refrigerant superheat. As shown in Fig. 4.3, while the two indoor units were both in an on-period, the refrigerant flow was evenly distributed into the two units. Furthermore, shutting off one of the indoor

units did not impact much on the other due to the decrease in compressor speed. The refrigerant flow to the other operating unit remained almost unchanged. This reflected the robustness of the novel control algorithm developed, which would be further evidenced in other tests.

Fig. 4.4 and Fig. 4.5 show the variations of indoor air dry-bulb temperatures in the Room 1 and Room 2, and the refrigerant flow rates to indoor unit 1 and 2 in Tests 2 and 3, respectively. The results in the first half were similar to those in Test 1. In the second half, at 2400 s, the LGU and indoor unit in one of the two rooms (Room 2 in Test 2 and Room 1 in Test 3) were shut off. Since the electrical heater inside the LGU, which was shut off, was still at a high temperature, air temperature in the room, in which the indoor unit was shut off, kept rising. There was only one indoor unit On-Off controlled by using compressor. As seen from the figures, while the air temperature in the room where its indoor unit was stopped was keeping rising, the air temperature in the other room where its indoor unit was operated remained under control. Furthermore, as shown in Table 4.4, *SD*s in both tests were reduced in the second half since the interaction between the two indoor units diminished.

In Test 4, indoor air temperature's settings in the two rooms differed by 2 °C (22.5 °C in Room 1 and 24.5 °C in Room 2). As shown in Fig. 4.6 and Table 4.4, the variation magnitudes and *SD*s for T_1 in the first half of the test were the highest among all Tests. This was caused by two reasons. Firstly, as shown in Fig. 4.6, one On-Off cycle for T_1 covered two On-Off cycles for T_2. When T_1 reached its low boundary of the dead-band, T_2 was still at its second on-cycle. Therefore, in that cycle, the On-Off control for indoor unit 1 was determined by the opening of EEV_1,

which would prolong an off-period for indoor unit 1. Secondly, the increased heat gain in Room 1 because of a lower indoor air temperature setting accelerated the rising of T_1 during the Off-period. This led to a concern that the indoor air temperature controlled by the NCCA would be subjected to significant fluctuation under a certain operating condition.

In the second half of Test 4, the cooling load in Room 1 was reduced. The On-Off cycling period for indoor unit 1 was consequently shortened; swap the operation control for indoor unit 1 from determined by the opening of EEV1 to be determined by the operation of compressor, which further decreased its off-period. On the other hand, the off-period of indoor unit 2 was prolonged since the On-Off control for indoor unit 2 was determined by EEV2 in the second half of the test. However, the variation magnitude of T_2 did not significantly increase, due probably to a lower cooling load in Room 2.

Figures. 4.7 to 4.9 show the variations of indoor air dry-bulb temperatures in both rooms and the refrigerant flow rates to both indoor units in Tests 5-7, when the cooling loads in both rooms were fixed but indoor air temperature settings were varied. The use of the NCCA showed good control robustness in the three tests, i.e., the changes in air temperature settings in one room did not significantly disturb the indoor air temperature in the other room.

Table 4.4 Statistical data for the measured indoor air dry-bulb temperatures (°C) in Tests 1-7

Test	Room	First half of the test (before 2400 s)				Second half of the test (after 2400 s)			
		Max.	*Min.*	*Avg.*	*SD*	*Max.*	*Min.*	*Avg.*	*SD*
1	1	25.51	23.92	24.72	0.39	25.61	23.96	24.73	0.41
	2	25.42	23.80	24.59	0.45	25.27	23.71	24.43	0.43
2	1	25.80	24.13	24.85	0.38	25.45	24.05	24.75	0.44
	2	25.72	24.15	24.88	0.40	NA	NA	NA	NA
3	1	25.54	23.97	24.72	0.42	NA	NA	NA	NA
	2	25.41	23.71	24.61	0.48	25.07	23.87	24.42	0.35
4	1	24.43	21.85	23.20	0.65	23.83	21.84	22.91	0.49
	2	25.53	23.95	24.69	0.40	25.12	23.78	24.48	0.42
5	1	26.11	24.11	25.02	0.46	25.76	24.05	24.94	0.43
	2	25.82	23.95	24.88	0.48	23.55	21.92	22.74	0.39
6	1	25.59	23.96	24.76	0.42	27.64	25.98	26.71	0.40
	2	25.41	23.71	24.58	0.47	25.31	23.78	24.51	0.42
7	1	25.67	23.93	24.77	0.45	27.50	25.79	26.64	0.41
	2	25.50	23.74	24.63	0.50	22.92	20.84	21.62	0.40

Max.: The maximum value of the measured indoor air temperature during the period

Min.: The minimum value of the measured indoor air temperature during the period

Avg.: The averaged measured indoor air temperature during the period

SD : As defined by Eq. (4.6)

4.5 Improvement to the NCCA

As presented in Section 4.4, although the use of NCCA resulted in good control robustness and sensitivity in most of the tests, the indoor air temperature controlled was still subjected to significant fluctuation under certain specific conditions. This was mainly caused by the use of temperature dead-band and time delay for compressor start-up, and the interaction between two indoor units. However, the elimination of temperature dead-band and time delay may cause frequent change in compressor speed. Therefore, an improvement to the NCCA was made to achieve better control accuracy without requiring frequent change in compressor speed, as follows:

For i^{th} ($1 \le i \le m$) indoor unit, X, an additional control signal, was defined as:

$$\text{If } T(t)_i > T_{set,i} - \Delta T \qquad \text{X}(t)_i = 1 \tag{4.7}$$

$$\text{If } T(t)_i \le T_{set,i} - \Delta T \qquad \text{X}(t)_i = 0 \tag{4.8}$$

Moreover, Y, an additional On-Off control signal for EEV, was defined as

$$Y(t)_i = E(t)_i + \left(mX(t)_i - \sum_{j=1}^{\text{m}} X(t)_j \right) \tag{4.9}$$

when $Y(t)_i \ge 1$, EEV_i functioned to control the degree of refrigerant superheat, and when $Y(t)_i \le 0$, EEV_i was closed. The compressor speed was still determined by the number of opened EEVs.

As seen in Eq. (4.7), the On-Off status of EEV_i was determined not only by the air temperature status in Room *i* but also air temperature in all other rooms. Assuming that all indoor units in an MEAC system were initially turned on, and then in Room *j* ($1 \le j \le m$), its air dry-bulb temperature, T_j, was the first one that reached $T_{set,j} - \Delta T$. At this time point, $E_j=0$, $X_j=0$, and $Y_j=1-m$. Hence, indoor unit *j* would be turned off and the compressor speed changed from $f(\sum_{i=1}^{m} Q_i)$ to $f(\sum_{i=1}^{m} Q_i - Q_j)$. Afterwards air temperature in Room *k*, T_k ($1 \le k \le m$) may also reach $T_{set,k} - \Delta T$, but T_j was higher than $T_{set,j} - \Delta T$ and lower than $T_{set,j} + \Delta T$. Therefore, $E_j=0$, $X_j=1$, $Y_j=1$, $E_k=0$, $X_k=0$, and $Y_k=1-m$. When under the original NCCA, since $E_j=0$, indoor unit *j* would remain at Off-status. However, using the improved novel capacity control algorithm (INCCA), since $Y_j=1$, indoor unit *j* would be turned on again and indoor unit *k* would be turned off. Meanwhile, the compressor speed was changed from $f(\sum_{i=1}^{m} Q_i - Q_j)$ to $f(\sum_{i=1}^{m} Q_i - Q_k)$. If Q_j was equal to Q_k, compressor speed remained unchanged. As it can be seen, using the INCCA, the magnitude of temperature variation could be restrained and the frequent switching in compressor speed avoided.

4.5.1 Experimental procedure for controllability tests of the INCCA

Three tests (Test 8 to Test 10) were carried out to validate the controllability of the INCCA, as detailed in Table 4.5. Each test lasted for 4800 s and may be separated into two halves. Changes were introduced between two the halves. In Tests 8 and 9, the experimental DEAC system was controlled by original NCCA in the first half but

by the INCCA in the second half. In Test 10, the experimental DEAC system was controlled by the INCCA, with the change in air temperature setting in Room 2 introduced at the beginning of the second half of the test.

All other experimental settings were identical to those in Tests 1-7.

Table 4.5 Experimental condition in Tests 8-10

Test	Room	Fixed Setting		Changes Introduced	
		Setting (°C)	Loads (kW)	Control Algorithm	
8	1	24.5	0.90	NCCA	INCCA
	2	24.5	0.50	NCCA	INCCA
9	1	24.5	0.90	NCCA	INCCA
	2	24.5	0.65	NCCA	INCCA
Test	Room	Fixed Setting		Changes Introduced	
		Control	Loads (kW)	Setting Point (°C)	
10	1	INCCA	0.90	24.5	24.5
	2	INCCA	0.65	24.5	22.5

4.5.2 Experimental results and discussions

Figures. 4.10 to 4.12 show the variations of indoor air dry-bulb temperatures in both rooms and refrigerant flow rates to both indoor units in Tests 8-10. Table 4.6 shows the statistics for the measured indoor air dry-bulb temperature (°C) in Tests 8-10.

As shown in Fig. 4.10 and Table 4.6, in the first half in Test 8, since the cooling load in Room 1 was larger than that in Room 2, both the variation magnitude and *SD* for T_1 were much larger than that for T_2. However, when the original NCCA was replaced by INCCA in the second half, the variation magnitude and *SD* for T_1 were significantly reduced to lower than those for T_1 in all previous tests. It should be further noted that the compressor speed remained unchanged for 700 s while the two EEVs were alternately opened.

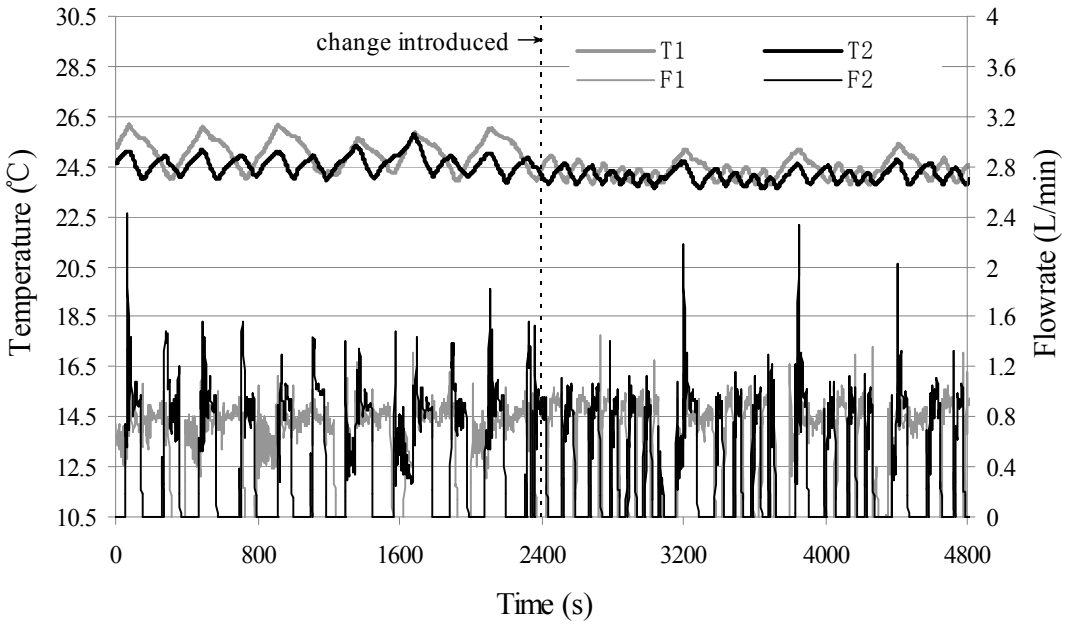

Fig. 4.10 Variations of indoor air dry-bulb temperatures and refrigerant flow rates in Test 8

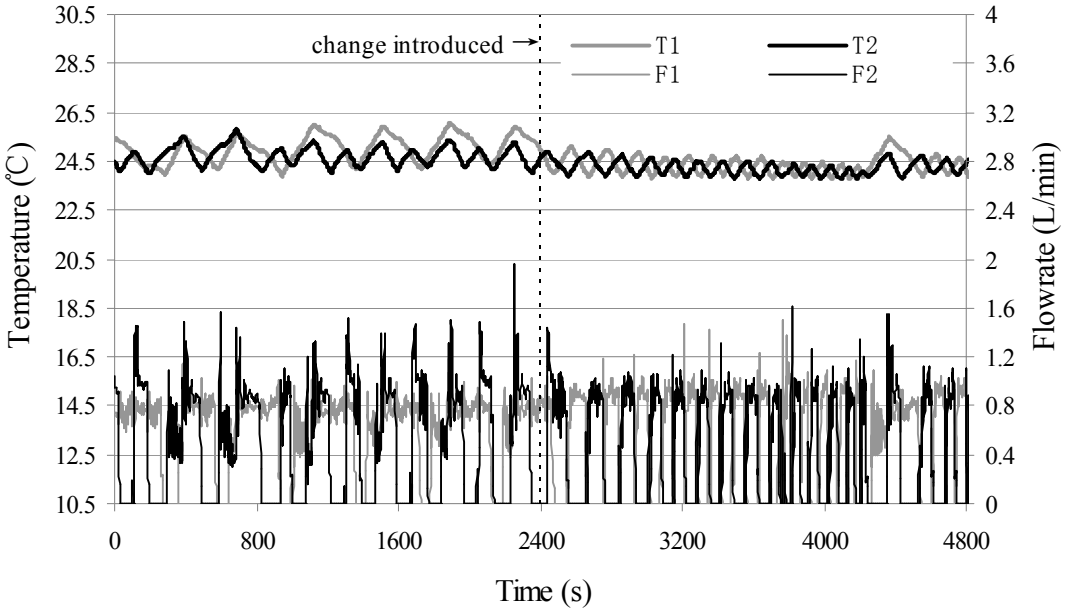

Fig. 4.11 Variations of indoor air dry-bulb temperatures and refrigerant flow rates in Test 9

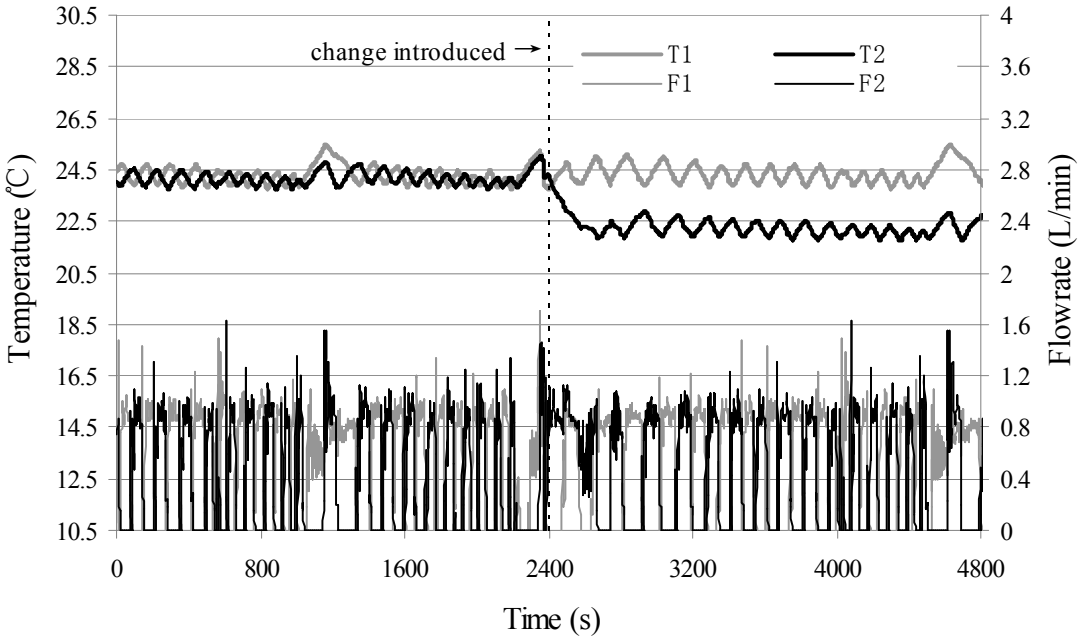

Fig. 4.12 Variations of indoor air dry-bulb temperatures and refrigerant flow rates in Test 10

Table 4.6 Statistical data for the measured indoor air dry-bulb temperatures (°C) in Tests 8-10

Test	Room	First Half (before 2400 s)				Second Half (after 2400 s)			
		Max.	*Min.*	*Avg.*	*SD*	*Max.*	*Min.*	*Avg.*	*SD*
8	1	26.17	23.93	25.10	0.59	25.41	23.76	24.39	0.38
	2	25.78	23.87	24.62	0.36	24.77	23.60	24.11	0.27
9	1	26.08	23.88	25.02	0.54	25.49	23.76	24.36	0.36
	2	24.83	23.74	24.72	0.39	24.83	23.74	24.20	0.25
10	1	25.49	23.76	24.30	0.36	25.48	23.76	24.35	0.37
	2	25.00	23.74	24.17	0.26	22.87	21.74	22.21	0.26

Theoretically, the length of an on-period for compressor would be increased when the cooling loads in all rooms were increased. When the sum of the cooling load in all rooms was larger than the cooling capacity at the lowest compressor speed assigned by the NCCA, the compressor speed would keep switching between high and low without an off-period. As shown in Fig. 4.11, the compressor speed remained unchanged for ~1800 s in the second half in Test 9, when the cooling load in Room 2 was 0.65 kW, larger than that in Test 8 at 0.5 kW. It can be predicted that when the number of indoor units was increased, the possibility of the sum of the cooling load in all rooms being larger than the output cooling capacity at the lowest compressor speed assigned by the controller would increase, and then the compressor controlled by the INCCA would have a greater chance to be continuously operated. Therefore, the control performance of an MEAC using the INCCA was expected to be better with increased number indoor units.

The experimental results in Test 10 proved the control robustness of the INCCA. After air temperature setting in Room 2 was changed from 24.5 to 22.5 °C at 2400 s, the variation of air temperature in Room 1, T_1, remained almost unchanged. Furthermore, the variation magnitude and *SD*s for T_2 in the second half in Test 10 were close to those in the first half.

It should be noted however that using the INCCA may cause more frequent On-Off switching of EEVs than using the original NCCA. Therefore, a digital stop valve may be placed upstream of an EEV to implement the shut-off function which was originally done by the EEV so as to protect the EEV.

4.6 Conclusions

A novel capacity control algorithm for an MEAC system has been developed and is reported in this Chapter. Experimental tests which a DEAC system validated its control accuracy and robustness. However, indoor air temperature controlled using the NCCA may still be subjected to significant fluctuations under certain operating conditions due to the use of temperature dead-band and time delay for compressor start-up, and the interaction among indoor units. An INCCA was therefore further developed, and further controllability test were carried out. The test results showed that the INCCA was simple but could effectively restrain the magnitude of temperature variations and avoid the frequent switching in compressor speed.

Chapter 5

A modeling study on the effects of refrigerant pipeline length on the operational performance of a DEAC system

5.1 Introduction

In an actual MEAC system, its pipelines are much more complicated than those in an SEAC system, with much longer total pipeline length and more pipe fittings such as elbows and valves. A longer pipeline with more fittings would cause a greater refrigerant pressure drop [Wijaya and Spatz 1995], which could in turn further lower evaporating temperature, increase condensing temperature, reduce system's operational efficiency [Lee and Yoo 2000] and result in refrigerant mal-distribution among evaporators as compared to what would happen in an SEAC system. Neglecting the influence of the length of pipeline with fittings on the operational performance may be reasonable for a simple SEAC system. However, this can be problematic for an MEAC system. Nonetheless, only a few researches have been so far looked into this issue [Hirao et al. 1992, Rajat et al. 2004, Shao et al. 2008, Shi et al. 2008]. However, in these studies, their primary objectives were not on studying the influence of the refrigerant pipelines on system performance, but on other issues such as evaluating refrigerant mass flow rate at each evaporator outlet or building a generic simulation model which can be used to study different complex refrigeration systems.

It could therefore be seen, as mentioned in Chapter 2, that although the relationship among the coupled operational parameters in an MEAC system have been extensively studied and the method of evaluating the pressure drop along refrigerant pipelines is readily available, the influence of the refrigerant pipeline length on the operational performance of an MEAC system has not yet been studied. Furthermore, for new MEAC system designs, guidelines are needed so as to optimize refrigerant pipework layout for the best possible system operational efficiency.

This Chapter reports on a modeling study on the effects of refrigerant pipeline length on the operational performance of a DEAC system. To facilitate the intended modeling study, a physical-based steady-state mathematic model for the DEAC system has been developed and is presented firstly. In addition to having the sub-models for all system components in a DEAC system, the model contained a sub-module specifically devoted to accounting for the influence of refrigerant pipeline length on system operational performance. The model was validated by comparing its predictions with the experimental results previously reported by others. Using the model developed, the effects of refrigerant pipeline length on the operational performance of the DEAC system have been studied and are then reported. Finally, the application of the DEAC model developed to studying the layout optimization of a DEAC system for the highest possible operational efficiency is presented.

5.2 Model development

5.2.1 Sub-models for system components in a DEAC system

The schematic diagram of a DEAC system to be modeled is shown in Fig. 5.1. The model was established by zoning the DEAC system. The complete conceptual model which depicts the zoning of the DEAC is shown in Fig. 5.2. Each zone was treated as a stirred tank; and the model so developed was of partial-lumped-parameter type. When presenting the sub-models in Sections 5.2, reference is made to Fig. 5.2 for symbols representing the zones and subscripts indicating the locations in the DEAC system.

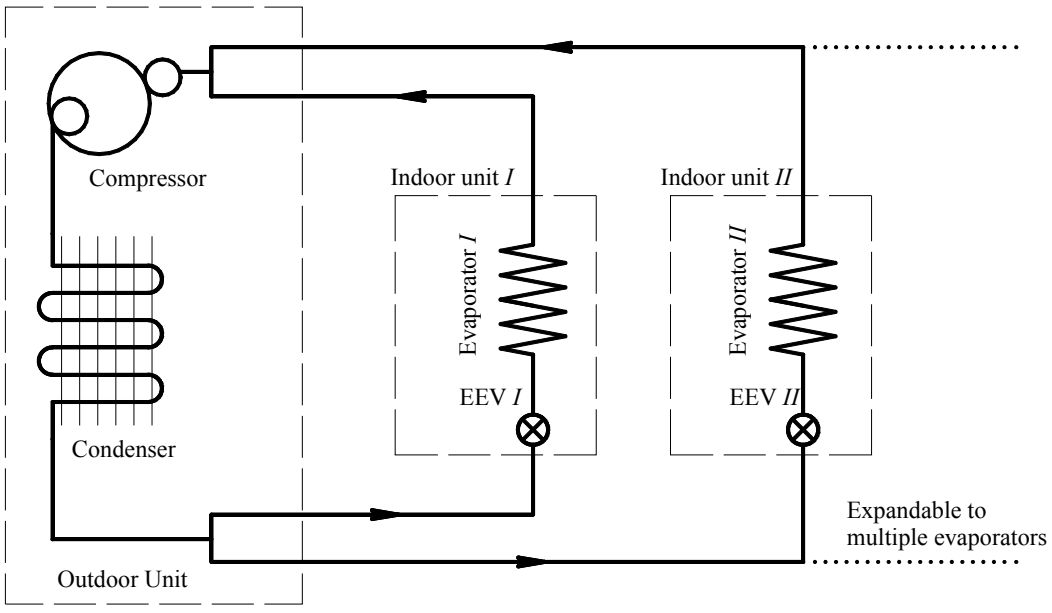

Fig. 5.1 Schematic diagram of a DEAC system

The major system components included a variable-speed compressor, an air-cooled condenser, two EEVs and two DX evaporators (indoor units), and all refrigerant pipelines.

Assuming that R22 was used as refrigerant, so that the State Equations developed by Wagner et al. [1993] for R22 covering the entire fluid region from 116 K to 550 K at pressures up to 200 MPa were used to calculate refrigerant thermal properties. State Equations for air were obtained from ASHRAE Handbook [2009].

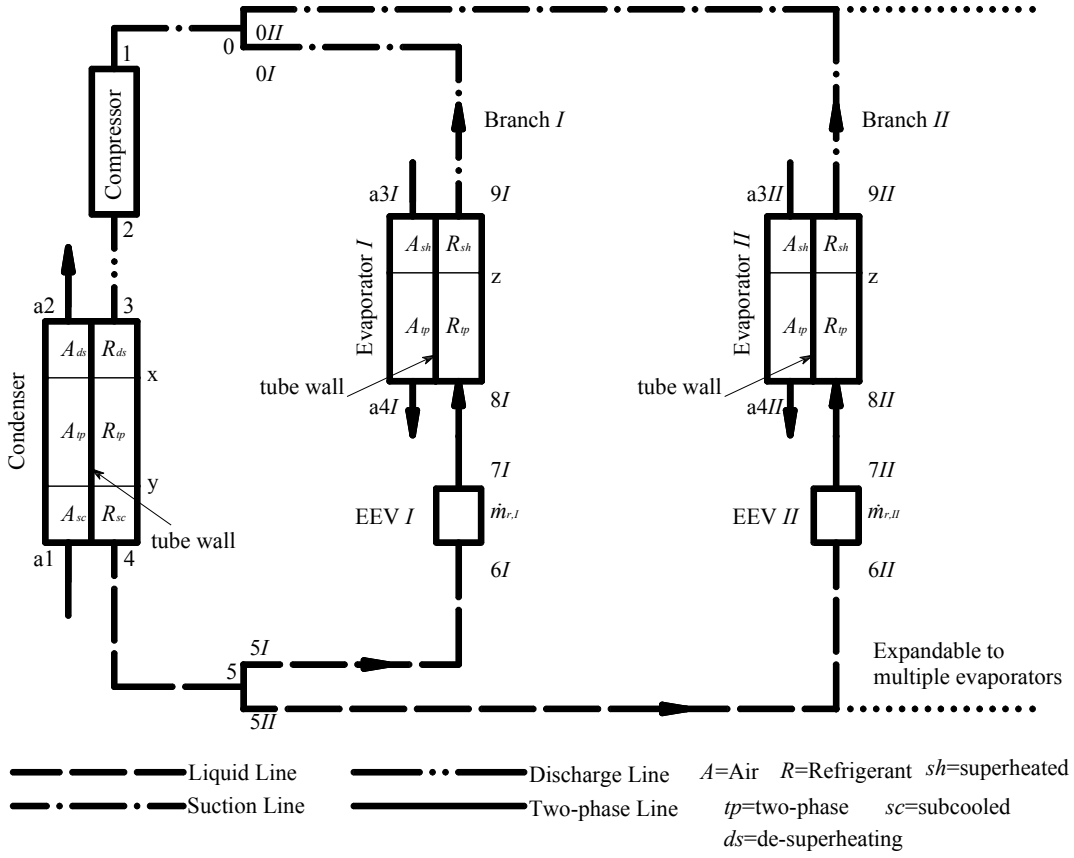

Fig. 5.2 Conceptual model of a DEAC

5.2.1.1 Sub-model for variable-speed compressor

An isentropic compression process and quasi-steady conditions were assumed. As shown in Fig. 5.2, points 1 and 2 are the compressor suction and discharge, respectively. This compressor was modeled using the principle of energy and mass balance, rather than using curve-fitting its performance data. Such a modeling approach has been commonly adopted [Jolly et al. 1990, Deng 2002, Chen et al. 2005].

The refrigerant mass flow rate leaving the compressor was assumed to be equal to that at compressor inlet:

$$\dot{m}_{r1} = \dot{m}_{r2} \tag{5.1}$$

and was calculated by:

$$\dot{m}_{r1} = \lambda_{cm} V_{cm} \rho_{r1} \tag{5.2}$$

The refrigerant volumetric flow rate passing through the compressor can be determined by:

$$V_{cm} = \frac{\pi}{240} D_{cm}{}^{2} L_{cm} S_{cm} \tag{5.3}$$

where D_{cm} is the cylinder bore, L_{cm} the stroke of cylinder, S_{cm} the rotational speed of compressor and can be calculated from the frequency of its motor drive:

$$S_{cm} = \frac{F_{cm}\left(1 - s_{cm}\right)}{PL_{cm}} \tag{5.4}$$

where F_{cm} is the input frequency of the variable-frequency drive (VFD) for compressor's motor; s_{cm} the slip factor of the motor with a value between 2% and 6%; and PL_{cm} the number of electrode couple of the motor.

The overall displacement coefficient, λ_{cm}, was determined by:

$$\lambda_{cm} = \lambda_v \lambda_p \lambda_t \lambda_l \tag{5.5}$$

where, λ_p is the pressure loss coefficient with an approximate value of 1.0; λ_l the leakage coefficient, 0.98~0.92; the compressor volumetric coefficient, λ_v, given by:

$$\lambda_v = 1 - 0.015 \times \left[\left(\frac{P_{r2}}{P_{r1}} \right)^{\frac{1}{N}} - 1 \right] \tag{5.6}$$

The temperature coefficient, λ_t, was evaluated by:

$$\lambda_t = 2.57 \times 10^{-3} T_{r0} - 1.06 \times 10^{-3} \times \left(T_{r3} - T_{r4} \right) \tag{5.7}$$

The theoretical isentropic work done by the compressor was given by:

$$w_{cm} = \lambda_w \frac{N}{N-1} \frac{P_{r1}}{\rho_{r1}} \left[\left(\frac{P_{r2}}{P_{r1}} \right)^{\left(\frac{N}{N-1} \right)} - 1 \right] \tag{5.8}$$

where N is the polytropic index of compression, and N=1.18 for R22. The indicated coefficient, λ_w , was evaluated by:

$$\lambda_w = \frac{1}{\lambda_t \lambda_l} \left[1 + \frac{\left[1.5 \times \Delta P_m \times \left(\frac{P_{r2}}{P_{r1}} \right)^{\frac{1}{N}} \right]}{\left[\frac{(h_{r2} - h_{r1})}{v_{r1}} \right]} \right] \tag{5.9}$$

where ΔP_m is the compressor discharge pressure loss and was evaluated by:

$$\Delta P_m = 25 \times (T_{r0} - 27315)^{-1.01} \times 10^{\frac{-0.15 \times P_{r2}}{P_{r2}}} \tag{5.10}$$

Based on the principle of energy conservation, the enthalpy of the vapour refrigerant leaving the compressor was evaluated by:

$$h_{r2} = h_{r1} + w_{cm} \tag{5.11}$$

Taking into account the energy loss inside the motor and transmission assembly, the total electrical work input to the compressor, W_{cm}, was given as follows:

$$W_{cm} = \frac{w_{cm}\dot{m}_{r1}}{\eta_{mec}\eta_{motor}} \tag{5.12}$$

where η_{mec} is the mechanical coefficient with a value between 0.7 and 0.85; η_{motor} is the motor coefficient with a value of 0.8.

5.2.1.2 Sub-model for EEV

The refrigerant mass flow rate passing through EEVs could be represented by an orifice equation. Taking EEV *I* as example, its sub-model could be expressed by:

$$\dot{m}_{r6I} = \xi_{ev,I} A_{ev,I} \sqrt{(P_{r6I} - P_{r7I})\rho_{r6I}} \tag{5.13}$$

The flow coefficient of the EEV was given by [Chen 2005]:

$$\xi_{ev,I} = 0.82 - 0.053\chi_{7I} \tag{5.14}$$

Generally, an EEV had a linear inherent flow characteristic. The valve opening was assumed to be linear with the actual pulse output of the EEV's controller, $EC_{ev,I}$:

$$A_{ev,I} = K_{ev,I} \times EC_{ev,I} \tag{5.15}$$

Where $K_{ev,I}$ is the valve opening per unit of pulse output and is obtainable from the performance date of the EEV.

Refrigerant flowing through an EEV may be regarded as an isenthalpic throttling process. Hence, the refrigerant enthalpy after the throttling process through the EEV was assumed to be equal to that upstream of the EEV it, i.e.,

$$h_{r6I} = h_{r7I} \tag{5.16}$$

5.2.1.3 Sub-model for evaporator

Since the evaporators in the DEAC system could be represented using the same sub-model, Evaporator *I*, as shown in Fig. 5.2, was therefore chosen as an example for illustrating the modeling process.

In this study, louver-fin-tube type of DX evaporators and counter-flow heat exchange between refrigerant and air were assumed. For each of the two evaporators, its zoning is also depicted in Fig. 5.2. The refrigerant side was divided into two regions: a two-phase region and a superheated region. Furthermore, dry-cooling and wet-cooling conditions on air side were separately treated when modeling.

5.2.1.3.1 Refrigerant side of two-phase region

Mass and energy balances in the two-phase region required:

$$\dot{m}_{r8I} = \dot{m}_{rz} \tag{5.17}$$

$$\dot{m}_{r8I} h_{r8I} + Q_{r,e,tp} = \dot{m}_{rz} h_{rz} \tag{5.18}$$

where the enthalpies of refrigerant, h_{r8I} and h_{rz}, could be calculated from refrigerant State Equations developed by Wagner et al. [1993] for R22.

Since the heat transfer coefficient on the refrigerant side in the two-phase region was relatively large, the increase in tube wall temperature could be neglected and was assumed to be constant. The heat transfer between two-phase refrigerant and the tube wall in the two-phase region was given as:

$$Q_{r,e,tp} = \alpha_{r,e,tp} A_{r,e,tp} \Delta T_{r,e,tp} \tag{5.19}$$

The convective heat transfer coefficient, $\alpha_{r,e,tp}$, on the refrigerant side in the two-phase region was determined using the *Kandlikar* Equation [Kandlikar 1990]:

$$\alpha_{r,e,tp} = \alpha_{r,li} C_o C_1 C_2 \left(25 Fr_r\right)^{C_3} + C_4 B_o^{\,C_5} F f_r \tag{5.20}$$

The assumed convective heat transfer coefficient for liquid refrigerant in the two-phase region, $\alpha_{r,li}$, was calculated by:

$$\alpha_{r,li} = 0.023 \times \mathrm{Re}_{r,li}^{0.8} \mathrm{Pr}_{r,li}^{0.4} \frac{\lambda_r}{d_{i,e}} \tag{5.21}$$

where $\mathrm{Re}_{r,li}$ is defined as:

$$\mathrm{Re}_{r,li} = \frac{g_r d_{i,e}}{\mu_{r,li}} \tag{5.22}$$

where g_r is the refrigerant mass flux, and $\mu_{r,li}$ the dynamic viscosity of liquid refrigerant. The refrigerant convection characteristic number was:

$$C_o = \left(\frac{1-\chi_e}{\chi_e} \right)^{0.8} \left(\frac{\rho_{r,va}}{\rho_{r,li}} \right) \tag{5.23}$$

The constants C_1 to C_5 in Eq. (5.20) were given according to the value of C_o, as shown in Table 5.1.

The refrigerant *Froude* number was:

$$Fr_r = \frac{g_r}{9.8 \rho_{r,li}^{\ 2} d_{i,e}} \tag{5.24}$$

Table 5.1 Values of constants used in Eq. (5.20)

	When $C_o \le 0.65$	When $C_o > 0.65$
C_1	1.1360	0.6683
C_2	-0.9	-0.2
C_3	0.30	0.30
C_4	667.2	1058.0
C_5	0.7	0.7

The refrigerant boiling characteristic number was:

$$B_o = \frac{q_{r,tp}}{g_r \gamma_e} \tag{5.25}$$

where $q_{r,tp}$ is the heat flux in the two-phase region.

Further in Eq. (5.20), Ff_r is a dimensionless factor of refrigerant property, and was 2.20 for R22.

5.2.1.3.2 Refrigerant side of superheated region

Similarly, both mass flow rate and energy balance in the superheated region could be evaluated by:

$$\dot{m}_{rz} = \dot{m}_{r9I} \tag{5.26}$$

$$\dot{m}_{rz} h_{rz} + Q_{r,e,sp} = \dot{m}_{r9I} h_{r9I} \tag{5.27}$$

Since the length of this region was short, to simplify calculation, the tube-fin temperature of the superheated region was assumed to be maintained at the outlet tube-fin temperature of the two-phase region. Log mean temperature difference, $LMTD_{r,e,sh}$, was used to calculate the heat transfer between refrigerant and the tube wall in the superheated region. The heat transfer was given as:

$$Q_{r,e,sh} = \alpha_{r,e,sh} A_{r,e,sh} LMTD_{r,e,sh} \tag{5.28}$$

where,

$$LMTD_{r,e,sh} = \frac{T_{r9I} - T_{rz}}{\ln\left[\dfrac{T_{wl,e,sh} - T_{rz}}{T_{wl,e,sh} - T_{r9I}}\right]} \tag{5.29}$$

The convective heat transfer coefficient for vapour refrigerant in the superheated region was evaluated using the *Petukhov-Popov* Equation [Baughn and Roby 1992]:

$$\alpha_{r,e,sh} = \lambda_r \times \frac{Nu_{r,sh}}{d_{i,e}} \quad (\mathrm{Re}=10^4 \sim 5.3\times10^6,\ \mathrm{Pr}=0.5\sim2000) \tag{5.30}$$

where λ_r is the thermal conductivity of refrigerant and the *Nusselt* number was:

$$Nu_{r,sh} = \frac{\frac{f_e}{8}\mathrm{Re}_{r,sh}\,\mathrm{Pr}_{r,sh}}{1.07 + 12.7(\frac{f_e}{8})^{0.5}(\mathrm{Pr}_{r,sh}{}^{0.667} - 1)} \tag{5.31}$$

where the turbulent skin-friction coefficient, f_e, is:

$$f_e = \left[1.82 \times \lg\left(\mathrm{Re}_{r,sh}\right) - 1.64\right]^{-2} \tag{5.32}$$

5.2.1.3.3 Air side of the evaporator

On the air side of both superheated region and two-phase region, the tube-fin temperature was used to determine whether dehumidifying occurred in this region. In both regions, wet-cooling of air occurred when the tube-fin surface temperature was below the dew point temperature of air entering the respective region; otherwise, dry-cooling of air occurred. Dry-cooling and wet-cooling of air were separately modeled and the modeling in the two-phase region is presented in the section, since the modeling in the superheated region might be similarly treated.

a) Wet-cooling

Because the thermal capacitance and mass storage of air were negligible, mass and energy balances yielded:

$$\frac{\dot{m}_{az}}{\dot{m}_{a4I}} = \frac{1+\omega_{az}}{1+\omega_{a4I}} \tag{5.33}$$

$$\dot{m}_{az} h_{az} - Q_{a,e,wt} = \dot{m}_{a4I} h_{a4I} \tag{5.34}$$

where the enthalpies of moisture air, h_{az} and h_{a4I}, and the moisture contents, ω_{az} and ω_{a4I}, could be calculated using the air State Equations from ASHRAE Handbook [2009].

The heat transfer between air and tube-fin surface in the two-phase region could be expressed as:

$$Q_{a,e,wt} = U_{a,e,wt} A_{a,e,tp} LMTD_{a,e,wt} \tag{5.35}$$

The log mean temperature difference, $LMTD_{a,e,wt}$, between the tube-fin and air was:

$$LMTD_{a,e,wt} = \frac{T_{az} - T_{a4I}}{\ln\left[\frac{T_{az} - T_{wl,e,tp}}{T_{a4I} - T_{wl,e,tp}}\right]} \tag{5.36}$$

where the overall heat transfer coefficient in Eq. (5.35) is:

$$U_{a,e,wt} = \frac{1}{\frac{1}{\alpha_{a,e,wt}\zeta_a \eta_{a,e,wt}} + R_e} \tag{5.37}$$

where R_e is the combined total thermal resistance from the evaporator tube wall, surface contact and fouling. Generally, the contact and fouling thermal resistance

could account for about 20% of the total thermal resistance in a heat exchanger. Therefore, it should not be neglected and a fixed value might be assumed.

The dehumidifying factor in Eq. (5.37) was evaluated by:

$$\zeta_a = 1 + 2.46 \times \frac{\omega_a - \omega_{az}}{T_a - T_{az}} \tag{5.38}$$

where ω_{az} is the moisture content of saturated air under temperature, T_{az}, and the average moisture content and temperature of air were:

$$\omega_a = \frac{(\omega_{az} + \omega_{a4I})}{2} \tag{5.39}$$

$$T_a = \frac{(T_{az} + T_{a4I})}{2} \tag{5.40}$$

The process line in a psychrometric chart for air cooling and dehumidification taking place in a DX cooling coil could be determined by using the state points of both the incoming air and saturated air at the tube-fin surface temperature. Once the process line was determined, the moisture content of exiting air, g_{a4I}, could be obtained from the exiting air temperature, T_{a4I}.

The following correlations provided by *Wang* [Wang et al. 2000] were selected to derive the sensible convective heat transfer coefficient for the louver-finned evaporator under wet-cooling conditions:

$$\alpha_{a,e,wt} = j_{e,wt}\rho_a \upsilon_{a,\max}\frac{C_{p,a}}{\mathrm{Pr}_a^{0.667}} \tag{5.41}$$

Where $j_{e,wt}$ is the *colburn* factor, and was calculated by:

$$j_{e,wt} = 9.717\mathrm{Re}_a^{j_1}\left(\frac{PI_{f,e}}{d_{c,e}}\right)^{j_2}\left(\frac{S_{2,e}}{S_{1,e}}\right)^{j_3}\left[\ln\left(3-\frac{PI_{L,e}}{PI_{f,e}}\right)\right]^{j_4} NR_e^{-0.543} \tag{5.42}$$

Where various correlation parameters are:

$$j_1 = -0.023634 - 1.2475\left(\frac{PI_{f,e}}{d_{c,e}}\right)^{0.65}\left(\frac{S_{2,e}}{S_{1,e}}\right)^{0.2} NR_e^{-0.18} \tag{5.43}$$

$$j_2 = 0.856\times e^{\tan\theta_l} \tag{5.44}$$

$$j_3 = 0.25\ln\left(\mathrm{Re}_a\right) \tag{5.45}$$

$$j_4 = 0.07162 \tag{5.46}$$

The fin surface efficiency was:

$$\eta_{a,e,wt} = 1 - \frac{A_{f,e}}{A_{tu,e}}\left(1-\eta_{f,e,wt}\right) \tag{5.47}$$

Where $A_{f,e}$ is the fin surface area, $A_{tu,e}$ the outside tube surface area. The existence of condensate within fin channels may increase the non-uniformity of the fin temperature, lowering the fin efficiency of an evaporator under a wet-cooling condition. The *Hong-Webb* Equation [Hong and Webb 1996] which took into

account the influence of condensate on heat transfer performance has been used to calculate the fin efficiency of the evaporator:

$$\eta_{f,e,wt} = \frac{th\left(\dot{m}_{e,wt}' h_e'\right) cos\left(0.1\dot{m}_{e,wt}' h_e'\right)}{\dot{m}_{e,wt}' h_e'} \tag{5.48}$$

$$\dot{m}_{e,wt}' = \sqrt{\frac{2\alpha_{a,e,wt}\zeta_a}{\lambda_{f,e}\delta_{f,e}}} \tag{5.49}$$

$$h_e' = 0.5 d_{o,e}\left(\frac{S_{tr,e}}{d_{o,e}} - 1\right)\left[1 + 0.35\ln\left(\frac{1.063 S_{tr,e}}{d_{o,e}}\right)\right] \tag{5.50}$$

where $\lambda_{f,e}$ is thermal conductivity tube-fin metal; $\delta_{f,e}$ the fin thickness; $S_{tr,e}$ the transverse tube pitch, $d_{o,e}$ the evaporator tube outside diameter.

b) Dry-cooling

Under a dry-cooling condition when the tube-fin surface temperature was above the dew point temperature of incoming air, no water vapor from air would be condensed. The mass and energy balances were given by:

$$\dot{m}_{az} = \dot{m}_{a4I} \tag{5.51}$$

$$\omega_{az} = \omega_{a4I} \tag{5.52}$$

$$\dot{m}_{az} h_{az} - Q_{a,e,dr} = \dot{m}_{a4I} h_{a4I} \tag{5.53}$$

The heat transfer between air and tube-fin metal in the two-phase region could be expressed as:

$$Q_{a,e,dr} = U_{a,e,dr} A_{a,e,tp} LMTD_{a,e,dr} \tag{5.54}$$

The log mean temperature difference, $LMTD_{a,e,dr}$, between the tube-fin and air was:

$$LMTD_{a,e,dr} = \frac{T_{az} - T_{a41}}{\ln\left[\frac{T_{az} - T_{wl,e,tp}}{T_{a41} - T_{wl,e,tp}}\right]} \tag{5.55}$$

where the overall heat transfer coefficient in Eq. (5.54) is:

$$U_{a,e,dr} = \frac{1}{\frac{1}{\alpha_{a,e,dr}\eta_{a,e,dr}} + R_e} \tag{5.56}$$

The fin surface efficiency was:

$$\eta_{a,e,dr} = 1 - \frac{A_{f,e}}{A_{tu,e}}\left(1 - \eta_{f,e,dr}\right) \tag{5.57}$$

The *Schmidt* Equation [Schmidt 1945] was used to determine the evaporator's fin efficiency under dry-cooling conditions:

$$\eta_{f,e,dr} = \frac{th\left(\dot{m}_{e,dr}' h_e'\right)}{\dot{m}_{e,dr}' h_e'} \tag{5.58}$$

$$\dot{m}_{e,dr}' = \sqrt{\frac{2\alpha_{a,e,dr}}{\lambda_{f,e}\delta_{f,e}}} \tag{5.59}$$

where h_e' could be calculated in the same way as that for the wet-cooling condition, using Eq. (5.50).

The correlations developed by Wang [Wang et al. 1999] for louver-finned evaporators under dry-cooling condition have been adopted to calculate the air side theoretical heat transfer coefficient, $\alpha_{a,e,dr}$,

$$\alpha_{a,e,dr} = j_{e,dr}\rho_a \upsilon_{a,\max} \frac{C_{p,a}}{\mathrm{Pr}_a^{0.667}} \tag{5.60}$$

$$j_{e,dr} = 1.1373\,\mathrm{Re}_a^{\,j_5}\left(\frac{PI_{f,e}}{S_{2,e}}\right)^{j_6}(\tan\theta_l)^{j_7}\left(\frac{S_{2,e}}{S_{1,e}}\right)^{j_8} NR_e^{\,0.3545} \tag{5.61}$$

where various correlation parameters are:

$$j_5 = -0.6027 + 0.02593\left(\frac{S_{2,e}}{d_{h,e}}\right)^{0.52} NR_e^{\,-0.5}\ln(\tan\theta_l) \tag{5.62}$$

$$j_6 = -0.4776 + 0.40774\left[\frac{NR_e^{\,0.7}}{\ln(\mathrm{Re}_a) - 4.4}\right] \tag{5.63}$$

$$j_7 = -0.58655\left(\frac{PI_{f,e}}{d_{h,e}}\right)^{2.3}\left(\frac{S_{2,e}}{S_{1,e}}\right)^{-1.6} NR_e^{\,-0.65} \tag{5.64}$$

$$j_8 = 0.0814\left[\ln\left(\mathrm{Re}_a\right) - 3\right] \tag{5.65}$$

By solving these correlations and using air State Equations, the temperature and moisture content of the air exiting the evaporator could be obtained.

5.2.1.4 Sub-model for condenser

The condenser in this DEAC system was air-cooled and of plate-fin-tube type and its conceptual model is shown in Fig. 5.2. Counter-flow heat exchange was assumed between the refrigerant and cooling air. According to the state of refrigerant, the condenser was divided into three regions, i.e., a de-superheating region, a two-phase region and a subcooling region. The superheated vapour refrigerant discharged from the compressor was cooled to become saturated vapour refrigerant and then flowed into the two-phase region. Afterwards, the refrigerant became sub-cooled.

The modeling processes in the de-superheating and the two-phase regions of the condenser on refrigerant side were similar to that in the superheated and two-phase regions of the evaporator. Since the degree of refrigerant subcooling inside the condenser was usually set within a certain range by using a control valve to best use the condenser and avoid refrigerant flashing, a fixed value was adopted. This could simplify the simulation with an acceptable accuracy. Since the condenser was used to reject heat, its fined surface was therefore regarded as fully dry. The heat transfer equations for the air side of the condenser were therefore similar to those on the air side of evaporator under a dry-cooling condition.

5.2.1.4.1 Refrigerant side of de-superheating region

Counter-flow heat transfer was assumed to take place between the refrigerant and the tube wall in this region. The energy and mass conservation equations were given as follows:

$$\dot{m}_{r3} = \dot{m}_{rx} \tag{5.66}$$

$$\dot{m}_{r3} h_{r3} = \dot{m}_{rx} h_{rx} + Q_{r,c,ds} \tag{5.67}$$

The heat transfer rate in the de-superheating region could be evaluated by using the log mean temperature difference between the refrigerant and the corresponding tube wall,

$$Q_{r,c,ds} = \alpha_{r,c,ds} A_{r,c,ds} LMTD_{r,c,ds} \tag{5.68}$$

where $LMTD_{r,c,ds}$ is calculated by:

$$LMTD_{r,c,ds} = \frac{T_{r3} - T_{rx}}{\ln\left[\frac{T_{r3} - T_{wl,c,ds}}{T_{rx} - T_{wl,c,ds}}\right]} \tag{5.69}$$

The refrigerant flow inside the tube could be regarded as being fully developed turbulent. The heat transfer coefficient in the de-superheating region was calculated using the *Petukhov-Popov* Equation [Baughn and Roby 1992]:

$$\alpha_{r,c,ds} = \lambda_r \times \frac{Nu_{r,ds}}{d_{i,c}} \quad (\mathrm{Re}=10^4\sim5\times10^6,\ \mathrm{Pr}=0.5\sim2000) \tag{5.70}$$

where λ_r is the thermal conductivity of refrigerant. The *Nusselt* number was:

$$Nu_{r,ds} = \frac{\left(\frac{f_c}{8}\right)\mathrm{Re}_{r,ds}\ \mathrm{Pr}_{r,ds}}{1+3.4f_c+\left(11.7+\frac{1.8}{\mathrm{Pr}_{r,ds}^{\ 0.333}}\right)\left(\frac{f_c}{8}\right)^{0.5}\left(\mathrm{Pr}_{r,ds}^{\ 0.667}-1\right)} \tag{5.71}$$

Where f_c is the predicted turbulent skin-friction factor, defined as:

$$f_c = \left[1.82\times\lg\left(\mathrm{Re}_{r,ds}\right)-1.64\right]^{-2} \tag{5.72}$$

5.2.1.4.2 Refrigerant side of two-phase region

Similarly, the mass and energy balances of this region yielded:

$$\dot{m}_{rx} = \dot{m}_{ry} \tag{5.73}$$

$$\dot{m}_{rx}h_{rx} = \dot{m}_{ry}h_{ry} + Q_{r,c,tp} \tag{5.74}$$

The heat transfer rate in the two-phase region, $Q_{r,c,tp}$, was calculated using:

$$Q_{r,c,tp} = \alpha_{r,c,tp}A_{r,c,tp}\Delta T_{r.c.tp} \tag{5.75}$$

The corresponding convective heat transfer coefficient, $\alpha_{r,c,tp}$, could be derived by *Nusselt* heat transfer equation for laminar flow [Zhang 1986]:

$$\alpha_{r,c,tp} = 0.555 \times r_c^{0.25} B_m \left(T_{r,c,tp} - T_{wl,c,tp}\right)^{-0.25} d_{i,c}^{-0.25} \tag{5.76}$$

where r_c is the refrigerant latent heat of vaporization and B_m the integrated refrigerant thermophysical property obtained by:

$$B_m = \left(\frac{9.81 \times \rho_r^{\,2} \lambda_r^{\,3}}{\mu_r}\right)^{0.25} \tag{5.77}$$

5.2.1.4.3 Refrigerant side of sub-cooling region

The mass and energy conservation equations were given by:

$$\dot{m}_{ry} = \dot{m}_{r4} \tag{5.78}$$

$$\dot{m}_{ry} h_{ry} = \dot{m}_{r4} h_{r4} + Q_{r,c,sc} \tag{5.79}$$

The heat transfer in the sub-cooling region was calculated as:

$$Q_{r,c,sc} = \alpha_{r,c,sc} A_{r,c,sc} LMTD_{r,c,sc} \tag{5.80}$$

The log mean temperature difference was calculated by:

$$LMTD_{r,c,sc} = \frac{T_{ry} - T_{r4}}{\ln\left(\frac{T_{ry} - T_{wl,c,sc}}{T_{r4} - T_{wl,c,sc}}\right)} \tag{5.81}$$

The refrigerant flow inside the tube could be regarded as being fully-developed turbulent. The heat transfer coefficient for the sub-cooled liquid refrigerant was evaluated using the *Dittus-Boelter* Equation [Kay and London 1984]:

$$Nu_{r,sc} = 0.023 \times \mathrm{Re}_{r,sc}^{0.8} \mathrm{Pr}_{r,sc}^{0.3} \quad (\mathrm{Re}=10^4 \sim 1.2\times10^5,\ \mathrm{Pr}=0.7\sim100) \tag{5.82}$$

5.2.1.4.4 Air side of the condenser

Since in a condenser the moisture content of cooling air forced across the condenser remained unchanged, the mass balance of air flow was given by:

$$\dot{m}_{a1} = \dot{m}_{a2} \tag{5.83}$$

It was assumed that the same overall heat transfer coefficient, $U_{a,c}$, between the tube-fin and cooling air was applied to all the regions in the condenser:

$$U_{a,c} = \frac{1}{\frac{1}{\alpha_{a,c}\eta_{a,c}} + R_c} \tag{5.84}$$

where R_c is the combined total thermal resistance from the tube wall, surface contact and fouling. Furthermore, when deriving the actual average convective heat transfer coefficient between tube-fin and cooling air, the surface coefficient of the condenser

tube-fin and cooling air, $\eta_{a,c}$, which accounted for the non-homogeneous temperature distribution over the plate-fin, was used:

$$\eta_{a,c} = 1 - \frac{A_{f,c}}{A_{tu,c}}\left(1 - \eta_{f,c}\right) \tag{5.85}$$

The fin efficiency, $\eta_{f,c}$, of the condenser's plate-fin was calculated by the *Schmidt* Equation [Schmidt 1945]:

$$\eta_{f,c} = \frac{th(m_c^{'} h_c^{'})}{m_c^{'} h_c^{'}} \tag{5.86}$$

where h_c' and m_c' could be calculated in the same way as that of an evaporator for the dry-cooling condition. The air heat transfer coefficient for forced convection was calculated by the *McQuiston* Equation [McQuiston 1978]:

$$\alpha_{a,c} = 0.0014 + 0.2168\,\mathrm{Re}_a - 0.4 \times \left(\frac{A_{o,c}}{A_{tu,c}}\right)^{-0.15} \tag{5.87}$$

where the *Reynolds* Number for air flow is:

$$\mathrm{Re}_a = \frac{\rho_a \upsilon_{a,\max} d_{o,c}}{\mu_a} \tag{5.88}$$

The heat transfer between the condenser tube-fin and cooling air was thus evaluated by:

$$Q_{a,c} = U_{a,c} A_{a,c} LMTD_{a,c} \tag{5.89}$$

where the log mean temperature difference between the tube-fin and cooling air in the de-superheating region was:

$$LMTD_{a,c} = \frac{T_{a2} - T_{a1}}{\ln\left(\frac{T_{a2} - T_{wl,c}}{T_{a1} - T_{wl,c}}\right)} \tag{5.90}$$

5.2.2 Development of the sub-model for evaluating pressure losses along the refrigerant pipelines and components in the DEAC system

Refrigerant pipelines might be classified into a liquid line, a suction line, a discharge line and a two-phase line, according to their locations and the refrigerant state inside, as shown in Fig. 5.2.

The refrigerant in a liquid line, a suction line or a discharge line was of single-phase state, and the total pressure loss was the sum of the friction losses along the pipelines and passing through fittings (valves, elbows, tees, mass flow meters, etc.) and section changes (contractions or expansions). The *Darcy-Weisbach* Equation [Brown 2002] was applied to each of the single-phase pipelines to calculate its pressure loss. Taking the pipeline between points 5*I* and 6*I* (a liquid line with a fixed diameter) as an example, its pressure drop could be evaluated as follows:

$$\Delta P_{5I-6I} = \frac{1}{2\rho_{r,5I-6I}} \left[f_{5I-6I} \frac{l_{5I-6I}}{d_i} + \zeta_{5I-6I} \right] \left(\frac{4\dot{m}_r}{\pi d_i} \right)^2 \tag{5.91}$$

For a two-phase pipeline, Brown [2002] recommended the following equation to calculate pressure drop for R22, which consisted of not only friction losses as in single phase pipelines, but also the kinetic energy change caused by refrigerant state change. Taking the pipeline between points 7*I* and 8*I* (a two-phase line with a fixed diameter) as an example, its pressure drop could be evaluated as follows:

$$\Delta P_{7I-8I} = \frac{1}{2\rho_{r,7I-8I}}\left[f_{7I-8I}\frac{l_{7I-8I}}{d_i} + \varsigma_{7I-8I} + \frac{2\left(\chi_{8I}-\chi_{7I}\right)}{\bar{\chi}}\right]\left(\frac{4\dot{m}_r}{\pi d_i}\right)^2 \tag{5.92}$$

In Eqs. (5.91) and (5.92), the local friction coefficient, ς, covers the contributions from all the fittings used in pipelines, and could be obtained from ASHRAE Handbook [Wile 1947, Baines and Peterson 1951, Deissler 1951, Ito 1962, ASHRAE Handbook 2009]. Further, *f* is a friction factor of pipes, and the relationship developed by Churchill [1973] to evaluate the value of *f*, which is valid for all ranges of *Reynolds* numbers, was used:

$$f = 8\left[\left(\frac{8}{\mathrm{Re}}\right)^{12} + \frac{1}{\left(K1+K2\right)^{1.5}}\right]^{\frac{1}{12}} \tag{5.93}$$

$$K1 = \left[2.457\ln\left(\frac{1}{\left(\frac{7}{\mathrm{Re}}\right)^{0.9} + \left(\frac{0.27\varepsilon}{d_i}\right)}\right)\right]^{16} \tag{5.94}$$

$$K2 = \left(\frac{37530}{\mathrm{Re}}\right)^{16} \tag{5.95}$$

Where the pipeline absolute roughness, ε, could be obtained from ASHRAE Handbook [2009].

The use of the Eqs. (5.91) and (5.92) can be extended to evaluating the pressure drops along the other pipelines in the DEAC system, as shown in Fig. 5.2. It was further assumed that all pipelines were thermally insulated, so that there was no heat exchange with the ambient.

Furthermore, the use of Eqs. (5.91) and (5.92) was also extended to evaluating the pressure losses in an evaporator and a condenser by changing the inlet and outlet dryness fraction of refrigerant. The refrigerant entered the condenser as superheated vapor and left as subcooled liquid, thus the dryness fractions of refrigerant at condenser inlet and outlet were 1 and 0, respectively. Similarly, the refrigerant left an evaporator as superheated vapor with a dryness fraction of 1. The inlet dryness fraction to an evaporator was evaluated based on the inlet enthalpy and pressure of refrigerant.

5.3 Calculation procedure of the DEAC system model developed

The complete DEAC model, as detailed in Section 5.2, had a flexible configuration, which would therefore enable the extension of DEAC system modeling to modeling an MEAC system having more than two numbers of evaporators by adding one or more branches.

As expected, the calculation procedure for solving the DEAC model developed was more complicated than that for an SEAC model. Sequential solving method was

therefore used to solve the complete DEAC system model, since when using this solving method only the knowledge of how the component sub-models were connected was required. The detailed explanations for the calculation procedures are given below.

The flow chart for solving the complete DEAC system model is shown in Fig. 5.3. When solving the complete DEAC system model, the DEAC system was considered to have two parallel evaporator branches, separated at Point 5 and merged at Point 0. In each branch, there was an evaporator, an EEV, connecting refrigerant pipelines and fittings. The initial values of both the total refrigerant mass flow rate, i.e., the refrigerant mass flow rate passing through the compressor, $\dot{m}_{r,1}$, and the compressor discharge pressure, $P_{r,1}$, were firstly assumed. The pressure drop along pipeline 2-3 could be evaluated, and both the pressure loss and heat exchange process in the condenser could be calculated by the sub-model of condenser, whose calculation procedures would be described later.

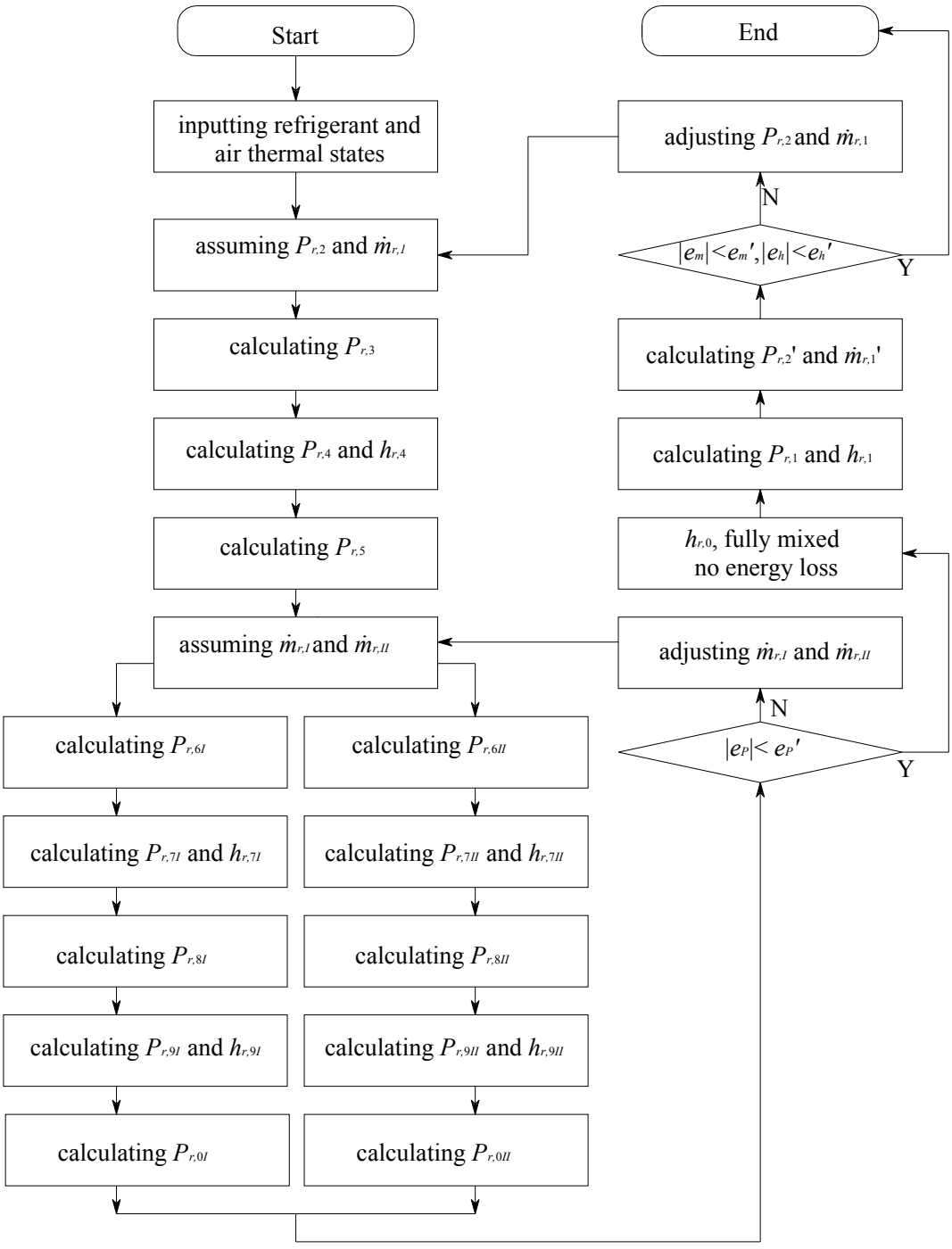

Fig. 5.3 Flow chart of the calculation procedure of the complete DEAC system model

After the pressure drop along pipeline 4-5 was evaluated, the refrigerant mass flow rates in each branch, $\dot{m}_{r,I}$ and $\dot{m}_{r,II}$ were assumed. Then the pressure drop along pipelines in Branch *I* and *II*, i.e., the refrigerant pressures at each branch outlet, $P_{r,0I}$, and $P_{r,0II}$, could be evaluated by solving the pressure drop equations and the evaporator sub-model, whose calculation procedures would also be described later. Since the two branches were connected in parallel to a common compressor and a condenser, the refrigerant pressure at each branch outlet should be equal to each other, and a change in one branch would cause the change in the other. This coupling effect determined the distribution of refrigerant mass flow rate to each branch. Therefore, the assumed mass flow rate for each branch should be updated using the Relaxation Algorithm [Zheng 2006] to ensure that $P_{r,0I}$ was equal to $P_{r,0II}$.

It was assumed that after leaving the two branches, the refrigerant was fully mixed but no energy was lost during mixing. The enthalpy of the mixed refrigerant at point 0 could then be evaluated based on energy balance. Then, the pressure drop along pipeline 0-1 was evaluated using Eq. (5.91), and the refrigerant thermal state at compressor suction, i.e., point 1 in Fig. 5.2, could be obtained using refrigerant State Equations [Wagner 1993]. By knowing the refrigerant pressure and enthalpy at compressor suction, $P_{r,1}$, $h_{r,1}$, and the assumed discharge pressure, $P_{r,2}$, a new refrigerant mass flow rate, $\dot{m}_{r,1}'$ and new discharge enthalpy $h_{r,2}^{'}$, would be obtained by solving the compressor sub-model. The assumed values of $\dot{m}_{r,1}$ and $P_{r,2}$ could then be updated.

The relative errors, e_p, e_m and e_h, for each calculating iteration were defined as follows:

$$e_P = \frac{P_{r,0I} - P_{r,0II}}{P_{r,0I}} \tag{5.96}$$

$$e_m = \frac{\dot{m}_{r,1} - \dot{m}_{r,1}'}{m_{r,1}} \tag{5.97}$$

$$e_h = \frac{h_{r,2} - h_{r,2}'}{h_{r,2}} \tag{5.98}$$

When these relative errors were less than their respective preset acceptable values, e_p', e_m', e_h', an iterative calculation process was ended.

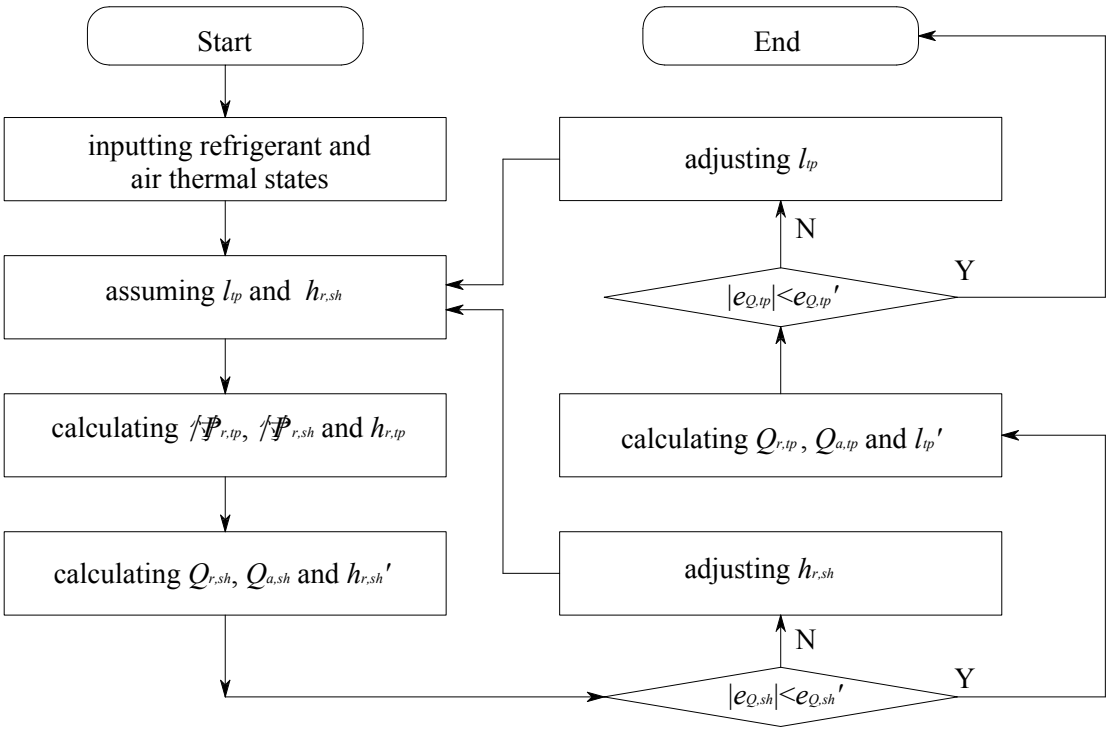

Fig. 5.4 Flow chart of the calculation procedure of an evaporator model

During solving the complete DEAC system model, solving an evaporator sub-model was needed and its calculation procedure is shown in Fig. 5.4. The refrigerant thermal states (i.e., pressure, temperature and enthalpy), as well as its mass flow rate, would be firstly input using the outcomes from solving the complete DEAC model. In addition, the air thermal states (i.e., temperature and humidity), as well as its mass flow rate at evaporator inlet were set as constants, based on the thermal settings in the two rooms. Initial values of the length of two-phase region in an evaporator, l_{tp}, and refrigerant enthalpy at the exit of the superheated region, $h_{r,sh}$, were respectively assumed. Afterwards, the pressure drops along both the two-phase region, $\Delta P_{r,tp}$, and the superheated region, $\Delta P_{r,sh}$, could be evaluated using Eqs (5.91) and (5.92), and thermal states of refrigerant at the exits of both two-phase region and superheated region by State Equations [Wagner 1993]. By chasing the energy balances between air side and refrigerant side in both regions, the assumed values of the two parameters, i.e., l_{tp}, and $h_{r,sh}$, could be updated.

The relative errors, $e_{Q,sh}$ and $e_{Q,tp}$, for each calculating iteration were defined as follows:

$$e_{Q,sh} = \frac{Q_{r,sh} - Q_{a,sh}}{Q_{r,sh}} \tag{5.99}$$

$$e_{Q,tp} = \frac{Q_{r,tp} - Q_{a,tp}}{Q_{r,tp}} \tag{5.100}$$

When these relative errors were less than their respective preset acceptable values, $e_{Q,sh}'$ and $e_{Q,tp}'$, an iterative calculation process was ended.

Furthermore, to solve the condenser sub-model, the inlet refrigerant pressure and mass flow rate, a fixed setting of degree of refrigerant sub-cooling and the inlet air thermal states were firstly input. Then the initial values of three parameters, i.e., the inlet refrigerant enthalpy, the lengths of both subcooled region and two-phase region, were assumed. The length of the superheated region may then be evaluated. Similar to the calculation procedure for an evaporator sub-model, the pressure drops and the refrigerant thermal states at the inlet and outlet of each region could be evaluated. By chasing the energy balance between air side and refrigerant side in the three regions, the assumed values of the three parameters could be updated.

5.4 Model validation

The validation of the DEAC model developed was performed by comparing its simulation results with the experimental data from Choi and Kim [2003], where the performance of an inverter-driven multi-air conditioner with two indoor units was tested by varying the EEV opening and indoor thermal loads. When validating the current DEAC model, model's parameters settings followed exactly the experimental conditions used in Choi and Kim's study [2003]. Figures. 5.5 and 5.6 show the comparisons between the predictions using the DEAC model developed and Choi and Kim's experimental results in terms of refrigerant mass flow rate and cooling capacity, respectively, as a function of EEV *I* opening, for Indoor Unit *I* and Indoor Unit *II*. It can be seen from the diagrams that the differences between simulation results and experimental data were all less than 10% for refrigerant mass flow rate and cooling capacity, suggesting that the DEAC model developed can well represent the operational performance of a real DEAC system.

It should be mentioned here that the DEAC experimental rig reported in Chapter 4 was not used for validating this DEAC system model, since the refrigerant pipe length in the DEAC experimental rig was not long enough for a meaningful validation. On the other hand, previous experimental results by others were readily available, enabling the experimental validations as shown in Fig. 5.5 and Fig. 5.6.

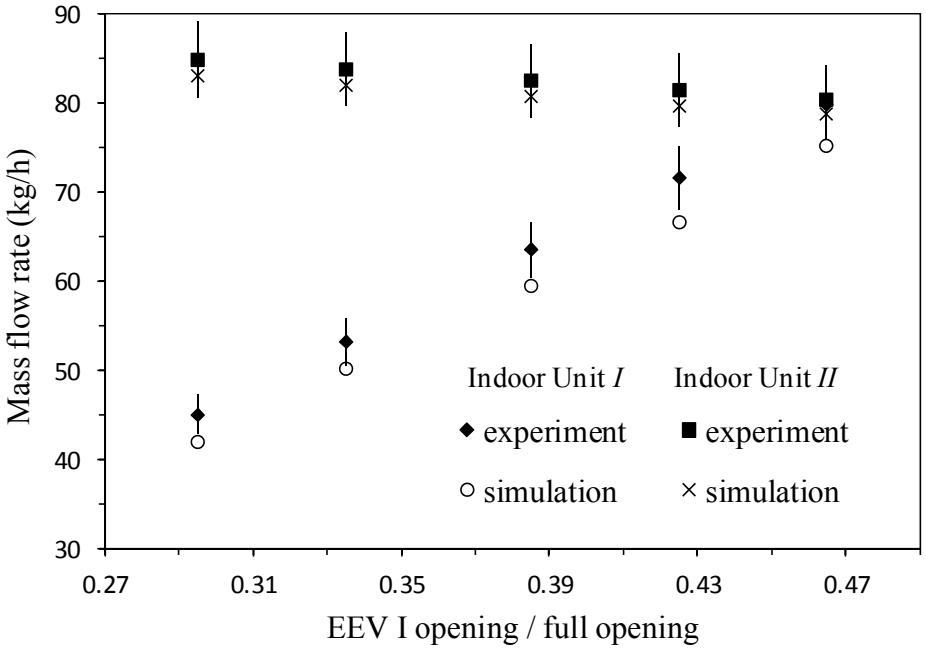

Fig. 5.5 Comparison of Choi and Kim's experimental data [2003] and simulation results: refrigerant mass flow rate

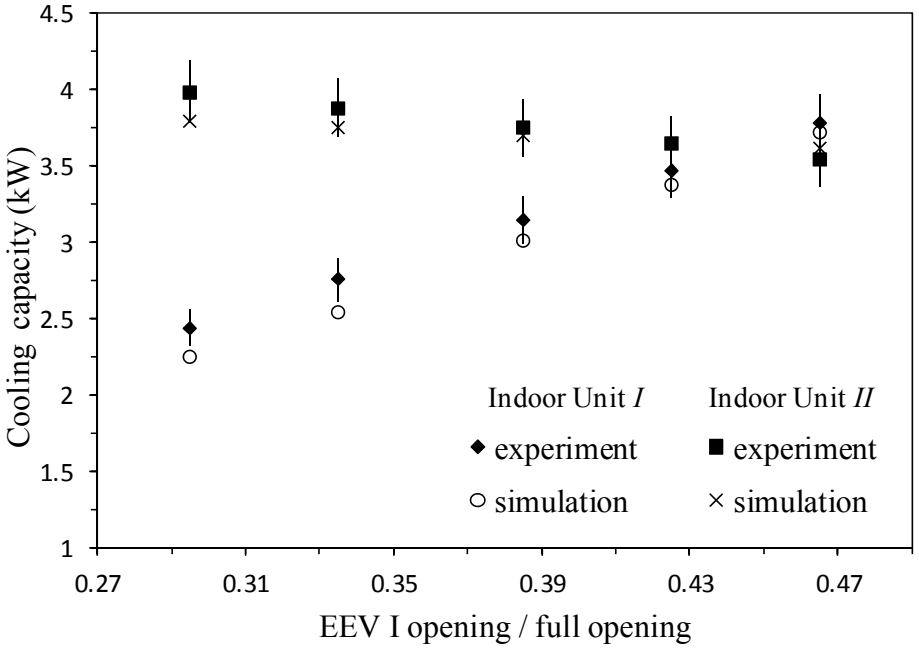

Fig. 5.6 Comparison of Choi and Kim's experimental data [2003] and simulation results: cooling capacity

5.5 Model application

Since a special sub-module on accounting for the pressure losses along refrigerant pipelines and components was included in the DEAC model developed, it can be applied to studying the effects of refrigerant pipeline length on the operational performance of a DEAC system and to optimizing the layout design of a DEAC system, both being the focus of the study reported in this chapter.

5.5.1 The influence of refrigerant pipeline length in evaporator branch on system performance

To study the influence of refrigerant pipeline length on system performance, the length of two selected pipes in Branch *I*, i.e., pipelines 5-6*I* and 9*I*-0, was each identical and varied from 2 to 20 m at an increment of 2 m, with the lengths of all other pipelines remained unchanged, as shown Table 5.2. It should be noted that the two selected pipelines were the supply and return pipes, therefore their changes were synchronized. This is to say, when the length of pipeline 5-6*I* was increased by 10 m; the length of pipeline 9*I*-0 would also be increased by 10 m, and vice versa. The thermal states and mass flow rate of inlet air to the condenser and evaporators used in simulation are shown in Table 5.3. The openings of two EEVs were fixed at a constant value.

COP, as defined by Eq. (5.101) was used to evaluate the system performance:

$$COP = \frac{Q_{r,e,tp} + Q_{r,e,sh}}{W_{cm}} \tag{5.101}$$

Fig. 5.7 shows the variations of refrigerant pressure with an increase in the length of refrigerant pipelines in Branch *I*. It can be seen that evaporating pressure in Branch *I* changed remarkably, but evaporating pressure in Branch *II*, suction pressure and condensing pressure only slightly changed. When the length of the two selected pipelines in Branch *I* was each increased from 2 to 20 m, the evaporating pressure in Branch *I* increased from 5.49 to 7.18 bar in order to overcome the increase in pressure loss in the branch. Consequently, evaporating temperature in Branch *I*

increased from 4.05 to 12.74 °C. This would decrease the temperature difference between the refrigerant and air in Evaporator *I*, deteriorating the heat transfer between the two. Furthermore, due to the coupling effect between the two evaporators, evaporating pressure in Branch *II* slightly reduced from 5.91 to 5.78 bar, while the operating conditions at Branch *II* remained unchanged

Table 5.2 Detailed configuration for refrigerant pipelines in the DEAC system modeled

	pipeline No.	l (m)	d_i (mm)	ς*(-)
Branch *I*	5-6*I*	from 2 to 20	9.30	6.756
	7*I*-8*I*	1	9.30	2.252
	9*I*-0	from 2 to 20	9.30	2.252
Branch *II*	5-6*II*	6	9.30	6.756
	7*II*-8*II*	1	9.30	2.252
	9*II*-0	6	9.30	2.252
Outdoor pipelines	0-1	1	9.30	3.378
	2-3	1	9.30	3.378
	4-5	1	9.30	3.378

* The local friction coefficient for all fittings

Table 5.3 Thermal states and mass flow rates of inlet air to condenser and indoor units

	T (℃)	RH (%)	$\dot{m}_a$ (kg/s)
Outdoor unit	35.00	60	0.389
Indoor unit *I*	25.00	60	0.200
Indoor unit *II*	25.00	60	0.200

The change in flow resistance due to the change in pipeline length in two branches would cause the re-distribution of refrigerant mass flow rate, as shown in Fig. 5.8. As seen, due to the increase in flow resistance in Branch *I*, less refrigerant would flow through the Branch *I*, forcing more refrigerant to enter Branch *II*. The mass flow rate in Evaporator *I* dropped from 0.0141 to 0.0138 kg/s, while that in Evaporator *II* increased from 0.0139 to 0.0143 kg/s when the length of the two selected pipelines in Branch *I* was each increased from 2 to 20 m. It should be noted however that the total refrigerant mass flow rate remained virtually unchanged during the re-distribution of the refrigerant mass flow rate to two evaporators, since the operating condition for compressor remained also virtually unchanged.

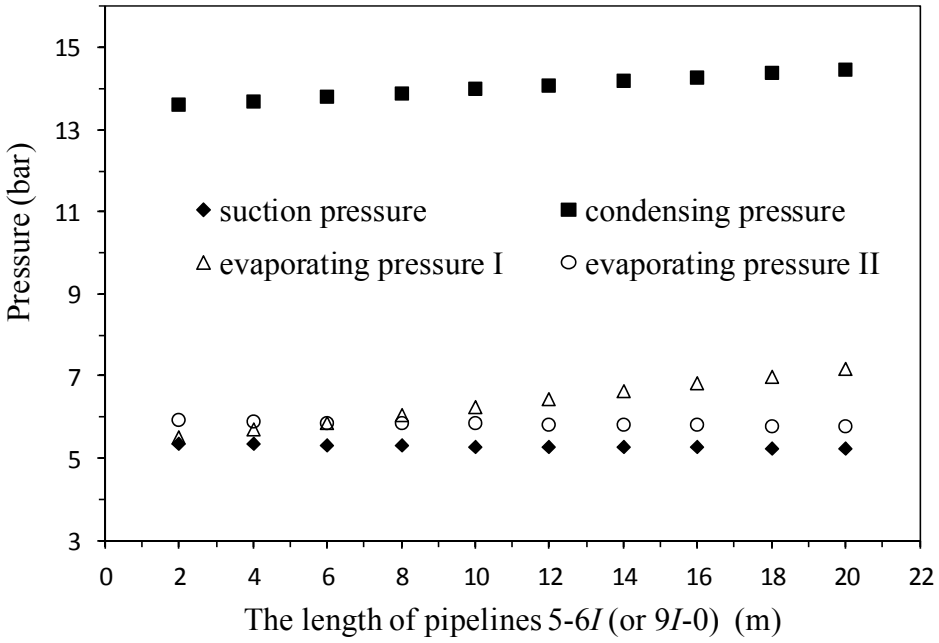

Fig. 5.7 Variations of pressure with the increase in the length of refrigerant pipelines in Branch *I*

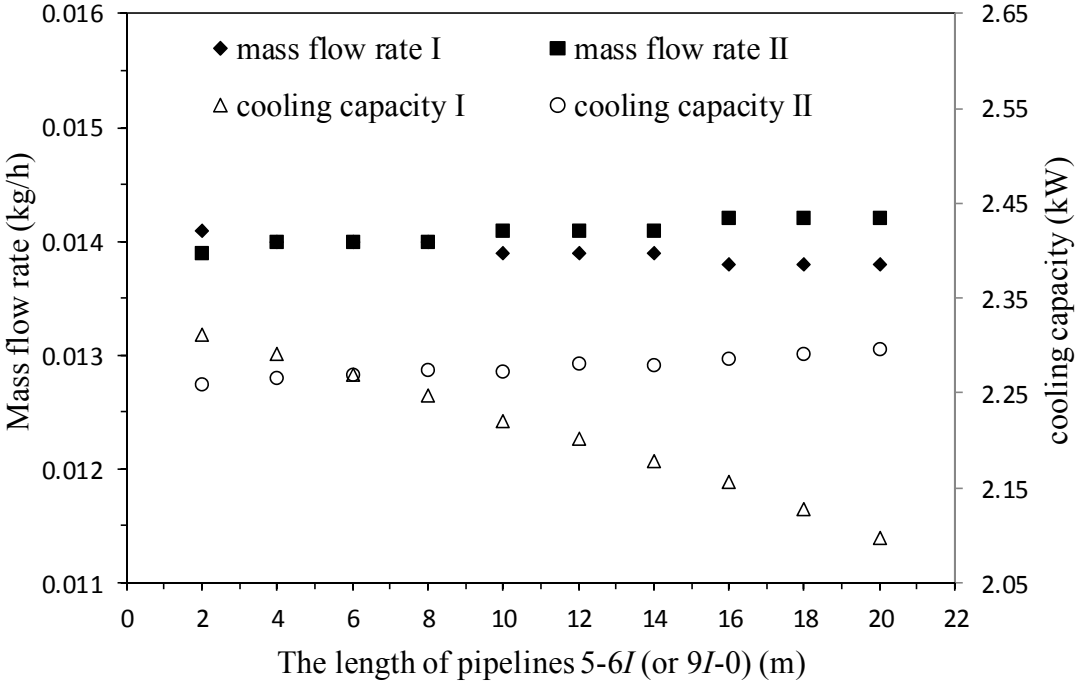

Fig. 5.8 Variations of mass flow rate and cooling capacity with the increase in the length of refrigerant pipelines in Branch *I*

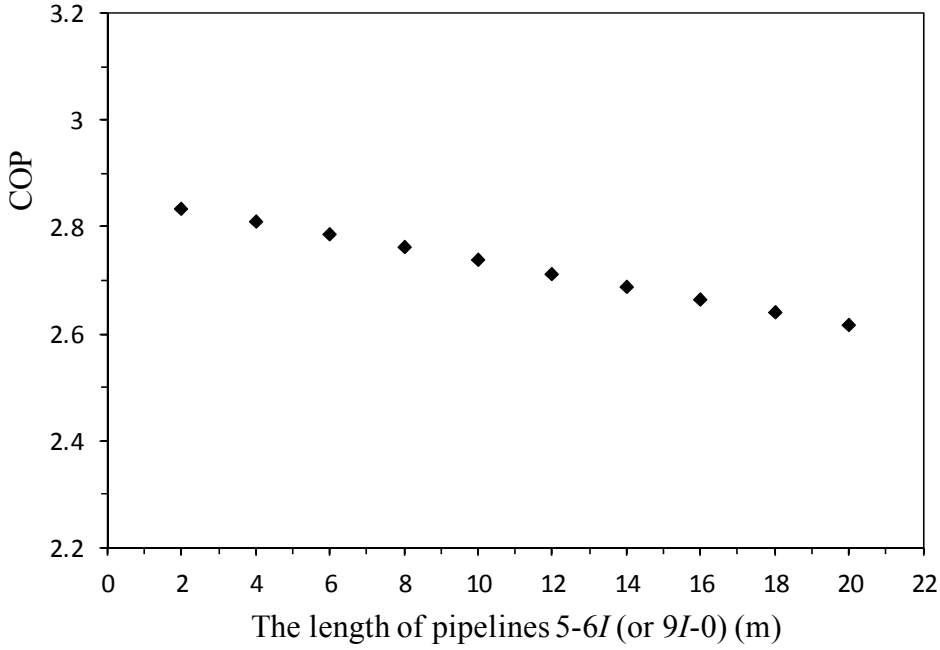

Fig. 5.9 Variation of COP with the increase in the length of refrigerant pipelines in Branch *I*

The re-distribution of refrigerant mass flow rate would certainly influence the cooling capacities of the two evaporators when the pipeline length in Branch *I* increased from 2 to 20 m. The cooling capacity of Evaporator *I* dropped from 2.31 to 2.10 kW, while that in Evaporator *II* increased from 2.26 to 2.30 kW, with the total cooling capacity reduced from 4.57 to 4.40 kW. Moreover, with the decrease in the total cooling capacity, the COP of the DEAC system also decreased with the increase in refrigerant line length Branch *I*, as shown in Fig. 5.9. When the length of the two selected pipelines was each increased from 2 to 20 m, the COP of the DEAC system dropped from 2.84 to 2.62, or a 7.7% reduction. In practical applications, keeping refrigerant pipeline of a DEAC system as short as possible would help not only increase the system energy efficiency but also save the initial installation cost.

5.5.2 Optimization of the layout design of a DEAC system

The optimization in the layout design for a DEAC system was studied using the DEAC model developed. According to the results obtained in Section 5.5.1, it was clear that a longer pipeline would result in a lower COP. Therefore, using fewer pipelines with a shorter length in a DEAC system could help achieve a higher system performance, therefore an outdoor unit should be best located between the two indoor units after their locations were fixed. Figure. 5.10 shows the location arrangement of outdoor unit studied using the DEAC model developed, with the distance between two rooms fixed at 20 m. The length of the two pipelines in Branch *I* (i.e., pipeline 5-6*I* and 9*I*-0) was each increased from 2 to 18 m at an increment of 2 m while that in Branch *II* (i.e., pipeline 5-6*II* and 9*II*-0) was each reduced from 18 to 2 m also at increment of 2 m, so that the total length of the two branches remained unchanged. The other conditions used in the study were the same as those in Section 5.5.1.

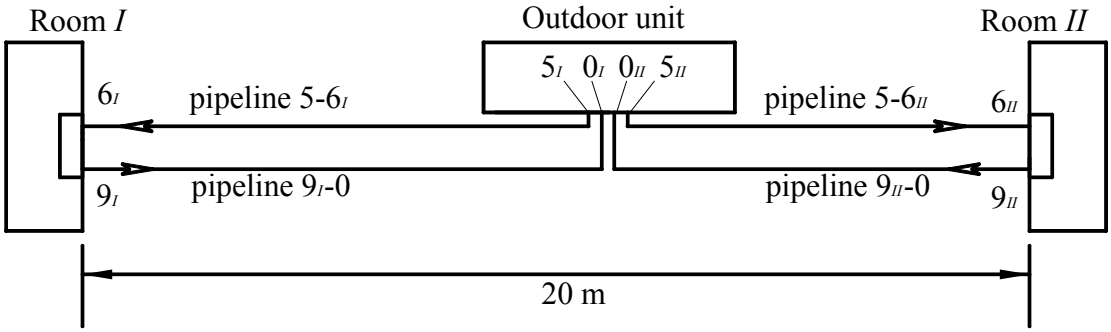

Fig. 5.10 The arrangement of outdoor unit location in a DEAC system

Fig. 5.11 shows the variations of pressure with the ratio of the length of pipeline 5-6*I* over the room distance of 20 m. It could be seen that while suction pressure and

condensing pressure did not change much at 5.2 bar and 14.2 bar, respectively, evaporating pressures in both evaporators were remarkably changed. The relatively stable suction and condensing pressure resulted however from the fact that the total length of pipelines in the DEAC system remained the same. Hence, the total pressure loss in the system remained unchanged although in each of the two branches, its pressure loss might be different. Evaporating pressure in Branch *I* was increased from 5.41 to 7.01 bar and evaporating pressure in Branch *II* was decreased from 7.01 to 5.41 bar, due to the increase in the length in both pipelines in Branch *I* from 2 to 18 m and the decrease in the length in both pipelines in Branch *II* from 18 to 2 m. When the pipeline lengths in the two branches were the same, the evaporating pressures in both evaporators were the same, at 6.21 bar.

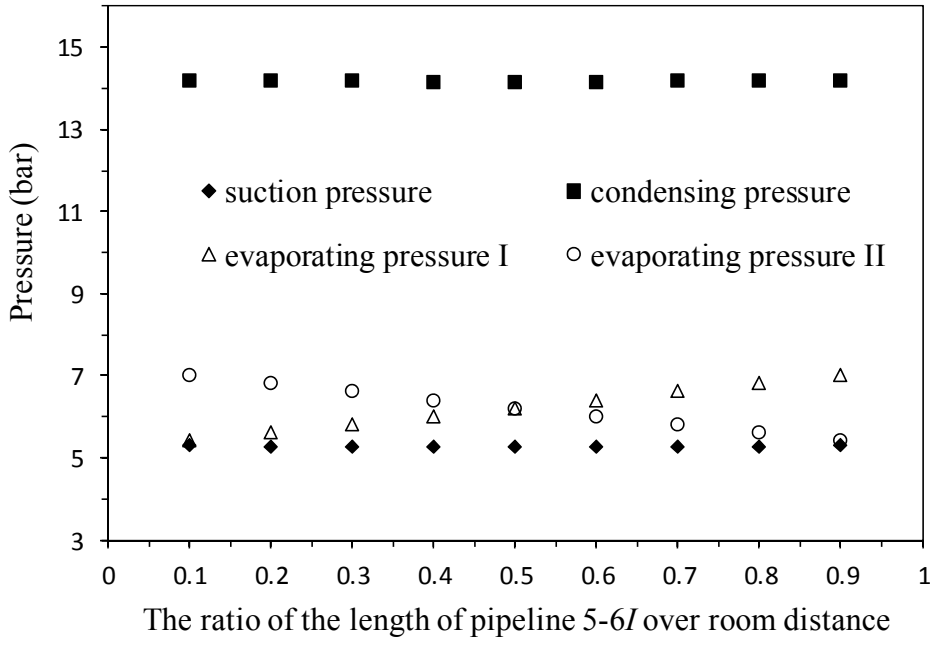

Fig. 5.11 Variations of pressure with the ratio of the length of pipeline 5-6*I* over room distance

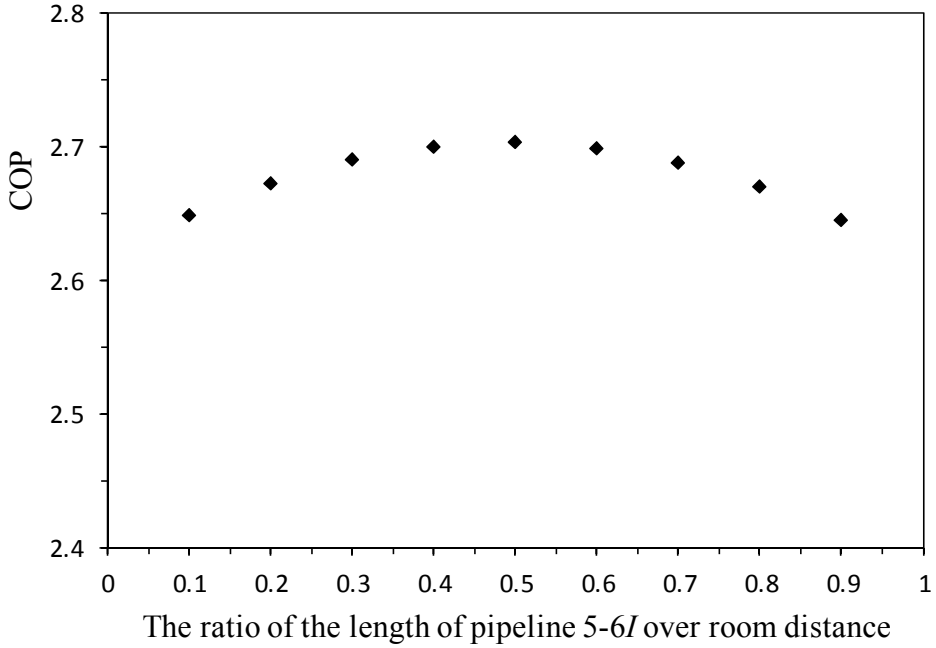

Fig. 5.12 Variation of COP with the ratio of the length of pipeline 5-6*I* over room distance

Figure 5.12 shows the variation of the DEAC system's COP with the ratio of the length of pipeline 5-6*I* over the room distance of 20 m. It could be seen that the highest system's COP would be resulted in when the outdoor unit was located equally between the two indoor units and the lowest COP resulted in when the outdoor unit was located close to either of the indoor unit. This suggested that although the total length of the refrigerant pipelines remained the same, the different layout of outdoor unit, resulting in different pipeline lengths, would also influence system's COP. Theoretically, the system COP could be increased through layout optimization without any additional cost. In this study, the COP increased from 2.65 to 2.70 when the outdoor unit was positioned from close to either indoor unit to right in the middle between the two indoor units.

5.6 Discussions

In this Chapter, using the DEAC model developed, both the impact of refrigerant pipeline length on the operational performance and the layout optimization of a DEAC system have been investigated. For the former case, the change in the length of refrigerant pipeline in the modeling study was only up to 20 m, and a reduction in COP of 7.7% was suggested by simulation. In practice, the actual length of refrigerant pipeline may however be much longer; therefore, the impact on system operational efficiency can be much more significant, and efforts should therefore be paid to minimizing pipe length as much as possible. For the latter case, it appeared when there were multiple branches, care should be exercised not to make excessive pressure drop in any single branch, but to ensure that all branches should experience a pressure drop of similar magnitude.

Furthermore, for both cases, pressure drops along refrigerant pipelines may be reduced by using pipes of larger diameters, under a given required pipe length. However, this would incur additional costs for larger diameter pipelines and their fittings, and may be further investigated.

5.7 Conclusions

A modeling study on the effects of refrigerant pipeline length on the operational performance of a DEAC system has been carried out and is reported in this Chapter. Simulation results indicated that the DEAC system's COP decreased with an increase in the refrigerant pipeline length. The simulation results also suggested that

for a DEAC system, its highest COP would be resulted in when the outdoor unit was located equally between the two indoor units and its lowest COP when the outdoor unit was located close to either of the indoor unit.

The outcomes from the study presented in this Chapter clearly suggest that different refrigerant pipework design in an MEAC system would significantly affect its operational performance, and this deserves more research attention from fundamental thermodynamic point of view. Therefore, in the next Chapter, an analytical study on applying the Constructal Theory to discovering the highest operational efficiency for an MEAC system is presented.

Chapter 6

The application of the Constructal Theory to the design of MEAC systems: a thermodynamic analysis approach

6.1 Introduction

The modeling study presented in Chapter 5 clearly suggested that when a large-scale pipework is present in a DX A/C system, the refrigerant pressure drop along pipelines can be significant, impacting system performance. This is particularly true for an MEAC system whose pipework is more complicated than that in an SEAC system. The current research literature does not contain too much information on the refrigerant pipework in MEAC systems and its influence on system performance.

The study reported in Chapter 5 identified the effects of refrigerant pipeline length on the operational performance of a DEAC system. The simulation results suggest that for the DEAC system, its highest COP will be obtained when the outdoor unit is located equally between the two indoor units; and its lowest COP when the outdoor unit is located close to either of the indoor unit. This suggests that more research attention be paid to the layout design of the refrigerant pipeline in an MEAC system.

The Constructal Theory teaches how to construct the flow architecture and provides a new way of thinking with epistemological and philosophical implications. This theory holds that every flow system exits with purpose (or objective, function). The constructal designs allow the system to flow more easily, to measurably move more

current farther and faster for less unit of useful energy consumed [Bejan 2006, Bejan and Lorente 2010]. This theory, also known as the Constructal Law, was stated by Bejan [Bejan 2006] in 1996, as follows: “For a finite-size system to persist in time (to live), it must evolve in such a way that it provides easier access to the imposed currents that flow through it.”

The Constructal Law is as a summary of all design generation and evolution phenomena in nature. For example, a heat engine is supposed to extract maximum useful work from heat currents that flow between systems at different temperatures. Performance is a measure of the degree to which each system realizes its purpose. The design of engineered systems evolves in time toward configurations that offer better performance, i.e., better achievement of their purpose. The system purpose is global and it should be under existing global constraints, including the space allocated to the system, available material and components, allowable temperature, pressure or stress ranges, etc. Inside the finite space, the system design is free to morph.

Flow architectures are ubiquitous in nature, in both natural and engineered systems. They evolve toward better performance, and persist in time (they survive) while the older designs disappear [Bejan 1996, Bejan and Lorente 2004, Bejan and Lorente 2006, Bejan and Lorente 2011]. Thus, the Constructal Theory could be used to explain the structures of nature flow and optimize flow architectures as well. However, no previous studies on applying the Constructal Theory to the pipework layout design of MEAC systems may be identified. Given that an MEAC system has a complicated pipework of several hundred meters long with height differences. It is

an ideal candidate for the application of the Constructal Theory to discover the best possible pipework layout for the highest possible operational efficiency, at fixed initial installation costs.

In this Chapter, an analytical study of applying the Constructal Theory to an MEAC system for minimizing its total power input is presented. The Constructal Theory is applied to discovering the best possible pipework layout design of an MEAC system, for the highest possible operational efficiency.

6.2 Two approaches

The thermodynamic optimization of a refrigeration system can be conducted by the following two approaches. Both consist of reducing the thermodynamic imperfection of the system.

The first approach is more common, and consists of changing the configuration of the refrigeration system in such a way that the work required per unit of heat removed from the conditioned space is reduced. In the refrigeration (R) system defined in Fig. 6.1, where R is a closed system that executes an integral number of cycles (or functions in steady-state); this approach leads to a lower ratio:

$$\frac{W}{Q_0} = \frac{1}{COP} \tag{6.1}$$

or a higher coefficient of performance.

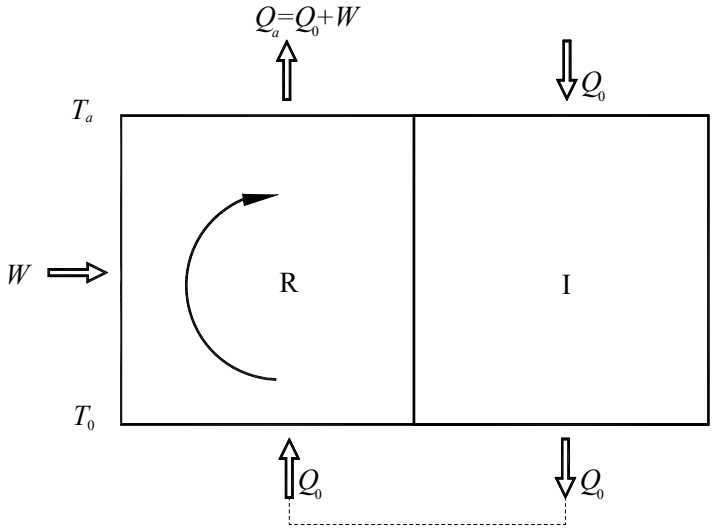

Fig. 6.1 Refrigeration as a closed system operating in an integral number of cycles in parallel with its leaky installation

The second approach is to reduce the irreversibility of the system, and this requires the correct calculation of the entropy generated during refrigeration. With reference to Fig. 6.1, it is noted that a steady-state operation is required because of the steady leakage of heat from T_a to T_0, through the insulation system (I) that separates a conditioned space at T_0, from the ambient at T_a.

The combined system (R+I) experiences a net heat transfer only with T_a, because the heat transfer with T_0 is zero [noting that the heat leak Q_0 that enters the conditioned space is removed at the same time by the R system]. The entropy generated by the (R+I) system is:

$$S_{gen} = \frac{Q_a}{T_a} - \frac{Q_0}{T_a} \tag{6.2}$$

where $Q_a = Q_0 + W$, based on the first law of thermodynamics for the R system. It follows that:

$$S_{gen} = \frac{W}{T_a} \tag{6.3}$$

or that the refrigeration work is proportional to the entropy that is generated in both R and I:

$$W = T_a S_{gen} \tag{6.4}$$

It will be shown later that the use of the two approaches would yield equivalent analysis results.

In the next few sections, the analyses for an SEAC system, a DEAC system and an MEAC system will be presented. All analyses are based on the first approach, except for the case for the SEAC system where both approaches are used.

6.3 Thermodynamic analysis for an SEAC system

6.3.1 First law analysis, the heat leak Q_L originates from T_B, Case 1

For the following thermodynamic analysis, the system (Fig. 6.2) consists of a room of temperature T_B, an evaporator (or indoor unit) of surface A and temperature T_E, the refrigerant pipeline of total length L, diameter D, and temperature T_E, and an

outdoor unit R, situated between T_E and the ambient at T_a. In this study case, the refrigerant pipeline is placed indoor, so that heat leak, Q_L, originates from T_B.

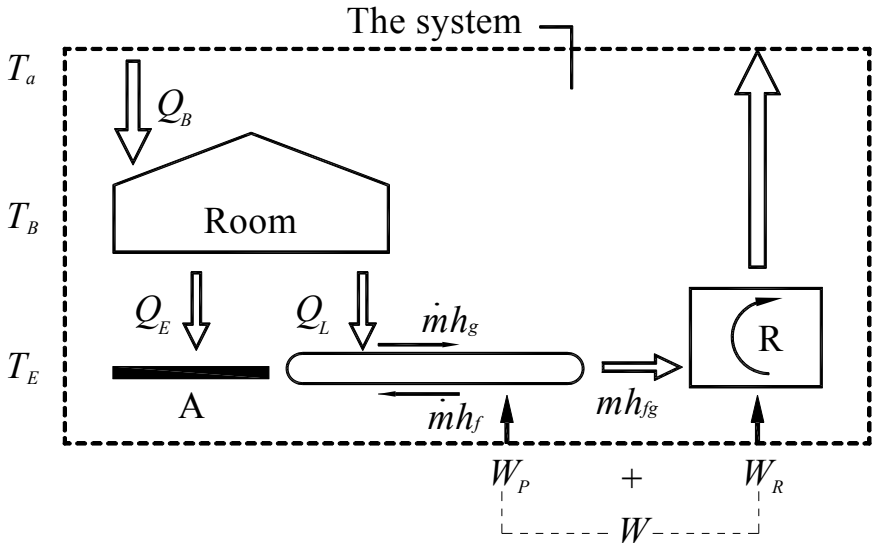

Fig. 6.2 Refrigeration and distribution pipeline for one room,

with heat leak from the room to the distribution pipeline

The system occupies a space at the temperature below ambient. The system operates in a steady-state. From the ambient, heat leaks into the room at the rate:

$$Q_B = Q_E + Q_L \tag{6.5}$$

The heat leak from the room interior to the evaporator surface is：

$$Q_E = U_E A \Delta T_B \tag{6.6}$$

and the heat leak from the room interior to the refrigerant pipeline is:

$$Q_L = U_L DL\Delta T_B \tag{6.7}$$

where $\Delta T_B = T_B - T_E$ is specified. The counter flows of refrigerant carries the enthalpy current $\dot{m}h_{fg}$ between the evaporator and the outdoor unit,

$$\dot{m}h_{fg} = Q_E + Q_L + W_P \tag{6.8}$$

where W_P is the pumping power required in order to circulate the refrigerant between the evaporator and outdoor unit. The efficiency for the compression taking place in the outdoor unit, R, is:

$$\eta_R = \frac{\dot{m}h_{fg}}{W_R} \tag{6.9}$$

The total power required by the SEAC system is:

$$W = W_R + W_P = \frac{Q_E + Q_L + W_P}{\eta_R} + W_P \tag{6.10}$$

Where in Equations (6.9) and (6.10), W_R is the power required for the refrigerant compression taking place in R and W_P is the pumping power required to circulate the refrigerant between outdoor unit and indoor unit. The objective here is to minimize W subject to the variable dimensions of the SEAC system. For this purpose, it is noted that Q_B is fixed by building design:

$$Q_B = U_B A_B \Delta T_1, \text{ constant} \tag{6.11}$$

where $\Delta T_1 = T_a - T_B$. The heat currents from the room air to the evaporator surface and to the refrigerant pipelines are given by Eqs. (6.6) and (6.7), where U_E and U_L are the respective overall heat transfer coefficients of the two surfaces, A and DL. Substituting Eqs. (6.6), (6.7) and (6.11) into Eq. (6.5), it is found that the sum of the two surfaces, A and DL, must satisfy the constraint:

$$A + \frac{U_L}{U_E} DL = \frac{U_B \Delta T_1}{U_E \Delta T_B} A_B \tag{6.12}$$

This constraint comes from the building enclosure design, not from material cost considerations. The total power requirement, Eq. (6.10), becomes:

$$W = \frac{Q_B}{\eta_R} + \left(1 + \frac{1}{\eta_R}\right) W_P \tag{6.13}$$

In this expression, Q_B is fixed by the size and building enclosure design. Assuming single-phase turbulent flow in all the distribution pipelines, W_P can be evaluated by:

$$W_P = C_6 \frac{\dot{m}^3 L}{D^5} \tag{6.14}$$

where C_1 is a constant proportional to the friction factor.

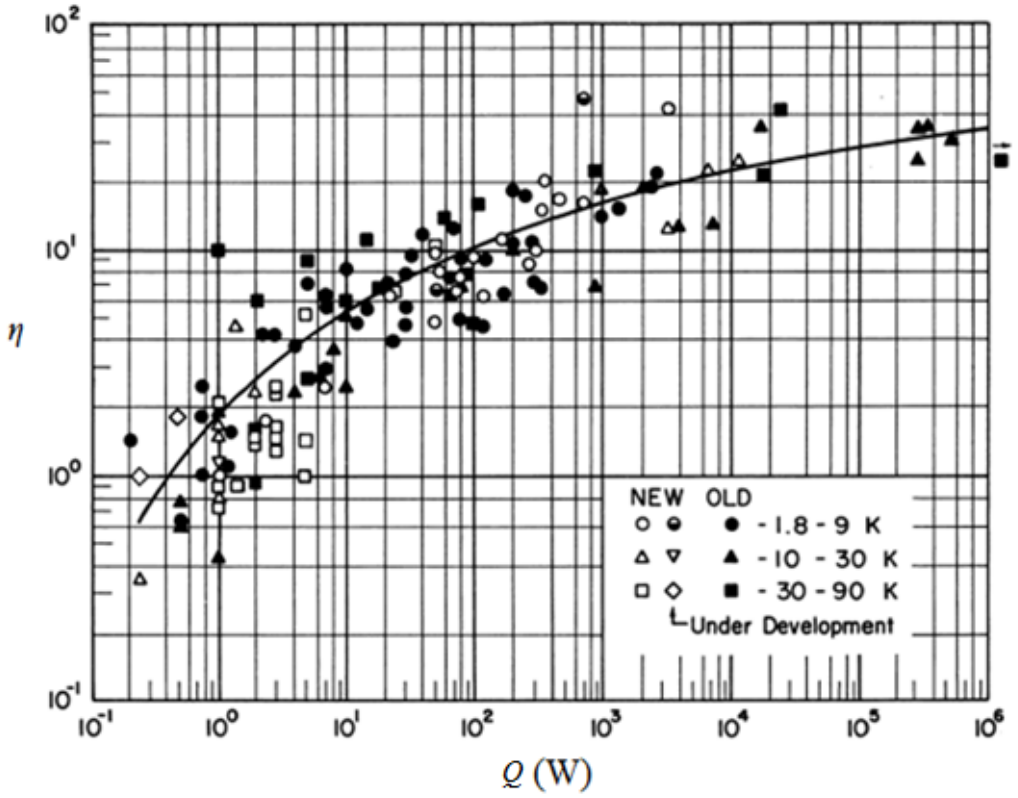

Fig. 6.3 Second-law efficiencies of refrigerators and liquefiers [Bejan 2006]

The compression efficiency, η_R , increases monotonically with the size of the refrigeration installation, cf., Fig. 6.3[Bejan 2006].

$$\eta_R = C_7 \left(Q_E + Q_L + W_P \right)^{\beta} \tag{6.15}$$

where β is positive and less than 1, and $Q_E + Q_L + W_P$ is the cooling capacity. According to Fig. 6.3, β is of order 0.26~0.35. In view of $Q_B = Q_E + Q_L$, which is constant, Eq. (6.13) becomes:

$$W = \frac{Q_B}{C_7\left(Q_B + W_P\right)^{\beta}} + \left[1 + \frac{1}{C_7\left(Q_B + W_P\right)^{\beta}}\right] W_P \tag{6.16}$$

or approximately:

$$W \sim \frac{Q_B}{C_7\left(Q_B + W_P\right)^{\beta}} + W_P \tag{6.17}$$

This shows that there is a trade-off between the power required for pumping the refrigerant (the second term) and that for compression refrigerant in the outdoor unit (the first term). The minimum total power required occurs when:

$$\frac{Q_B}{C_7\left(Q_B + W_P\right)^{\beta}} \sim W_P \tag{6.18}$$

which means:

$$\frac{W_P}{Q_B}\left(1 + \frac{W_P}{Q_B}\right)^{\beta} \sim \frac{1}{C_7 {Q_B}^{\beta}} \tag{6.19}$$

When $W_p << Q_B$, Eqs. (6.17) and (6.19) become:

$$W \sim W_P \sim {C_7}^{-1} {Q_B}^{1-\beta} \tag{6.20}$$

When $W_p >> Q_B$, the conclusion is:

$$W \sim W_P \sim C_7^{\frac{1}{1+\beta}} Q_B^{\frac{1}{1+\beta}} \tag{6.21}$$

Furthermore, one constraint comes from the total cost:

$$C_T = C_E A + C_L DL \tag{6.22}$$

where C_E is the cost per unit area of evaporator, C_L the cost per unit area of refrigerant pipeline, and C_T the total cost. Equation (6.22) can be written per unit C_E as:

$$c_T = A + c_L DL \tag{6.23}$$

where $c_T = C_T / C_E$ and $c_L = C_L / C_E$ .The total power requirement becomes:

$$\begin{aligned} W = W_R + W_P &= \frac{\dot{m} h_{fg}}{\eta_R} + W_P \\ &= \frac{Q_E + Q_L}{\eta_R} + \left(\frac{1}{\eta_R} + 1 \right) W_P \\ &= \frac{U_E A \Delta T_B + U_L DL \Delta T_B}{\eta_R} + \left(\frac{1}{\eta_R} + 1 \right) C_6 \frac{\dot{m}^3 L}{D^5} \end{aligned} \tag{6.24}$$

From Eqs. (6.22)-(6.24), it follows:

$$W = K_E + K_L DL + K_P \frac{L}{D^5} \tag{6.25}$$

where the coefficients are:

$$K_E = \frac{c_T U_E \Delta T_B}{\eta_R} \tag{6.26}$$

$$K_L = \frac{U_L \Delta T_B - c_L U_E \Delta T_B}{\eta_R} \tag{6.27}$$

$$K_P = \left(\frac{1}{\eta_R} + 1 \right) C_6 \dot{m}^3 \tag{6.28}$$

In sum, the total power requirement, W, has a minimum with respect to the diameter of the distribution lines. Solving $\partial W / \partial D = 0$ gives:

$$D_{opt} = \left(\frac{5K_P}{K_L} \right)^{\frac{1}{6}} \tag{6.29}$$

which is independent of the duct length L.

According to constraints (6.12) and (6.23), the area of evaporator, A, is specified:

$$\begin{aligned} A &= \frac{c_L Q_B - c_T U_L \Delta T_B}{\Delta T_B \left(c_L U_E - U_L \right)} \\ &= \frac{Q_B - c_T B_1}{\Delta T_B U_E - B_1} \end{aligned} \tag{6.30}$$

where $B_1 = U_L \Delta T_B / c_L$, and Q_B is fixed because of the cooling load of the room. Substituting Eqs. (6.29) and (6.30) into Eq. (6.23), the length, L, under the optimum D_{opt} is:

$$L_{opt} = \frac{1}{D_{opt}} \left(\frac{Q_B - \eta_R K_E}{\eta_R K_L} \right) \tag{6.31}$$

6.3.2 Second law analysis, also for Case 1

Here the system shown in Fig. 6.2 is used in order to illustrate the general principle developed in Eqs. (6.2) to (6.4). The system shown in Fig. 6.2 generates entropy at the rate of:

$$S_{gen} = \frac{W_R + W_P + Q_E + Q_L}{T_a} - \frac{Q_B}{T_a} \tag{6.32}$$

In view of Eq. (6.5), this means that the total power requirement is proportional to the total rate of enthalpy generation in the system, i.e., in the conditioned space situated below T_a.

$$W_R + W_P = T_a S_{gen} \tag{6.33}$$

This matches the conclusion reached in Eq. (6.4), proving that the use of the two approaches would yield equivalent result, as mentioned at the end of Section 6.2.

Since the first approach is simpler and more familiar by people and it does not require the calculation and discussion of entropy generation. The analysis in the following sections is therefore based on the first approach.

6.3.3 If the heat leak Q_L originates from T_a, Case 2

Considering an alternative when the refrigerant pipelines are surrounded by air at T_a, as shown in Fig. 6.4. In this study case, the refrigerant pipeline is placed outdoor, so that the heat leak, Q_L, originates from T_a.

The analysis presented in Section 6.3.2 is changed as follows. Equation (6.7) is replaced by:

$$Q_L = U_L DL\Delta T_a \tag{6.34}$$

where $\Delta T_a = T_a - T_E$ is specified. Equation (6.5) becomes:

$$Q_B = Q_E \text{ constant} \tag{6.35}$$

Therefore, the area of evaporator, A, must satisfy the constraint:

$$\frac{A}{A_B} = \frac{U_B \Delta T_1}{U_E \Delta T_B} \tag{6.36}$$

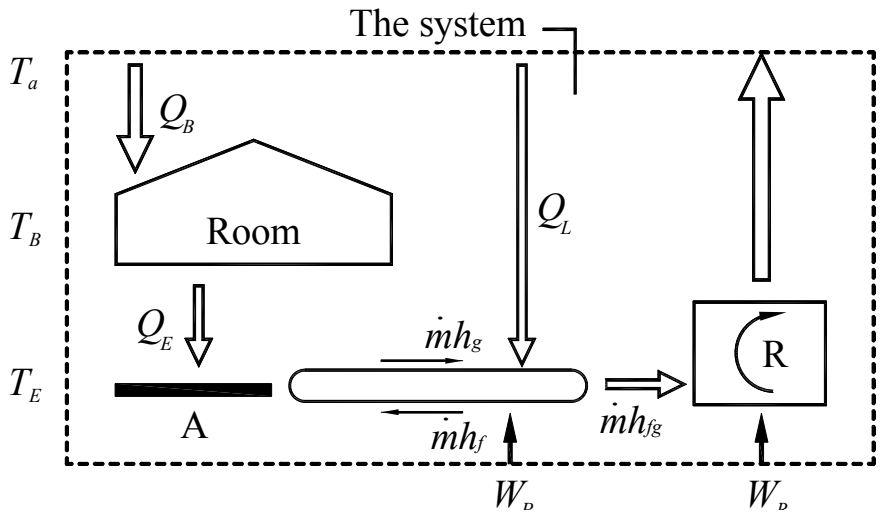

Fig. 6.4 Refrigeration and distribution pipeline for one room,

with heat leak from the ambient to the distribution pipeline

Equation (6.12) disappears, but Eqs. (6.8)-(6.10) continue to hold, except that in Eq. (6.10) only Q_E is fixed (because of Q_B), and Q_L varies. The total power requirement becomes:

$$\begin{aligned} W &= W_R + W_P \\ &= \frac{U_E A \Delta T_B + U_L D L \Delta T_a}{\eta_R} + \left(\frac{1}{\eta_R} + 1 \right) C_6 \frac{\dot{m}^3 L}{D^5} \end{aligned} \tag{6.37}$$

The cost constraints represented by Eqs. (6.22) and (6.23) continue to hold, and Eq. (6.37) is replaced by:

$$W = K_E + K_L' D L + K_P \frac{L}{D^5} \tag{6.38}$$

where the constant coefficients, K_E, and , K_P , are the same as that in Case 1, as shown in Eqs. (6.26) and (6.28). However,

$$K_L' = \frac{U_L \Delta T_a - c_L U_E \Delta T_B}{\eta_R} \tag{6.39}$$

In sum, the total power requirement W has a minimum with respect to the diameter of the refrigerant pipeline. Solving $\partial W / \partial D = 0$ would give:

$$D_{opt} = \left(\frac{5K_P}{K_L'} \right)^{\frac{1}{6}} \tag{6.40}$$

which is again independent of the duct length L.

Substituting Eqs. (6.36) and (6.40) into Eq. (6.23), it is found that the evaporator area and pipeline length are:

$$A = \frac{Q_B}{U_E \Delta T_B} \tag{6.41}$$

$$L_{opt} = \frac{1}{D_{opt}} \left(\frac{Q_B - \eta_R K_E}{\eta_R K_L' - U_L \Delta T_a} \right) \tag{6.42}$$

where Q_B is fixed because it is the cooling load of the room.

The results of the two cases shown in Fig. 6.2 and Fig. 6.4 are compared:

- The evaporator surfaces in the two cases are both decided by the cooling load of the room, Q_B. According to the cost constraint, A is fixed by Q_B, and a trade-off exists between D and L of the pipeline. This shows that if the cooling load of the room is specified, the performance of an SEAC is influenced by the design of its refrigerant pipeline.

- The optimum diameters, $D_{opt,1}$ (Fig. 6.2) and $D_{opt,2}$ (Fig. 6.4) follow from Eqs. (6.29) and (6.40), and from the ratio of the two:

$$\begin{aligned}\frac{D_{opt,1}}{D_{opt,2}} &= \left(\frac{K_L'}{K_L}\right)^{1/6} \\ &= \left(\frac{U_L\Delta T_a - c_L U_E \Delta T_B}{U_L\Delta T_B - c_L U_E \Delta T_B}\right)^{1/6}\end{aligned} \tag{6.43}$$

because $\Delta T_a > \Delta T_B$, this ratio shows that:

$$\frac{D_{opt,1}}{D_{opt,2}} > 1 \tag{6.44}$$

- According to Eqs. (6.30) and (6.41), the areas of evaporators in these two cases are subject to the heat leakage per unit area, $U_L\Delta T_B$, and cost of the material, c_L.

- Substituting Eqs. (6.29) (6.31) (6.40) and (6.42) into Eq. (6.14), respectively, the ratio of the pumping power required under the optimum pipeline diameters in the two cases is:

$$\frac{W_{P,1}}{W_{P,2}} = \frac{\left(c_L U_E \Delta T_B\right)\left(c_L U_E \Delta T_B - U_L \Delta T_a\right)}{\left(c_L U_E \Delta T_B - U_L \Delta T_B\right)^2} \tag{6.45}$$

Which means, because $\Delta T_a > \Delta T_B$:

$$\frac{W_{P,1}}{W_{P,2}} > 1 \tag{6.46}$$

6.4 Thermodynamic analysis for a DEAC system

The schematic diagrams of the DEAC system, under study in this section are shown in Fig. 6.5 and Fig. 6.6.

6.4.1 Heat leak Q_L originates from T_B, Case 3

In this study case, refrigerant distribution pipelines are placed indoor. Considering the heat leak from the interiors of Rooms 1 and 2 to the evaporator surfaces, A_1 and A_2, as shown in Fig. 6.5:

$$Q_{E1} = U_E A_1 \Delta T_{B1} \tag{6.47}$$

$$Q_{E2} = U_E A_2 \Delta T_{B2} \tag{6.48}$$

Fig. 6.5 Refrigeration and distribution pipelines for two rooms, with heat leak from the rooms to the distribution pipelines

and the heat leak from the interiors of rooms to the refrigerant pipeline:

$$Q_{L1} = U_L D_1 L_1 \Delta T_{B1} \tag{6.49}$$

$$Q_{L2} = U_L D_2 L_2 \Delta T_{B2} \tag{6.50}$$

The temperature differences are assumed to be the same:

$$\Delta T_{B1} = \Delta T_{B2} = \Delta T_B \tag{6.51}$$

From the ambient, heat leaks into room 1 and 2 at the rate:

$$Q_{B1} = Q_{E1} + Q_{L1} \text{ constant} \tag{6.52}$$

$$Q_{B2} = Q_{E2} + Q_{L2} \text{ constant} \tag{6.53}$$

$$Q_B = Q_{B1} + Q_{B2} \text{ constant} \tag{6.54}$$

The power inputs for pumping the refrigerant to the two rooms are calculated as：

$$W_{P1} = C_6 \frac{\dot{m}_1^{\,3} L_1}{D_1^{\,5}} \tag{6.55}$$

$$W_{P2} = C_6 \frac{\dot{m}_2^{\,3} L_2}{D_2^{\,5}} \tag{6.56}$$

The counter flows of refrigerant carries the enthalpy current between the evaporator and the outdoor unit,

$$\dot{m}_1 h_{fg} = Q_{E1} + Q_{L1} + W_{P1} \tag{6.57}$$

$$\dot{m}_2 h_{fg} = Q_{E2} + Q_{L2} + W_{P2} \tag{6.58}$$

The compression efficiency, η_R, of the system is：

$$\begin{aligned} \eta_R &= \frac{\dot{m}_1 h_{fg} + \dot{m}_2 h_{fg}}{W_R} \\ &= \frac{Q_{E1} + Q_{L1} + W_{P1} + Q_{E2} + Q_{L2} + W_{P2}}{W_R} \end{aligned} \tag{6.59}$$

The total power requirement becomes：

$$W = W_R + W_{P1} + W_{P2} \tag{6.60}$$

Substituting Eq. (6.59) into Eq. (6.60)：

$$W = \frac{Q_{E1} + Q_{L1} + Q_{E2} + Q_{L2}}{\eta_R} + \left(\frac{1}{\eta_R} + 1 \right) \left(W_{P1} + W_{P2} \right) \tag{6.61}$$

The total cost constraint is:

$$C_T = C_E \left(A_1 + A_2 \right) + C_L \left(D_1 L_1 + D_2 L_2 \right) \tag{6.62}$$

which can be written per unit of C_E as:

$$c_T = A_1 + A_2 + c_L\left(D_1 L_1 + D_2 L_2\right) \tag{6.63}$$

Combining Eqs. (6.61) and (6.63) would lead to:

$$W = K_E + K_L\left(D_1 L_1 + D_2 L_2\right) + K_{P1}\frac{L_1}{D_1^{\,5}} + K_{P2}\frac{L_2}{D_2^{\,5}} \tag{6.64}$$

where the constant coefficients are:

$$K_E = \frac{c_T U_E \Delta T_B}{\eta_R} \tag{6.65}$$

$$K_L = \frac{U_L \Delta T_B - c_L U_E \Delta T_B}{\eta_R} \tag{6.66}$$

$$K_{P1} = \left(\frac{1}{\eta_R} + 1\right) C_6 \dot{m}_1^{\,3} \tag{6.67}$$

$$K_{P2} = \left(\frac{1}{\eta_R} + 1\right) C_6 \dot{m}_2^{\,3} \tag{6.68}$$

In sum, the total power requirement W has a minimum with respect to the diameters of the refrigerant pipelines. Solving $\partial W/\partial D_1 = 0$ and $\partial W/\partial D_2 = 0$ gives:

$$D_{opt1} = \left(\frac{5K_{P1}}{K_L}\right)^{\frac{1}{6}} \tag{6.69}$$

$$D_{opt2} = \left(\frac{5K_{P2}}{K_L}\right)^{\frac{1}{6}} \tag{6.70}$$

which is independent of the duct length L.

On the other hand, the ratio of the two optimum diameters of pipelines linking two indoor units to the outdoor units is:

$$\frac{D_{opt1}}{D_{opt2}} = \left(\frac{\dot{m}_1}{\dot{m}_2} \right)^{\frac{1}{2}} \tag{6.71}$$

which indicates that the ratio is determined by their respective refrigerant mass flow rate.

According to Eqs. (6.54) and (6.63), the total evaporator area ($A_1 + A_2$) and pipeline area, ($D_1 L_1 + D_2 L_2$) are fixed by the total heat leakage and the cost constraint:

$$A_1 + A_2 = \frac{c_L Q_B - c_T U_L \Delta T_B}{\Delta T_B \left(c_L U_E - U_L \right)} \tag{6.72}$$

$$D_1 L_1 + D_2 L_2 = \frac{c_T}{c_L} - \frac{c_L Q_B - c_T U_L \Delta T_B}{c_L \Delta T_B \left(c_L U_E - U_L \right)} \tag{6.73}$$

If the total length between the two rooms is L, and n is the ratio of L_1 over the total length:

$$L_1 = nL \quad (0 < n < 1) \tag{6.74}$$

$$L_2 = (1 - n)L \quad (0 < n < 1) \tag{6.75}$$

Eq. (6.73) can be simplified to:

$$D_1 L_1 + D_2 L_2 = B_2 \tag{6.76}$$

and B_2 is:

$$B_2 = \frac{c_T}{c_L} - \frac{c_L Q_B - c_T U_L \Delta T_B}{c_L \Delta T_B \left(c_L U_E - U_L \right)} \tag{6.77}$$

which is independent of dimension factor and Eq.(6.73) becomes:

$$\left[nD_1 + (1-n) D_2 \right] L = B_2 \tag{6.78}$$

Substituting Eq. (6.78) into Eqs. (6.74) and (6.75) to obtain:

$$L_1 = \frac{nB_2}{nD_1 + (1-n) D_2} \tag{6.79}$$

$$L_2 = \frac{(1-n) B_2}{nD_1 + (1-n) D_2} \tag{6.80}$$

Since the optimum diameters, D_{opt1} and $D_{opt\,2}$, are known, the optimum lengths are:

$$L_{opt1} = \frac{nB_2}{nD_{opt1} + (1-n) D_{opt\,2}} \tag{6.81}$$

$$L_{opt\,2} = \frac{(1-n) B_2}{nD_{opt1} + (1-n) D_{opt\,2}} \tag{6.82}$$

The areas of evaporators in rooms 1 and 2 are obtained as follows:

$$A_{opt1} = \frac{Q_{B1}}{U_E \Delta T_B} - \frac{nU_L B_2 D_{opt1}}{nU_E D_{opt1} - (1-n)U_E D_{opt2}} \tag{6.83}$$

$$A_{opt2} = \frac{Q_{B2}}{U_E \Delta T_B} - \frac{(1-n)U_L B_2 D_{opt2}}{nU_E D_{opt1} - (1-n)U_E D_{opt2}} \tag{6.84}$$

The results show that the total evaporator area is fixed by total cooling load. However, the changes in length and diameter of refrigerant pipeline will influence on the evaporator area in each room. This conclusion will lead the designer of a DEAC system to figure out the optimum diameter first, and then decide the length and evaporator area according to the other constraint(s).

6.4.2 Heat leak Q_L originates from T_a, Case 4

In this study case, refrigerant distribution pipelines are placed outdoor as shown in Fig. 6.6. Where the distribution lines are surrounded by air at T_a. The analysis process is similar to that shown in Section 6.4.1.

The evaporator area in each room and the heat exchanger areas are:

$$A_1 = \frac{Q_{B1}}{U_E \Delta T_B} \tag{6.85}$$

$$A_2 = \frac{Q_{B2}}{U_E \Delta T_B} \tag{6.86}$$

$$A = A_1 + A_2 = \frac{Q_B}{U_E \Delta T_B} \tag{6.87}$$

The total power requirement W has a minimum with respect to the diameters of the refrigerant pipelines,

$$D_{opt1} = \left(\frac{5K_{P1}}{K_L'} \right)^{\frac{1}{6}} \tag{6.88}$$

$$D_{opt2} = \left(\frac{5K_{P2}}{K_L'} \right)^{\frac{1}{6}} \tag{6.89}$$

where, K_L' is defined by Eq. (6.39). The lengths of refrigerant pipeline to each room are:

$$L_{opt1} = \frac{nB_3}{nD_{opt1} + (1-n)} \tag{6.90}$$

$$L_{opt2} = \frac{(1-n)B_3}{nD_{opt1} + (1-n)D_{opt2}} \tag{6.91}$$

where B_3 is defined by:

$$B_3 = \frac{c_T U_E \Delta T_B - Q_B}{c_L U_E \Delta T_B} \tag{6.92}$$

Fig. 6.6 Refrigeration and distribution pipelines for two rooms, with heat leak from the ambient to the distribution pipelines

Comparing B_2 with B_3,

$$\frac{B_2}{B_3} = \frac{U_E}{U_E - (U_L/c_L)} \frac{(c_T U_E \Delta T_B - Q_B) + (c_T/c_L)\Delta T_B (U_E - U_L)}{c_T U_E \Delta T_B - Q_B} \tag{6.93}$$

When $U_L/c_L > 0$ and $(c_T/c_L)\Delta T_B(U_E - U_L) > 0$, the ratio shows that:

$$\frac{B_2}{B_3} > 1 \tag{6.94}$$

If *n* in Case 3 and Case 4 are the same, the lengths and diameters for these two cases are:

$$\frac{L_{opt1,3}}{L_{opt1,4}} = \frac{L_{opt2,3}}{L_{opt2,4}} = \frac{B_2}{B_3} > 1 \tag{6.95}$$

$$\frac{D_{opt1,3}}{D_{opt1,4}} = \frac{D_{opt2,3}}{D_{opt2,4}} = \left(\frac{K_L'}{K_L}\right)^{\frac{1}{6}} = \left(\frac{U_L \Delta T_a - c_L U_E \Delta T_B}{U_L \Delta T_B - c_L U_E \Delta T_B}\right)^{\frac{1}{6}} > 1 \tag{6.96}$$

Hence,

$$D_{opt\,1,3} L_{opt\,1,3} + D_{opt\,2,3} D_{opt\,2,3} > D_{opt\,1,4} L_{opt\,1,4} + D_{opt\,2,4} D_{opt\,2,4} \tag{6.97}$$

According to the cost constraint, when $c_{T,3} = c_{T,4}$:

$$A_{1,3} + A_{2,3} < A_{1,4} + A_{2,4} \tag{6.98}$$

This shows that the cost for evaporator in Case 3 is less than that in Case 4.

6.5 Thermodynamic analysis for an MEAC system

6.5.1 Heat leak Q_L originates from T_B, Case 5

In this study case, refrigerant distribution pipelines are placed indoor. Considering the heat leak from the interiors of m rooms in a building, the heat leak from the i^{th} room is calculated by:

$$Q_{Ei} = U_E A_i \Delta T_B \qquad (i = 1 - m) \tag{6.99}$$

and the heat leak from the interior in the i^{th} room to the refrigerant pipelines:

$$Q_{Li} = U_L D_i L_i \Delta T_B \tag{6.100}$$

The temperature differences are assumed to be the same. The power input for pumping the refrigerant to the i^{th} room is calculated as:

$$W_{Pi} = C_6 \frac{\dot{m}_i^{\,3} L_i}{D_i^{\,5}} \tag{6.101}$$

The counter flows of refrigerant carries the enthalpy current between the i^{th} indoor unit and outdoor unit are:

$$\dot{m}_i h_{fg} = Q_{Ei} + Q_{Li} + W_{Pi} \tag{6.102}$$

The η_R of the system is:

$$\eta_R = \frac{\sum_{i=1}^{m} \dot{m}_i h_{fg}}{W_R} \tag{6.103}$$

Therefore:

$$W_R = \frac{\sum_{i=1}^{m} \dot{m}_i h_{fg}}{\eta_R} = \frac{\sum_{i=1}^{m} Q_{Ei} + Q_{Li} + W_{Pi}}{\eta_R} \tag{6.104}$$

The total power requirement becomes:

$$W = W_R + \sum_{i=1}^{m} W_{Pi} \tag{6.105}$$

Substituting Eq.(6.104) into Eq. (6.105):

$$W = \frac{1}{\eta_R} \sum_{i=1}^{m} \left(Q_{Ei} + Q_{Li}\right) + \left(\frac{1}{\eta_R} + 1\right) \sum_{i=1}^{m} \left(W_{Pi}\right) \tag{6.106}$$

The total cost constraint could be:

$$C_T = C_E \sum_{i=1}^{m} A_i + C_L \sum_{i=1}^{m} D_i L_i \tag{6. 107}$$

which can be written per unit of C_E as:

$$c_T = \sum_{i=1}^{m} A_i + c_L \sum_{i=1}^{m} D_i L_i \tag{6.108}$$

Equation (6.106) follows:

$$W = K_E + K_L \sum_{i=1}^{m} D_i L_i + \sum_{i=1}^{m} K_{Pi} \frac{L_i}{D_i^{\,5}} \tag{6.109}$$

where the constant coefficients, K_E and K_L evaluated by Eqs. (6.65) and (6.66), except:

$$K_{Pi} = \left(\frac{1}{\eta_R} + 1 \right) C_6 \dot{m}_i^{\,3} \tag{6.110}$$

In sum, the total power requirement W has a minimum with respect to the diameter of the distribution lines. Solving $\partial W / \partial D_i = 0$ gives:

$$D_{opti} = \left(\frac{5K_{Pi}}{K_L} \right)^{\frac{1}{6}} \tag{6.111}$$

which is independent of the duct length L.

6.6 Conclusions

An analytical study of applying the Constructal Theory to discovering the best

possible layout design for an MEAC for the highest possible energy efficiency is presented in this Chapter. The following main results are obtained:

- It is shown that in an SEAC system, the evaporator area is fixed by the cooling load it has to deal with,

- In both a DEAC system and an MEAC system, the total evaporator area is decided by the total cooling load a system has to deal with, but the evaporator area in each room however is also influenced by the location of an outdoor unit when the distance among the rooms are fixed. The analytical results from all the cases indicated that the optimum diameters of the refrigerant pipeline are independent of the length. This conclusion can be used to guide the designer of an MEAC system to calculate an optimum pipeline and find out the total heat exchanger area first, and then decide the length of pipelines and the evaporator area in each room according the total cost and outdoor unit location.

Chapter 7

Conclusions and future work

7.1 Conclusions

A programmed research work on firstly developing a novel capacity control algorithm, secondly investigating on the effects of the large pressure drop along a refrigerant distribution pipework on the operational performance in a DEAC system, and finally discovering the best pipework layout design of an MEAC system for minimizing the total power input using the Constructal Theory has been successfully carried out and is reported in this thesis. The conclusions of the thesis are:

- A novel capacity control algorithm (NCCA) for an MEAC system has been developed and is reported in Chapter 4. Experimental tests validated its control accuracy and robustness. However, indoor air temperature controlled using the NCCA may still be subjected to significant fluctuations under certain operating conditions due to the use of temperature dead-band and time delay for compressor start-up, and the interaction among indoor units. An improved novel capacity control algorithm (INCCA) was therefore further developed, and further controllability test were carried out and the test results showed that the INCCA was simple but could effectively restrain the magnitude of temperature variations and avoid the frequent switching in compressor speed.

- A modeling study on the effects of refrigerant pipeline length on the operational performance of a DEAC system has been carried out and is reported in Chapter 5. A steady-state mathematical model for a DEAC system was developed and validated using the experimental results previously obtained by others. The study results indicated that the DEAC system's COP decreased with an increase in the refrigerant pipeline length. The results also suggested that for a DEAC system, its highest COP would be resulted in when the outdoor unit was located equally between the two indoor units and its lowest COP when the outdoor unit was located close to either of the indoor unit.

- Chapter 6 reports an analytical study of applying the Constructal Theory to discovering the best possible pipework layout design for MEAC systems for the highest possible operational efficiency. The study started with analyzing an SEAC system, and was extended to a DEAC system and an MEAC system. The study results for the SEAC system showed that the evaporator (or indoor unit) area was fixed by the cooling load it had to deal with, while for the DEAC and MEAC system, the total evaporator areas were decided by the total cooling load. The evaporator area in each room was however influenced by the length ratio of the refrigerant pipelines for one given room when the distance among the rooms was fixed. This suggested that if the cooling load in one room was specified, the operational performance of an MEAC system will be influenced by the layout design of its pipework. The study results also indicated that the optimum diameters of refrigerant distribution pipework were independent of the pipeline length. This could be used to guide the designer of an MEAC system to calculate

an optimum pipeline diameter and find out the total evaporator area first, and then decide the pipelines length and evaporator area in each room as a function of the total cost and the position of outdoor unit.

The outcomes of the programmed research work reported in this thesis have made significant contributions to advancing the technical development of MEAC systems. A better understanding of both the relationships among the operational parameters in the MEAC systems and their influences on the system design layout has been obtained. The long-term significance of the work is its contribution to the advancement of high efficiency building air conditioning technology and the sustainable development.

7.2 Proposed future work

A number of future studies following on the successful completion of the project reported in this thesis are proposed:

- An experimentally validated capacity control algorithm, NCCA, and its improved version, INCCA, have been developed and are reported in Chapter 4. Although the INCCA was simple and could effectively restrain the magnitude of temperature variations and avoid the frequent switching in compressor speed, temperature fluctuations still existed since it was still On/Off based. Therefore, it is highly desirable to develop control algorithms, which are not On/Off based, to further reduce, if not totally eliminate, the temperature fluctuations.

- The simulation study reported in Chapter 5 demonstrated the influence of refrigerant pipework on the operational performance. However, the study focused on a DEAC system, and the height differences of pipework were not considered. Hirao et al. [1992] found that the height differences in an SEAC system could cause serious refrigerant flashing. Therefore, it is suggested that the study be extended to considering also the height differences in an MEAC system.

- An analytical study of applying the Constructal Theory to MEAC systems to discovering the best possible layout design for an MEAC system for the highest possible energy efficiency is presented in Chapter 6. However, in this study, it was assumed that the outdoor unit and indoor units were installed horizontally, without considering the height difference of system installation. Therefore, further research on applying the Constructal Theory to MEAC systems with height difference in system installation is necessary.

Appendix A

Photos of the experimental DEAC system

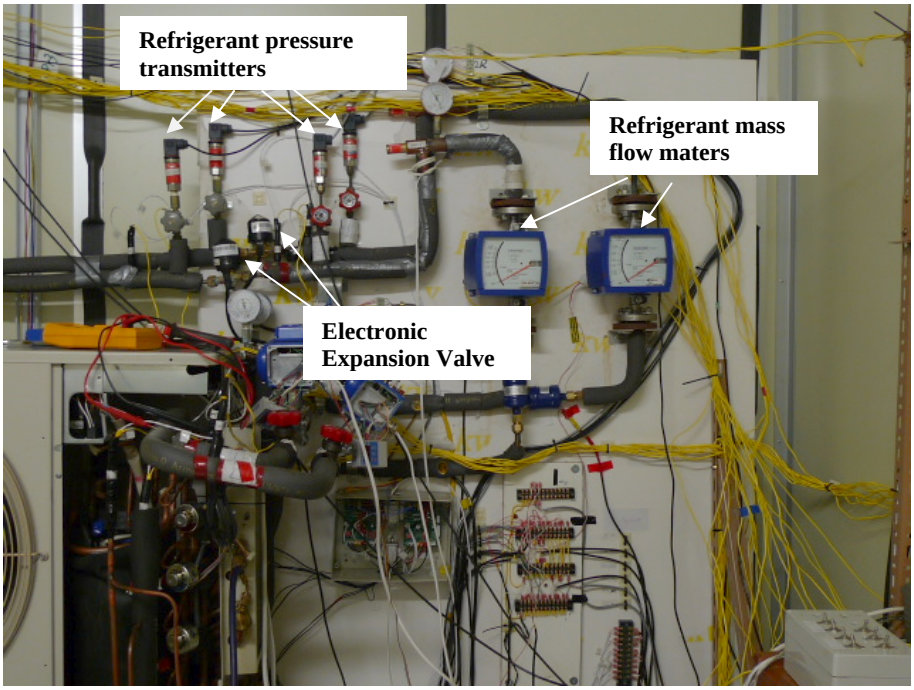

Photo 1 Overview of the experimental rig (1)

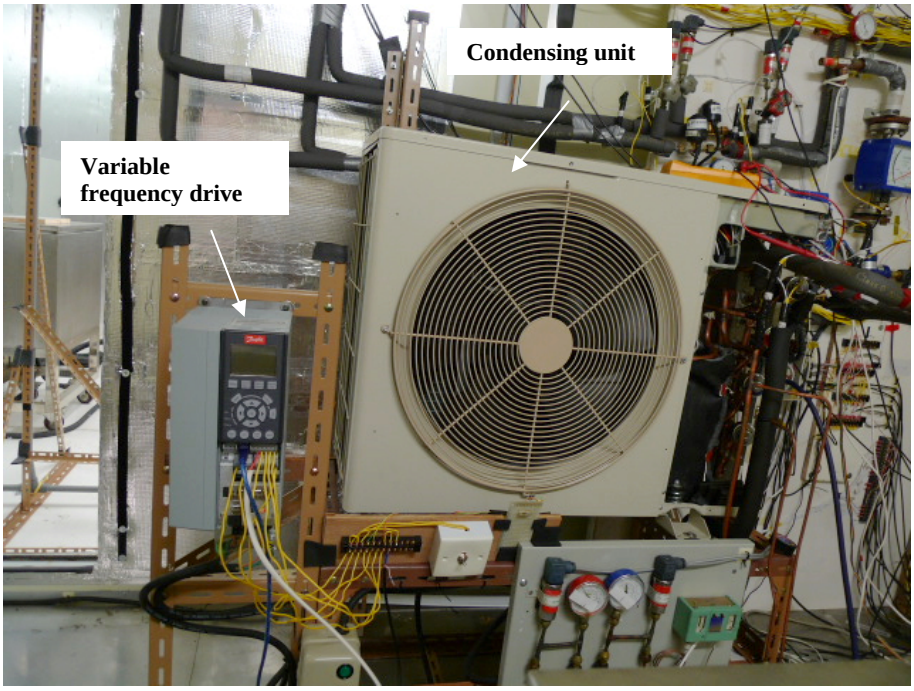

Photo 2 Overview of the experimental rig (2)

Photo 3 Overview of the indoor unit

Photo 4 Load generation unit inside conditioned space

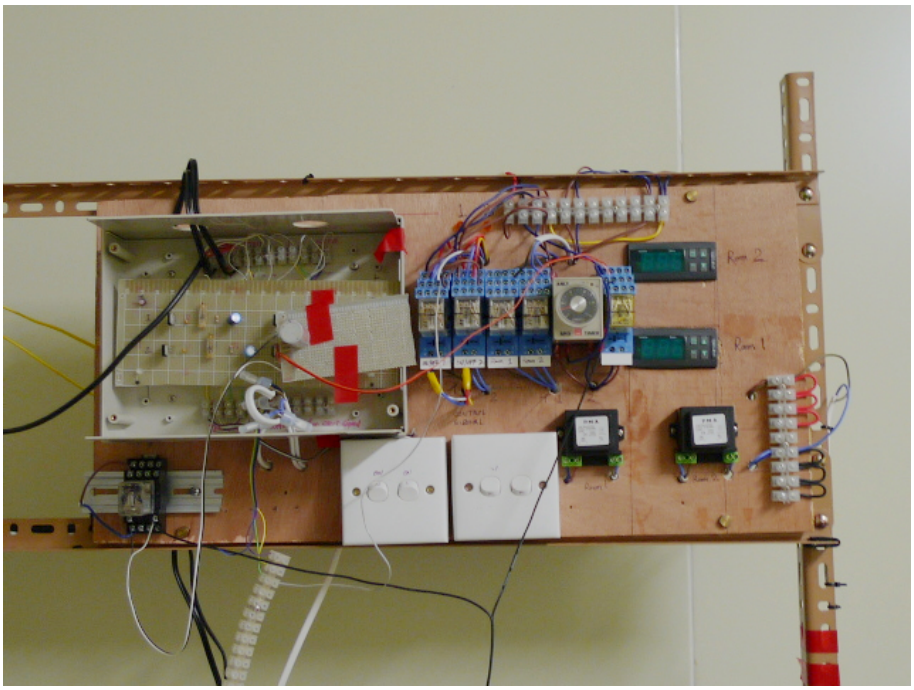

Photo 5 Control console

References

1. Afify 2008
   Afify R.
   Designing VRF systems. *ASHRAE Journal*, Vol. 50, No. 6, PP. 52-55 (2008)

2. Ahemd et al. 1998a
   Ahmed O., Mitchell J.W. and Klein S.A.
   Feedforward-feedback controller using general regression neural network (GRNN) for laboratory HVAC system, Part I: pressure control. *ASHRAE Transactions*, Vol. 104, No.2, PP. 613-625 (1998)

3. Ahemd et al. 1998b
   Ahmed O., Mitchell J.W. and Klein S.A.
   Feedforward-feedback controller using general regression neural network (GRNN) for laboratory HVAC system, part II: cooling control. *ASHRAE Transactions*, Vol. 104, No. 2, PP. 626-633 (1998)

4. Ahemd et al. 1998c
   Ahmed O., Mitchell J.W. and Klein S.A.
   Feedforward-feedback controller using general regression neural network (GRNN) for laboratory HVAC system, part III: heating control. *ASHRAE Transactions*, Vol. 104, No. 2, PP. 634-642 (1998)

5. Alebrahim and Bejan 1999
   Alebrahim A. and Bejan A.
   Constructal trees of circular fins for conductive and convective heat Transfer. *Intentional Journal of Heat and Mass Transfer*, Vol. 42, No. 19, PP. 3585-3597 (1999)

6. Almogbel and Bejan 1999
   Almogbel M. and Bejan A.

Conduction trees with spacing at the Tips. *Intentional Journal of Heat and Mass Transfer*, Vol. 42, No. 20, PP. 3739-3756 (1999)

7. Amarnath and Blatt 2008
   Amarnath A. and Blatt M.
   Variable refrigerant flow: where, why, and how. E*ngineered Systems,* Vol. 25, PP.54-60 (2008)

8. Anderson et al. 2002
   Anderson M., Young P., Hittle D., Anderson C., Tu J.L. and Hodgson D.
   MIMO robust control for heating, ventilation and air conditioning systems. *Proceedings of the 41st IEEE conference on decision and control. Las Vegas, Nevada, USA*, December 2002

9. ANSI/ARI 1999
   ANSI/ARI
   ARI standard 540-1999: standard for positive displacement refrigerant compressor sand compressor units. *Air-Conditioning & Refrigeration Institute, VA, USA*, 1999

10. Aprea and Mastrullo 2002
    Aprea C. and Mastrullo R.
    Experimental evaluation of electronic and thermostatic expansion valves performance using R22 and R407C. *Applied Thermal Engineering*, Vol. 22, No. 22, PP. 205-218 (2002)

11. Aprea et al. 2004
    Aprea C., Mastrullo R. and Renno C.
    Fuzzy control of the compressor speed in a refrigeration plant. *International Journal of Refrigeration*, Vol. 27, PP. 639-648 (2004)

12. ANSI/ASHRAE 2004
    ASHRAE

ANSI/ASHRAE Standard 55-2004, thermal environment conditions for human occupancy. *American Society of Heating, Refrigerating and Air-Conditioning Engineering, USA*, 2004

13. ANSI/ASHRAE 2007
ASHARE
ANSI/ASHRAE Standard 90.1-2007, energy standard for buildings except low-rise residential buildings. *American Society of Heating, Refrigerating and Air-Conditioning Engineering, USA*, 2007

14. Aureshi and Tassou 1996
Aureshi T.A. and Tassou S.A.
Variable-speed capacity control in refrigeration systems. *Applied Thermal Engineering*, Vol. 16, No. 2, PP. 103–113 (1996)

15. Aynur 2008a
Aynur T.N.
Evaluation of a multi-split type air conditioning system under steady-state and transient conditions. *Ph.D. thesis, Department of Mechanical Engineering, Istanbul Technical University*, 2008

16. Aynur 2008b
Aynur T.N., Hwang Y. and Radermacher R.
Experimental evaluation of the ventilation effect on the performance of a VRV system in cooling mode—Part I: Experimental evaluation. *HVAC&R Research*, Vol. 14, No. 4, PP. 615-630 (2008)

17. Aynur et al. 2008c
Aynur T.N., Hwang Y. and Radermacher R.
Field performance measurements of a heat pump desiccant unit in dehumidification mode. *Energy and Buildings*, Vol. 40, No. 12, PP. 2141-2147 (2008)

18. Aynur et al. 2008d
Aynur T.N., Hwang Y. and Radermacher R.
The effect of the ventilation and the control mode on the performance of a VRV system in cooling and heating modes. *Processing of the 12th International Refrigeration and Air Conditioning Conference at Purdue, West Lafayette, IN, USA*, 2008

19. Aynur 2010
Aynur T.N.
Variable refrigerant flow systems: A review. *Energy and Buildings*, Vol. 42, PP. 1106-1112 (2010)

20. Baines and Peterson 1951
Baines W.D. and Peterson E.G.
An investigation of flow through screens. *ASME Transactions*, PP. 73-457 (1951)

21. Bejan 1996
Bejan A.
Street network theory of organization in nature. *Journal of Advanced Transportation*, Vol. 30, No. 2, PP. 85-107 (1996)

22. Bensafi et al. 1997
Bensafi A., Borg S. and Parent D.C.
A computational model for the detailed design of plate-fin-and-tube heat exchangers using pure and mixed refrigerant. *International Journal of Refrigeration*, Vol. 20, No. 3, PP. 218-228 (1997)

23. Bejan and Lorente 2004
Bejan A. and Lorente S.
The constructal law and the thermodynamics of flow systems with configuration. *International Journal of Heat and Mass Transfer*, Vol. 47, No. 14-16, PP. 3203-3214 (2004)

24. Bejan 2005
Bejan T.M.
Natural Law and Natural Design.
http://www.dogma.lu/txt/TB-NaturalDesign.htm, 2005

25. Bejan and Reis 2005
Bejan A. and Reis A.H.
Thermodynamic optimization of global circulation and climate. *International Journal of Energy Research*, Vol. 29, No. 4, PP. 303-316 (2005)

26. Bejan and Almogbel 2000
Bejan A. and Almogbel M.
Constructal T-shaped fins. *International Journal of Heat and Mass Transfer*, Vol. 43, No. 12, PP. 2101-2115 (2000)

27. Biserni et al. 2004
Biserni C., Rocha L.A.O. and Bejan A.
Inverted fins: geometric optimization of the intrusion into a conducting wall. *Intentional Journal of Heat and Mass Transfer*, Vol. 47, No. 12-13, PP. 2577-2586 (2004)

28. Bonjour et al. 2004
Bonjour J., Rocha L.A.O., Bejan A. and Meunier F.
Dendritic fins optimization for a coaxial two-stream heat exchanger. *Intentional Journal of Heat and Mass Transfer*, Vol. 47, No. 1, PP. 111-124 (2004)

29. Cavallini et al. 2001
Cavallini A., Censi G. and Delcol D.
Experimental investigation on condensation heat transfer and pressure drop of new HFC refrigerants (R134a, R125, R32, R410a, R236ea) in a horizontal

smooth tube. *International Journal of Refrigeration*, Vol. 24, No. 1, PP. 73-87 (2001)

30. Chen et al. 2001
Chen W.Y., Chen Z.J., Zhu R.Q. and Wu Y.Z.
Control algorithm of electronic expansion valve in evaporator superheat regulation. *Journal of Shanghai Jiaotong University*, Vol. 35, No. 8, PP. 1228-1232 (2001)

31. Chen et al. 2002a
Chen Y., Halm N.P., Groll E.A. and Braun J.E.
Mathematical modeling of scroll compressors. Part I: compression process modeling. *International Journal of Refrigeration*, Vol. 25, PP.731-750 (2002).

32. Chen et al. 2002b
Chen Y., Halm N.P., Groll E.A. and Braun J.E.
Mathematical modeling of scroll compressors. Part II: overall scroll compressor modeling, *International Journal of Refrigeration*, Vol. 25, PP. 751-764 (2002)

33. Chen et al. 2005
Chen W., Zhou X.X. and Deng S.M.
Development of control for multi-evaporator air conditioners (MEAC) method and dynamic model. *Energy Conversion and Management*, Vol. 46, PP. 451-465 (2005)

34. Chen 2005
Chen W.
Modeling and control of a direct expansion (DX) variable-air-volume (VAV) air conditioning (A/C) system. *Ph.D. thesis, The Hong Kong Polytechnic University*, 2005

35. Chen and Deng 2006
Chen W. and Deng S.M.
Development of a dynamic model for a DX VAV air conditioning system. *Energy Conversion and Management*, Vol. 47, No. 18-19, PP. 2900-2924 (2006)

36. Chen and Deng 2010
Chen W. and Deng S.M.
Research on a novel DDC-based capacity controller for the direct-expansion variable-air-volume A/C system. *Energy Conversion and Management*, Vol. 451, No. 1, PP. 1-8 (2010)

37. Chi and Didion 1982
Chi J. and Didion D.
A simulation model of the transient performance of a heat pump. *International Journal of Refrigeration*, Vol. 5, No. 3, PP. 176-184 (1982)

38. Cho and Kim 2000
Cho H.H. and Kim Y.
Experimental study on an Inverter-Driven Scroll Compressor with an Injection System. *Proceedings of Purdue International Compressor Engineering Conference, Purdue, USA*, 2000

39. Choi and Kim 2003
Choi J.M. and Kim Y.C.
Capacity modulation of an inverter-driven multi-air conditioner using electronic expansion valves. *Energy*, Vol. 28, PP. 141-155 (2003)

40. Corberan and Melon 1998
Corberan J.M. and Melon M.C.
Modeling of plate finned tube evaporators and condensers working with R134a. *International Journal of Refrigeration*, Vol. 21, No. 4, PP. 273-284 (1998)

41. Cohen et al. 1974
Cohen R., Hamilton J.F. and Pearson J.T.
Possible energy conservation through the use of variable-capacity compressor. *Proceeding of Purdue Compressor Technology Conference, Purdue, USA*, 1974

42. Cuevas and Lebrun 2009
Cuevas C. and Lebrun J.
Testing and modeling of a variable speed scroll compressor. *Applied Thermal Engineering*, Vol. 29, No. 2-3, PP. 469-478 (2009)

43. DAIKIN 2011
DAIKIN Corporate Information, Corporate Profile/History.
http://www.daikin.com/company/history.html, 2011

44. Damasceno and Rooke 1990
Damasceno G.S. and Rooke S.P.
Comparison of three steady-state heat pump computer models. *ASHRAE Transaction*, Vol. 96, part 2, PP. 191-204 (1990)

45. Deissler 1951
Deissler R.G.
Laminar flow in tubes with heat transfer. *National Advisory Technical Note* 2410, Committee for Aeronautics

46. Deng 2000
Deng S.M.
A dynamic mathematical model of a direct expansion (DX) water-cooled air conditioning plant. *Building and Environment*, Vol. 35, No. 7, PP. 603-613 (2000)

47. Diaz et al. 1999
Diaz G, Yang K.T, McClain R.L and Sen M.
Simulation of heat exchanger performance by artificial neural networks. *HVAC&R Research*, Vol. 5, PP. 195-208 (1999)

48. Ding et al. 2000
Ding G.L., Zhang C.L., Zhan T. and Chen Z.J.
Compound fuzzy model for thermal performance of refrigeration compressors. *Chinese Science Bulletin*, Vol. 45, No. 14, PP. 1319-1322 (2000)

49. Ding 2007
Ding G.L.
Recent developments in simulation techniques for vapour-compression refrigeration systems. *International Journal of Refrigeration*, Vol. 30, PP. 1119-1133 (2007)

50. Domanski 1991
Domanski P.A.
Simulation of an evaporator with non-uniform one-dimensional air distribution. *ASHRAE Transactions*, Vol. 97, No. 1, PP. 793-802 (1991)

51. Domanski and Mclinden 1992
Domanski P. and Mclinden M.
A simplified cycle simulation model for the performance rating of refrigerants and refrigerant mixtures. *International Journal of Refrigeration*, Vol. 15, No. 2, PP.81-88 (1992)

52. Dyer 2006
Dyer M.
Approaching 20 years of VRF in the UK. *Modern Building Services*, http://www.modbs.co.uk/news/fullstory.php/aid/2127/Approaching_20_years_of_VRF_in_the_UK.html, 2006

53. Elliott and Rasmussen 2008
Elliott M.S. and Rasmussen B.P.
Model-based predictive control of a multi-evaporator vapor. *Proceedings of American control conference, Seattle, Washington, USA,* June 2008

54. Elliott and Rasmussen 2009
Elliott M.S. and Rasmussen B.P.
A model-based predictive supervisory controller for multi-evaporator HVAC systems. *Proceedings of American control conference, St. Louis, MO, USA,* June 2009

55. EPRI 2009
Electric Power Research Institute
Use of variable refrigerant flow in conjunction with ice thermal storage and dehumidification for space conditioning, In Chinese, PP. 1-2 (2009)

56. Errera and Bejan 1998
Errera M.R. and Bejan A.
Deterministic tree networks for river drainage basins. *Fractals,* Vol. 6, No. 3, PP. 245-261 (1998)

57. Fonseca and Fleming 1998
Fonseca C.M. and Fleming P.J.
Multi-objective optimization and multiple constraints handling with evolutionary algorithms. Part 1: A Unified Formulation. *Systems, man and Humans,* Vol. 28, No. 1, PP. 26-37 (1998)

58. Fong et al. 2006
Fong K.F. Hanby V.I. and Chow T.T.
HVAC system optimization for energy management by evolutionary programming. *Energy and Buildings,* Vol. 38, No. 3, PP. 220-231 (2006)

59. Fujita et al. 1992
Fujita Y., Kubo T. and Suma S.
Multi-air conditioner with two indoor units. *Refrigeration*, Vol. 67, PP. 171–176 (1992)

60. Giovanni and Lorenzo 1994
Giovanni C. and Lorenzo B.
Valve control for optimum performance in compression refrigeration cycles. *Heat recovery systems & CHP*, Vol. 14, No. 1, PP. 61-66 (1994)

61. Gordon et al. 1999
Gordon B.W., Liu S. and Asada H.H.
Dynamic modeling of multi-zone vapor compression cycles using variable order representation. *Proceedings of American control conference, S. Diego, GA, USA*, June 1999

62. Goetzler 2007
Goetzler W.
Variable refrigerant flow systems. *ASHRAE Journal*. Vol. 49, No. 4, PP. 24-31 (2007)

63. Gray and Webb 1986
Gray D.L. and Webb R.L.
Heat transfer and friction correlations for plate finned-tube heat exchangers having plain fins. *Proceeding of The Eighth International Heat Transfer Conference, SF, USA*, 1986

64. Gu et al. 2004
Gu Z., Liu H. and Li Y.
Thermal energy recovery of air conditioning system-heating recovery system calculation and phase change materials development. *Applied Thermal*

Engineering, Vol. 24, No. 17-18, PP. 2511-2526 (2004)

65. Hai et al. 2006a
Hai X.H., Jun S., Hand Z.Y. and Bin T.C
Design and research of the digital VRV multi-connected units with three pipes type heat recovery system. *Proceedings of the 11th International Refrigeration and Air Conditioning Conference at Purdue, West Lafayette, IN, USA*, 2006

66. Hai et al. 2006b
Hai X.H., Tao Z., Yun F.H. and Jun S.
Design and research of the commercial digital VRV multi-connected units with sub-cooled ice storage system. *Proceedings of the 11th International Refrigeration and Air Conditioning Conference at Purdue, West Lafayette, IN, USA*, 2006

67. Hardy 2009
Hardy M.
A practical guide to multi-split systems and variable refrigerant volume (VRV) systems.
http://www.ambthair.com/multisplit_and_vrv_systems.html, 2009

68. He et al. 1997
He X.D., Liu S. and Asada H.H.
Modeling of vapor compression cycles for multivariable feedback control of HVAC systems. *Transaction of the ASME: Journal of Dynamic Systems, Measurement, and Control*, Vol. 119, PP. 183-191 (1997)

69. He et al. 1998
He X.D., Liu S., Asada H.H. and Itoh H.
Multivariable control of vapor compression systems. *HVAC&R Research*, Vol. 4, No. 3, PP. 205-230 (1998)

70. Hirao et al. 1992
Hirao T., Ohzeki S. and Kobayashi S.
Prediction of performance and stability of heat pump systems with long pipes and high head. *ASHRAE Transactions*, Vol. 98, PP. 411-419 (1992)

71. Hu and Yang 2005
Hu S.C. and Yang R.H.
Development and testing of a multi-type air conditioner without AC inverters. *Energy Conversion and Management*, Vol. 46, PP. 373-383 (2005)

72. Islamoglu 2003
Islamoglu Y.
A new approach for the prediction of the heat transfer for rate of the wire-on-tube heat exchanger use of an artificial neural network model. *Applied thermal energy*, Vol. 23, No. 2, PP.243-249 (2003)

73. Ito 1962
Ito H.
Pressure losses in smooth pipe bends. *Journal of Basic Engineering*, Vol. 82, No. 1, PP. 131 (1962)

74. Joo et al. 2011
Joo Y., Kang H., Ahn J.H., Lee M. and Kim Y.
Performance characteristics of a simultaneous cooling and heating multi-heat pump at partial load conditions. *International Journal of Refrigeration*, Vol. 34, No. 4, PP. 893-901 (2011)

75. Kairouani et al. 2009
Kairouani L, Elakhdar M, Nehdi E and Bouaziz N.
Use of ejectors in a multi-evaporator refrigeration system for performance enhancement. *International Journal of refrigeration*, Vol. 32, No. 6, PP. 1173-1185 (2009)

76. Kang 2009
Kang H., Jooa Y.u, Chunga H., Kim Y. and Choi J.
Experimental study on the performance of a simultaneous heating and cooling multi-heat pump with the variation of operation mode. *International Journal of Refrigeration*, Vol. 32, No. 6, PP. 1452-1459 (2009)

77. Kesim et al. 2000
Kesim S.C., Albayrak K. and Ileri A.
Oil entrainment in vertical refrigerant piping. *International Journal of Refrigeration*, Vol. 23, PP. 626-631 (2000)

78. Kim et al. 2004
Kim K.R., Tae S.J., Cho K.N., Moon J.M., Kim J.Y. and Kwon H.J.
Experimental study on the performance and oil return characteristics of multi-split air-conditioning system for medium size building. *Proceedings of Purdue International Refrigeration and Air Conditioning Conference, Purdue, USA*, 2004

79. Klein and Alvarado 2002
Klein S.A. and Alvarado F.L.
EES: Engineering Equation Solver. F-chart software.
http://www.fchart.com/ees/, 2002

80. Kwon et al. 2004
Kwon Y.C., Kwon J.T., Jeong J.H., Lee S.J. and Kim D.H.
Performance of a 2 room multi-heat pump with a constant speed compressor. *International Journal of Air-conditioning and Refrigeration*, Vol. 12, PP. 184-191 (2004)

81. Kraus 2003
Kraus A.D.
Constructal theory and the optimization of finned arrays. *Proceedings of the 2003 ASME International Mechanical Engineering Congress, Washington,*

DC. USA, November 2003

82. Larsen and Thybo 2004
Larsen L.S. and Thybo C.
Potential energy saving in refrigeration systems using optimal. *Proceedings of the IEEE conference on control application. Taipei, Taiwan*, September 2004

83. Lee and Yoo 2000
Lee G.H. and Yoo J.Y.
Performance analysis and simulation of automobile air conditioning system. *International Journal of Refrigeration*, Vol. 23, PP. 243-254 (2000)

84. Lee et al. 2001
Lee T.H, Yun J.Y., Lee J.S., Park J.J. and Lee K.S.
Determination of airside heat transfer coefficient on wire-on-tube type heat exchanger. *International Journal of Heat and Mass Transfer*, Vol. 44, PP. 1767-1776 (2001)

85. Lee et al. 2002
Lee G., Kim M.S. and Cho Y.M.
An experimental study of the capacity control of multi-type heat pump system using predictive control logic. *Proceeding of the 7th International Energy Agency Heat Pump Conference*, 2002

86. Li et al. 2009
Li Y., Wu J. and Shiochi S.
Modeling and energy simulation of the variable refrigerant flow air conditioning system with water-cooled condenser under cooling conditions. *Energy and Buildings*, Vol. 41, No. 9, PP. 949-957 (2009)

87. Lijima et al. 1992
Lijima H., Tanaka N., Sumida Y. and Nakamura T.

Development of a new multi-system air conditioner with concurrent heating and cooling operation. *ASHRAE Transactions*, Vol. 98, PP. 309-315 (1992)

88. Li et al. 2004
Li X.Q., Chen J.P., Chen Z.J., Liu W.H., Hu W. and Liu X.B.
A new method for controlling refrigerant flow in automobile air conditioning. *Applied Thermal Engineering*, Vol. 24, PP. 1073-1085 (2004)

89. Lin and Yeh 2007a
Lin J.L. and Yeh T.J.
Modeling, identification and control of air-conditioning systems. *International Journal of Refrigeration*, Vol. 30, PP. 209-220 (2007)

90. Lin and Yeh 2007b
Lin J.L. and Yeh T.J.
Identification and control of multi-evaporator air conditioning systems. *International Journal of Refrigeration*, Vol. 30, No.8, PP. 1374-1385 (2007)

91. Lin and Yeh 2009a
Lin J.L. and Yeh T.J.
Control of multi-evaporator air-conditioning systems for flow distribution. *Energy Conversion and Management*, Vol. 50, No.6, PP. 1529-1541 (2009)

92. Lin and Yeh 2009b
Lin J.L. and Yeh T.J.
Mode switching control of dual-evaporator air-conditioning systems. *Energy Conversion and Management*, Vol. 50, No.6, PP. 1542-1555 (2009)

93. Liu et al. 2004
Liu J., Wei W.J., Ding G.L., Zhang C.L. Kukaya M. Wang K.J. and Inagaki T.
A general steady state mathematical model for fin-and-tube heat exchanger based on graph theory. *International Journal of Refrigeration*, Vol. 27, No.

8, PP. 965-973 (2004)

94. Lorente et al. 2002
Lorente S., Wechsatol W. and Bejan A.
Tree-shaped flow structures designed by minimizing path lengths. *International Journal of Heat and Mass Transfer*, Vol. 45, No. 16, PP. 3299-3312 (2002)

95. Lorente et al. 2003
Lorente S., Wechsatol W. and Bejan A.
Optimization of tree-shaped flow distribution structures over a disc-shaped area. *International Journal of Energy Research*, Vol. 27, No. 8, PP. 715-723 (2003)

96. MacArthur 1984
MacArthur J. W.
Transient heat pump behavior: a theoretical investigation. *International Journal of Refrigeration*, Vol. 7, No. 2. PP. 123-127 (1984)

97. Maisey and Milestone 2010
Maisey G.E. and Milestone B.
Optimizing HVAC life-cycle performance optimizing HVAC life-cycle performance. http://www.wbdg.org/resources/tqc.php, 2010

98. Margaret 1972
Margaret I.
Willis Haviland Carrier Father of Air Conditioning (Technology and Society Section). *Ayer Company Publisher, Inc.*, 1972

99. Masuda et al. 1991
Masuda M., Wakahara K. and Matsui K.
Development of a multi-split system air conditioner for residential use. *ASHRAE Transaction*, Vol. 97, No. 2, PP. 121-131 (1901)

100. Masy 2006

Masy G.

Dynamic simulation on simplified building models and interaction with heating systems. *Proceeding of the 7th International Conference on System Simulation in Buildings, Liège, Belgium*, October 2008

101. Masy 2008

Masy G.

Definition and validation of a simplified multi-zone dynamic building model connected to heating system and HVAC unit. *PhD thesis, University of Liège*, 2008

102. Matos et al. 2004a

Matos R.S., Vargas J.V.C. and Laursen T.A.

Optimally staggered finned circular and elliptic tubes in forced convection. *International Journal of Heat and Mass Transfer*, Vol. 47, No. 6-7, PP. 1347-1359 (2004)

103. Matos et al. 2004b

Matos R.S., Laursen T.A., Vargas J.V.C. and Bejan A.

Three-dimensional optimization of staggered finned circular and elliptic tubes in forced convection. *International Journal of Thermal Sciences*, Vol. 43, No. 5, PP. 477-487 (2004)

104. Matthew and Banasal 1998

Matthew W.B. and Banasal P.K.

Challenges in modeling vapor-compression liquid chillers. *ASHRAE Transaction*, Vol. 104, PP. 474-486 (1998)

105. Mosca 2001

Mosca E.

Model-based predictive control. *Control Systems, Robotics and Automation,* 2001

106. M&EI 2009
Market Research Group in Mechanical and Electrical Information
Air-conditioning industry analysis report: MEAC market analysis. *Mechanical and Electrical Information*, in Chinese, 2009

107. Nyers and Stoyan 1994
Nyers J. and Stoyan G.
Dynamical model adequate for controlling the evaporator of a heat pump. *International Journal of Refrigeration*, Vol. 17, PP. 101-108 (1994)

108. Omar and Mohammed 2004
Omar M.A. and Mohammed M.A.
A survey of energy efficient strategies for effective air conditioning. *Energy Conversion and Management*, Vol. 45, PP. 1643-1654 (2004)

109. Okuzawa 1992
Okuzawa Y.
One system family air conditioning: multi-system air conditioner for 4–6 rooms. *Refrigeration*, Vol. 67, PP. 149–156 (1992)

110. Park et al. 2001
Park Y.C., Kim Y.C. and Min M.K.
Performance analysis on a multi-type inverter air conditioner. *Energy Conversion and Management*, Vol. 42, PP. 1607-1621 (2001)

111. Park et al. 2002
Park Y.C., Kim Y.C. and Cho H.
Thermodynamic analysis on the performance of a variable speed scroll compressor with refrigerant injection. *International Journal of Refrigeration,* Vol. 25, No. 8, PP.1072-1082 (2002)

112. Park et al. 2007
Park C., Cho H., Lee Y. and Kim Y.
Mass flow characteristics and empirical modeling of R22 and R410a flowing through electronic expansion valves. *International Journal of Refrigeration*, Vol. 30, PP.1401-1407 (2007)

113. Pacheco-Vega et al. 2001
Pacheco-Vega A., Sen M., Yang K.T. and McClain R.
Neural network analysis of fin-tube refrigerating heat exchanger with limited experimental data. *International Journal of Heat and Mass Transfer*, Vol. 44, No. 4, PP. 763-770 (2001)

114. Qi 2009
Qi Q.
Multivariable control of air temperature and humidity in a space served by a direct expansion (DX) air conditioning (A/C) system. *Ph.D. thesis, The Hong Kong Polytechnic University*, 2009

115. Qureshi and Tassou 1996
Qureshi T.Q. and Tassou S.A.
Variable-speed capacity control in refrigeration systems. *Applied Thermal Engineering*, Vol. 16, No. 2, PP. 103-113 (1996)

116. Raja et al. 2007
Raja V. A.P., Basak T. and Das S.K.
Thermal performance of a multi-block heat exchanger designed on the basis of Bejan's constructal theory. *International Journal of Heat and Mass Transfer*, Vol. 51, No. 13-14, PP. 3582-3594 (2007)

117. Rajat et al. 2004
Rajat S., Andrew G.A. and Clark W.B.

Dynamic modeling and control of multi-evaporator air-conditioning systems. *ASHRAE Transactions*, Vol. 110, PP. 109-119 (2004)

118. Reis 2006
Reis A.H.
Constructal theory: from engineering to physics, and how flow systems develop shape and structure. *Applied Mechanics Reviews*, Vol. 59, No. 5, PP. 269-282 (2006)

119. Reis and Bejan 2006
Reis A.H. and Bejan A.
Constructal theory of global circulation and climate. *International Journal of Heat and Mass Transfer*, Vol. 49, No. 11-12, PP. 1857–1875 (2006)

120. Richardson et al. 2002
Richardson D.H., Jiang H., Lindsay D. and Radermacher R.
Optimization of vapor-compression systems via simulation. *Proceedings of the International Refrigeration and Air Conditioning Conference at Purdue University, West Lafayette, IN, USA*, July 2002

121. Richardson et al. 2004
Richardson D.H., Aute V., Winkler J. and Radermacher, R.
Numerical challenges in simulation of a generalized vapor compression refrigeration system. *Proceeding of the International Refrigeration and Air Conditioning Conference at Purdue University, West Lafayette, IN, US*, July 2004

122. Richardson 2006
Richardson D.H.
An object oriented simulation framework for steady-state analysis of vapor compression refrigeration systems and components. *Ph.D. thesis, Department of Mechanical Engineering, University of Maryland*, 2006

123. Rosa et al. 2004
Rosa R., Reis A. H. and Miguel F.
Bejan's constructal theory of shape and structure. *Évora Geophysics Centre*, 2004

124. Scalabrin and Bianco 1994
Scalabrin G. and Bianco G.
Experimental thermodynamic analysis of a variable-speed open reciprocating refrigeration compressor. *Internal Journal of Refrigeration*, Vol. 17, No. 1, PP. 68-75 (1994)

125. Scheuer et al. 2003
Scheuer C., Keoleian A.G. and Reppe P.
Life cycle energy and environmental performance of a new university building: modeling challenges and design. *Energy and Buildings*, Vol. 35, No. 10, PP. 1049-1064 (2003)

126. Shi et al. 2003
Shi W., Shao S., Li X., Peng X. and Yang X.
A network model to simulate performance of variable refrigerant volume refrigeration systems. *ASHRAE Transactions*, Vol. 109, No. 2, PP. 61-68 (2003)

127. Shah 2004a
Shah R., Alleyne A.G. and Bullard C.W.
Dynamic modeling and control of multi-evaporator air conditioning systems. *ASHRAE Transactions*, Vol. 110, Part 1, PP. 109-119 (2004)

128. Shah et al. 2004b
Shah R., Rasmussen B.P. and Alleyne A.G.
Application of a multivariable adaptive control strategy to automotive air conditioning systems. *International Journal of Adaptive Control and Signal Processing*, Vol. 18, PP. 199-221 (2004)

129. Shao et al. 2008a
Shao S.Q., Shi W.X., Li X.T. and Yan Q.S.
Simulation model for complex refrigerant systems based on two-phase fluid network. Part I: Model development. *International Journal of Refrigeration,* Vol. 31, PP. 490-499 (2008)

130. Shao et al. 2008b
Shao S.Q., Shi W.X., Li X.T. and Yan Q.S.
Simulation model for complex refrigerant systems based on two-phase fluid network. Part II: Model application. *International Journal of Refrigeration,* Vol. 31, PP. 500-509 (2008)

131. Shen et al. 2008
Shen J., Xiao H., Peng A. and Li T.
Research and design for digital multi-connected ground-source heat recovery unit. *Proceedings of the 11th International Refrigeration and Air Conditioning Conference at Purdue, West Lafayette, IN, USA,* 2008

132. Simizu 1990
Simizu K.
Inverter-aided multi-system air conditioner (air to air heat pump) for conditioning use in buildings. *The 3rd International Energy Agency Heat pump Conference, Tokyo, Japan,* 1990

133. Singh et al. 2006
Singh J., Singh N. and Sharma J.K.
Fuzzy modeling and control of HVAC systems: A review. *Journal of Scientific and Industrial Research,* Vol. 65, PP. 470-476 (2006)

134. Smith 2006
Smith L.

A Daikin perspective on VRF. *Daikin Air Conditioning, UK*, 2006

135. Tiwari et al. 2004
Tiwari M.K., Mukhopadhyay A. and Sanyal D.
Numerical simulation of optimal multiple-input, multiple-output control of jet impingement cooling of a glass plate. *Numerical Heat Transfer*, Vol. 46, PP. 401-424 (2004)

136. Thompson and Dexter 2005
Thompson R. and Dexter A.
A fuzzy decision-making approach to temperature control in air-conditioning systems. *Control Engineering Practice*, Vol.13, PP. 689-698 (2005)

137. Turaga et al. 1988
Turaga M., Lin S. and Fazio P.F.
Correlations for heat transfer and pressure drop factors for direct expansion air cooling and dehumidifying coils. *ASHRAE Transaction*, Vol. 94, PP. 616-629 (1988)

138. Vargas and Paris 1995
Vargas J.V.C. and Paris J.A.R.
Simulation in transient regime of a heat pump with closed0looped and on-off control. *International Journal of refrigeration*, Vol. 18, No. 4, PP. 235-243 (1995)

139. Vargas and Bejan 2002
Vargas J.V.C. and Bejan A.
The optimal shape of the interface between two conductive bodies with minimal thermal resistance. *Journal of heat transfer*, Vol. 124, No. 6, PP. 1218-1221 (2002)

140. Wang et al. 1999
Wang C.C., Lee C.J. and Chang C.T.

Heat transfer and friction correlation for compact louvered fin-and-tube heat exchangers. *International Journal of Heat and Mass Transfer*, Vol. 42, No. 11, PP. 1945-1956 (1999)

141. Wang et al. 2000
Wang C.C., Lin Y.T. and Lee C.J.
Heat and momentum transfer for compact louvered fin-and-tube heat exchangers in wet conditions. *International Journal of Heat and Mass Transfer*, Vol. 43, No. 18, PP. 3443-3452 (2000)

142. Webb 1990
Webb R.L.
Air-side heat transfer correlations for flat and wavy plate fin-and tube geometries. *ASHRAE Transaction*, Vol. 96, PP. 445-449 (1990)

143. Wechsatol et al. 2001
Wechsatol W., Lorente S. and Bejan A.
Tree-shaped insulated designs for the uniform distribution of hot water over an area. *International Journal of Heat and Mass Transfer*, Vol. 44, No. 16, PP. 3111-3123 (2001)

144. Wile 1947
Wile D.D.
Air flow measurement in the laboratory. *Refrigerating Engineering*, PP.515

145. Wijaya 1995
Wijaya H. and Spatz M.W.
Two-phase flow heat transfer and pressure drop characteristics of R22 and R32/125. *ASHRAE Transactions*, Vol. 101, PP. 1020-1027 (1995)

146. Winkler et al. 2008
Winkler J., Aute V. and Radermacher R.
Comprehensive investigation of numerical methods in simulating a steady-

state vapor compression system. *International Journal of Refrigeration*, Vol. 31, PP. 930-942 (2008)

147. Winandy and Cuevas 2003
Winandy E.L. and Cuevas C.B.
Analysis of the oil return in a pair of scroll compressors working in parallel at part load. *Applied Thermal Engineering*, Vol. 23, PP. 623-636 (2003)

148. Xiao et al. 1997
Xiao P.W., Johnson P. and Akbarzadeh A.
Application of heat pipe heat exchangers to humidity control in air-conditioning systems. *Applied Thermal Engineering*, Vol. 17, No. 6, PP. 561-568 (1997)

149. Xia et al. 2002
Xia J., Winandy E., Georges B. and Lebrun J.
Testing methodology for VRF systems. *Proceedings of the 9th International Refrigeration and Air Conditioning Conference at Purdue, West Lafayette, IN, USA*, July 2006

150. Xia et al. 2003
Xia J., Zhou X., Jin X. and Wu Y.
Simulation study on operating characteristics of multi-evaporator VRV air conditioner. *Proceedings of the 21st IIR international Congress of Refrigeration, Washington, DC, USA*, August, 2003

151. Yang and Lee 1991
Yang K.H and Lee M.L.
Analysis of an inverter-driven air-conditioning system and its application in a hot and humid area. *International Journal of Energy Research*, Vol. 15, No. 5, PP. 357-365 (1991)

152. You et al. 2010
You Y, Wu A. and Yang S.
An optimal control strategy for multi-evaporator vapor compression systems. *Proceedings of the International conference on electrical and control engineering, Wuhan, China,* June 2010

153. Zhang and Zhang 2006
Zhang W.J. and Zhang C.L.
A generalized moving-boundary model for transient simulation of dry-expansion evaporators under larger disturbances. *International Journal of Refrigeration,* Vol. 29, PP. 1119-1127 (2006)

154. Zhang and Zhang 2011
Zhang W.J. and Zhang C.L.
Transient modeling of an air conditioner with a rapid cycling compressor and multi-indoor units. *Energy Conversion and Management,* Vol. 52, No. 1, PP. 1-7 (2011)

155. Zhou et al. 2007
Zhou Y.P., Wu J.Y., Wang R.Z. and Shiochi S.
Energy simulation in the variable refrigerant flow air-conditioning system under cooling conditions. *Energy and Building,* Vol. 39, No. 2, PP. 212-220 (2007)

156. Zhou et al. 2008
Zhou Y.P., Wu J.Y., Wang R.Z., Shiochi S. and Li Y.M.
Simulation and experimental validation of the variable-refrigerant-volume (VRV) air-conditioning system in EnergyPlus. *Energy and Buildings,* Vol. 40, No. 6, PP. 1041-1047 (2008)